MITOCHONDRIAL DISEASE WITH ABNORMAL MITOCHONDRIAL MORPHOLOGY

Stephanie Grice

Master of Science by Research

Department of Biochemistry

University of Oxford

CONTENTS

Abstract 5

Acknowledgements 6

Abbreviations 7

Chapter 1: Introduction 12

1.1 Introduction to the structure and function of the mitochondrion 12

1.2 Mitochondrial morphology and dynamics 13

1.2.1 Fission and fusion of mitochondria 13

1.2.2 Mitochondrial transport 23

1.2.3 Anchoring of mitochondria to the microtubules and/or actin cytoskeleton 31

1.2.4 Mitophagy 33

1.2.5 Mitochondria and the endoplasmic reticulum 39

1.2.6 Mitochondria and peroxisomes 44

1.2.7 Localisation of nuclear mRNAs encoding mitochondrial proteins to the mitochondrial outer membrane: a putative role for AKAP149 50

1.3 Mitochondrial dynamics and respiratory function 52

1.3.1 Secondary effects on mitochondrial morphology resulting from genetic defects in oxidative phosphorylation 52

1.3.2 Secondary effects on mitochondrial metabolism resulting from genetic defects in mitochondrial dynamics 56

1.4 Mitochondrial dynamics in disease 58

1.4.1 Mutations in *MFN2* cause Charcot-Marie-Tooth disease type 2A 58

1.4.2 Mutations in *GDAP1* cause Charcot-Marie-Tooth disease type 4A 60

1.4.3 Mutations in *DNM1L* result in a combined defect in mitochondrial and peroxisomal fission 61

1.4.4 Mutations in *OPA1* result in autosomal dominant optic atrophy 62

1.5 The project 62

1.5.1 Introduction to the patients studied in the project 63

1.5.2 Hypothesis 63

1.5.3 Aims 63

Chapter 2: Materials and Methods 65

2.1 Clinical presentations of the patients 65

2.2 Tissue culture 66

2.2.1 Media and reagents 66

2.2.2 Culture of human skin fibroblasts 67

2.2.3 Screening for *Mycoplasma* infection 69

2.2.4 Cell culture in emetine 70

2.3 Assay for pyruvate dehydrogenase activity 70

2.3.1 Buffers and reagents 70

2.3.2 Outline of the protocol 71

2.3.3 Preparation of cell extracts 72

2.3.4 PDH assay 72

2.4 Assays for citrate synthase and cytochrome c oxidase activity 74

2.4.1 Buffers and reagents 74

2.4.2 Outline of the protocol 75

2.4.3 Preparation of cell extracts 76

2.4.4 Citrate synthase assay 77

2.4.5 COX assay 78

2.5 Lowry protein assay 79

2.6 Analysis of mitochondrial morphology 80

2.7 Analysis of the subcellular distribution of the pyruvate dehydrogenase complex 81

2.8 Analysis of the subcellular distribution of cytochrome c oxidase 82

2.9 Analysis of the amount and subcellular distribution of mitochondrial DNA 83

2.10 Analysis of mitochondrial membrane potential 84

2.11 Pairwise patient cell fusions for complementation studies 85

2.12 Sequence analysis of candidate genes 86

2.12.1 Selection of candidate genes 86

2.12.2 Selection of reference sequences 86

2.12.3 Oligonucleotide primer design 87

2.12.4 Template preparation 87

2.12.5 Polymerase chain reaction 88

2.12.6 Gel electrophoresis 89

2.12.7 Purification and quantification 89

2.12.8 Sequencing 89

2.12.9 Sequence analysis of *TRAK1* 90

Chapter 3: Results 92

3.1 Mitochondrial enzyme activities 92

3.2 Mitochondrial morphology 93

3.3 Subcellular distribution of the pyruvate dehydrogenase complex 94

3.4 Subcellular distribution/activity of cytochrome c oxidase 96

3.5 Amount and subcellular distribution of mitochondrial DNA 97

3.6 Mitochondrial membrane potential 97

3.7 Complementation analysis 98

3.8 Sequence analysis of candidate genes 117

3.8.1 *AKAP1* 117

3.8.2 *DNM1L* 119

3.8.3 *FIS1* 120

3.8.4 *MFN1* 120

3.8.5 *MFN2* 120

3.8.6 *RHOT1* 120

3.8.7 *RHOT2* 121

3.8.8 *TRAK1* 123

3.8.9 *TRAK2* 126

Chapter 4: Discussion and Future Work 129

4.1 Discussion 129

4.2 Further work 137

4.2.1 Characterisation of the cellular phenotype 137

4.2.2 Genetic studies 138

4.3 Concluding remarks 139

Appendix 1: Zeiss filter set specifications 140

Appendix 2: Approved gene symbols and their aliases 141

Appendix 3: Reference sequences 142

Appendix 4: Preparation of template nucleic acid for PCR 143

Appendix 5: Primers and protocols for PCR 145

Appendix 6: Primers and protocols for sequencing 147

Appendix 7: Gel electrophoresis 149

Appendix 8: Purification of PCR products 150

References 151

ABSTRACT

Mitochondrial encephalopathies are a clinically, biochemically and genetically heterogeneous group of disorders and less than 50 % of patients receive a molecular diagnosis. Due to the bi-directional relationship between mitochondrial morphology and metabolic function, it is thought that in many of these cases the primary defect lies in a gene involved in the regulation of mitochondrial dynamics, rather than in a gene directly involved in mitochondrial metabolism. To date, patients diagnosed with diseases of mitochondrial dynamics present first and foremost with neurological symptoms and onset occurs in the first two decades of life. This project has characterised a novel group of previously undiagnosed patients with early-onset mitochondrial disease apparently due to a primary genetic defect in mitochondrial dynamics. Key common symptoms were lactic acidosis and acute encephalopathy. Primary skin fibroblasts showed abnormalities in the distributions and activities of multiple mitochondrial enzymes, in the content and distribution of mitochondrial DNA, and in the morphology of the mitochondria. In each case, the primary genetic defect was not identified but progress was made towards understanding the nature of the defect in the context of the cellular phenotype and suggestions were made for future work.

ACKNOWLEDGEMENTS

I would like to thank my supervisor, Dr Garry Brown, for giving me the opportunity to do the project and for patience in teaching me the assay protocols. I would also like to thank Mrs Ruth Brown for excellent tuition in tissue culture techniques and for screening the primary cell cultures for *Mycoplasma* infection.

I am grateful to Dr R. Capaldi and Dr M. Marusich at MitoSciences for their gift of the anti-PDH E2 subunit monoclonal antibody conjugated to Oregon Green®. I am also grateful to Mrs Rosie Head, whose protocols I used for amplification and sequencing of *MFN1* and *MFN2* from cDNA.

Finally, special thanks go to Dr Sam Hughes, Dr Martin Dalziel, Hannah Sleven and Anne-Marie Couto, for their invaluable support, advice and friendship, and to Dot and Karen in the Biochem Café, for delicious coffee and cake in times of need.

ABBREVIATIONS

aa	amino acid residue(s)
ABC	ATP-binding cassette
ABCD1	ABC subfamily D, member 1
ADOA	autosomal dominant optic atrophy
ADP	adenosine diphosphate
AKAP	A kinase-anchoring protein
ALDP	adrenoleukodystrophy protein
AMN	adrenomyeloneuropathy
ATP	adenosine triphosphate
BLAST	basic local alignment search tool
bp	base pair(s)
cAMP	cyclic adenosine monophosphate
CCCP	carbonyl cyanide *m*-chlorophenylhydrazone
CCDS	collaborative consensus coding sequence
cDNA	complementary DNA
CMT2A	Charcot-Marie-Tooth disease type 2A
CMT4A	Charcot-Marie-Tooth disease type 4A
CNS	central nervous system
CoA-SH	coenzyme A
COX	cytochrome c oxidase
CPT1	carnitine palmitoyltransferase 1
CS	citrate synthase
CTP	cytidine triphosphate
3D	3-dimensional

DAB	3,3'-diaminobenzidine
dATP	deoxyadenosine triphosphate
DCA	dichloroacetate
dCTP	deoxycytidine triphosphate
dGTP	deoxyguanosine triphosphate
dH_2O	deionised water
DMEM/F-12 Ham	Dulbecco's Modified Eagle's Medium/Nutrient Mixture F-12 Ham
DMSO	dimethyl sulfoxide
DNA	deoxyribonucleic acid
DNM1/Dnm1	dynamin 1
DNM1L	dynamin 1-like
dNTP	deoxynucleotide triphosphate
$\Delta\psi_m$	mitochondrial membrane potential
DRG	dorsal root ganglion
DRP1/Drp1	dynamin-related protein 1
DTNB	dithiobis 2-nitrobenzoic acid
EDTA	ethylenediaminetetraacetic acid
ER	endoplasmic reticulum
EST	expressed sequence tag
EtBr	ethidium bromide
FAD^+/FADH	flavin adenine dinucleotide (oxidised/reduced)
FBS	fetal bovine serum
FIS1/Fis1	fission 1
FLIP	fluorescence loss in photobleaching
FRAP	fluorescence recovery after photobleaching
FRET	fluorescence resonance energy transfer
Fzo	fuzzy onions

GDAP1	ganglioside-induced differentiation-associated protein 1
gDNA	genomic DNA
GED	GTPase effector domain
GFP	green fluorescent protein
GS	goat serum
GTP	guanosine triphosphate
GTPγS	guanosine-5'-*O*-(3-thio)triphosphate
HBSS	Hank's Balanced Salt Solution
HEK	human embryonic kidney
HSP60	heat shock protein 60 kDa
HUGO	Human Genome Organisation
ID	identification
IM	mitochondrial inner membrane
IMS	mitochondrial intermembrane space
IP_3	inositol 1,4,5-triphosphate
IP_3R	IP_3 receptor
JC-1	5,5',6,6'-tetrachloro-1,1',3,3'-tetraethylbenzimidazolylcarbocyanine iodide
KH	K homology
Khc	kinesin heavy chain (*Drosophila*)
LCAD	long-chain fatty acyl-CoA dehydrogenase
LCFA	long chain fatty acid ($C_{>12:0}$)
3MA	3-methyladenine
MAM	mitochondria-associated ER membrane
MAPL	mitochondrial-anchored protein ligase
MDV	mitochondria-derived vesicle
MEF	mouse embryonic fibroblast
MFF/Mff	mitochondrial fission factor

MFN/Mfn	mitofusin
milt	milton (after the blind British poet, John Milton)
Miro	mitochondrial Rho
MnSOD	manganese superoxide dismutase
MPT	mitochondrial permeability transition
MRI	magnetic resonance imaging
mRNA	messenger RNA
mtDNA	mitochondrial DNA
mtGFP	mitochondrial matrix-targeted GFP
mtPA-GFP	mitochondrial matrix-targeted photoactivatable GFP
mtRFP	mitochondrial matrix-targeted RFP
mtYFP	mitochondrial matrix-targeted YFP
NAD^+/NADH	nicotinamide adenine dinucleotide (oxidised/reduced)
NMD	nonsense-mediated decay
OD	optical density
OM	mitochondrial outer membrane
OPA1	optic atrophy 1
OXPHOS	oxidative phosphorylation
4PBA	4-phenylbutyrate
PBS	Dulbecco's Phosphate Buffered Saline
PBD	peroxisomal biogenesis disorder
PCR	polymerase chain reaction
PDH	pyruvate dehydrogenase
PDK	pyruvate dehydrogenase kinase
PED	single peroxisomal enzyme deficiency
PEG	polyethylene glycol
PEX/Pex	peroxin

PI	phosphatidylinositol
PKA	cAMP-dependent protein kinase A
RFP	red fluorescent protein
RHOT1	Ras homolog gene family, member T1
RHOT2	Ras homolog gene family, member T2
RNA	ribonucleic acid
RNAi	RNA interference
ROS	reactive oxygen species
rRNA	ribosomal RNA
SNARE	soluble N-ethylmaleimide sensitive factor attachment protein receptor
SNP	single nucleotide polymorphism
SNPH	syntaphilin
TM	transmembrane
TMRE	tetramethylrhodamine ethyl ester
TMRM	tetramethylrhodamine methyl ester
TOM20	translocase of outer membrane 20 kDa subunit
TPP	thiamine pyrophosphate
TPR	tetratricopeptide repeat
(d)TTP	thymidine triphosphate
TRAK	trafficking protein, kinesin-binding
tRNA	transfer RNA
UTR	untranslated region
UV	ultraviolet
VDAC	voltage-gated anion channel
VLCFA	very long chain fatty acid ($C_{>22:0}$)
X-ALD	X-linked adrenoleukodystrophy
YFP	yellow fluorescent protein

CHAPTER 1: INTRODUCTION

1.1 INTRODUCTION TO THE STRUCTURE AND FUNCTION OF THE MITOCHONDRION

Mitochondria are ubiquitous eukaryotic organelles. They are the cellular sites of oxidative phosphorylation (OXPHOS) and generate most of the cell's supply of ATP. They also play crucial roles in FeS cluster assembly, calcium signalling and apoptosis. Mitochondria are particularly important in tissues with high energy requirements, namely the liver and the brain, and mutations in nuclear genes encoding mitochondrial proteins result in severe early-onset metabolic and neurological disorders.

The mitochondrion is a double membrane-bound organelle. The space enclosed by the outer membrane (OM) and the inner membrane (IM) is known as the intermembrane space (IMS). The space enclosed by the IM is called the matrix. The IM is further subdivided into an inner boundary membrane and the cristae compartment, which consists of bag-like folds of the IM connected at their mouth via narrow tubular junctions (Frey and Mannella, 2000). The matrix is the site of the citric acid cycle whereas the complexes of the respiratory chain reside predominantly in the cristae compartment and generate an electrochemical gradient across the IM (negative in the matrix), known as the mitochondrial membrane potential ($\Delta\psi_m$). Cytochrome c is concentrated in the intracristal space and is released by cristae remodelling in response to apoptotic stimuli to play an important role in apoptosis.

The majority of mitochondrial proteins are encoded by nuclear genes and post-translationally imported into the organelle. However, mitochondria contain their own genome, which replicates independently of nuclear DNA. Mitochondrial DNA (mtDNA) is complexed with protein in structures called nucleoids, which are evenly distributed throughout the mitochondrial matrix. In

humans, mtDNA contains 13 protein-coding genes, all of which encode subunits of the respiratory chain complexes, 22 transfer RNA (tRNA) genes and 2 ribosomal RNA (rRNA) genes.

Mitochondria are dynamic organelles that constantly fuse and divide. Their size, shape, connectivity and subcellular distribution vary dramatically between cell types and with different developmental stages and physiological and pathological states. Mitochondria can exist as numerous small, spherical organelles or as an organised, interconnected network (Bakeeva *et al.*, 1981; Bereiter-Hahn, 1990; Bereiter-Hahn and Voth, 1994).

1.2 MITOCHONDRIAL MORPHOLOGY AND DYNAMICS

For the purposes of this project, mitochondrial morphology is defined as the ultrastructure, size, shape, connectivity and subcellular distribution of mitochondria. Mitochondrial dynamics refers to the physiological processes that govern mitochondrial morphology, namely mitochondrial fission and fusion, mitochondrial transport and anchoring, mitochondrial degradation, and interactions between mitochondria and other organelles. Each of these processes will be discussed in turn with descriptions of the proteins involved, their mechanisms of action, and their effects on mitochondrial morphology.

1.2.1 Fission and fusion of mitochondria

Mitochondria undergo continuous cycles of fission and fusion all along their length (Twig *et al.*, 2006) and the balance of these processes determines overall mitochondrial morphology. A shift towards fusion results in a dense mitochondrial network consisting of highly elongated and interconnected mitochondrial tubules. This facilitates transmission of $\Delta\psi_m$ from oxygen-rich to oxygen-poor areas of the cell, to allow efficient dissipation of energy throughout the cytoplasm,

and allows complementation of mtDNA gene products in heteroplasmic cells that have accumulated different somatic mutations in their mtDNA. In contrast, a shift in the balance of fission/fusion towards fission generates numerous morphologically and functionally distinct small, spherical organelles. This is important for mitochondrial inheritance during cytokinesis, for apoptosis (prior to cytochrome c release and caspase activation), and for transport of mitochondria in neurons, where organelles must travel long distances down axons to synapses. This section will discuss the key components of the mitochondrial fission and fusion machineries in mammalian cells, as shown in Table 1.1, and the effects on mitochondrial morphology when these components are defective.

Process	*S. cerevisiae*	Mammals	Location	Proposed function
Fission	Dnm1	Drp1	Cytosol and OM	OM fission
	Fis1	Fis1	OM	Receptor for OM fission machinery
	Mdv1	-	Cytosol and OM	Adaptor between Fis1 and Dnm1
	Caf4	-	Cytosol and OM	Redundant with Mdv1
	Mdm33	MTP18	IM	Possible role in IM fission
Fusion	Fzo1	Mfn1 and Mfn2	OM	OM fusion
	Ugo1	-	OM	Co-ordination of OM and IM fusion
	Mgm1	OPA1	IM and IMS	IM fusion

Table 1.1 Core components of the mitochondrial fission and fusion machineries in yeast and mammals. Mammalian homologues of yeast Ugo1, Mdv1 and Caf4 have not been identified to date. OM, outer mitochondrial membrane. IM, inner mitochondrial membrane. IMS, intermembrane space.

1.2.1.1 Mitochondrial fission

Dynamin-related protein 1 (Drp1) was the first protein to be identified as a component of the mitochondrial fission machinery in mammalian cells (Smirnova *et al.*, 1998). Homologous proteins are Dnm1p in *S. cerevisiae* (Bleazard *et al.*, 1999; Otsuga *et al.*, 1998) and Drp1 in *C. elegans* (Labrousse *et al.*, 1999). Depletion of Drp1 by RNA interference (RNAi), expression of dominant-negative mutants of Drp1 (such as $Drp1^{K38A}$), or microinjection of function-blocking anti-Drp1 antibodies, results in the same abnormal mitochondrial morphology phenotype: very long and highly branched mitochondrial tubules, perinuclear clustering and the formation of

swollen, spherical mitochondria (Labrousse *et al.*, 1999; Pitts *et al.*, 1999; Smirnova *et al.*, 1998, 2001; Yoon *et al.*, 2001). Electron microscopy showed that these large mitochondria vary greatly in size, exist as club-shaped and ring-shaped structures as well as solid spherical structures, and display vesiculation and rarefaction of cristae (Smirnova *et al.*, 1998).

Drp1 is a member of the dynamin family of GTPases and, like dynamin, has an N-terminal GTPase domain, a "middle" domain and a C-terminal GTPase effector domain (GED domain) (Smirnova *et al.*, 1998). The human homologue, DRP1, is expressed at high levels in brain, at moderate levels in skeletal muscle and heart muscle, and at low levels in other tissues (Smirnova *et al.*, 1998). Drp1 has a punctate distribution throughout the cytoplasm, with less than 5 % of proteins associated with mitochondria and the remainder in the cytosol (Pitts *et al.*, 1999; Smirnova *et al.*, 2001). Time-lapse imaging of Drp1 tagged with green fluorescent protein (GFP) showed that Drp1 localised in spots on mitochondria where fission was about to occur. Spots were seen to appear and disappear during the course of experiments, indicating cycling of Drp1 between the cytosol and the OM. Spots tended to appear on mitochondrial tubules and points of constriction and disappear from tips, suggesting assembly of Drp1 prior to fission and disassembly of Drp1 after fission (Labrousse *et al.*, 1999; Smirnova *et al.*, 2001).

Electron microscopy of purified recombinant Drp1 showed that Drp1 can self-assemble into multimeric ring-like structures with dimensions similar to those of dynamin multimers (Smirnova *et al.*, 2001; Yoon *et al.*, 2001). This self-assembly was inhibited by GTP but enhanced by a non-hydrolysable GTP analogue, guanosine-5'-*O*-(3-thio)triphosphate (GTPγS), suggesting that GTP binding to Drp1 results in self-assembly of Drp1 into rings and that GTP hydrolysis results in disassembly into Drp1 monomers (Yoon *et al.*, 2001). Furthermore, the GTP-bound form of Drp1 was shown to tubulate membranes both *in vivo* and *in vitro*. Drp1^{K38A}, which binds but does not hydrolyse GTP, induced membrane tubulation in rat hepatocytes; transmission electron microscopy revealed that these tubules had a constant diameter with Drp1-associated

striations at regular intervals along their length. *In vitro*, in the presence of liposomes and GTPγS, Drp1 induced the formation of long membrane tubules with striations at regular intervals, similar to those formed by $Drp1^{K38A}$ *in vivo* (Yoon *et al.*, 2001). Taken together, these observations suggest that GTP-bound Drp1 wraps around the constriction points of dividing mitochondria, analogous to dynamin collars at the necks of budding vesicles, and that GTP hydrolysis drives membrane scission and disassembly of Drp1 for recycling to the cytosol. However, proper distribution and assembly of Drp1 on mitochondria depends on a protein called fission 1 (Fis1).

Genetic studies in *S. cerevisiae* identified *FIS1* as a gene that acts in the same pathway as *DNM1* to regulate mitochondrial fission, identifying Fis1p as a component of the mitochondrial fission machinery, together with Dnm1p (Mozdy *et al.*, 2000). The human homologue of Fis1p, FIS1, was also found to be essential for DRP1-mediated mitochondrial fission (James *et al.*, 2003). In mammalian cells, overexpression of FIS1 results in mitochondrial fragmentation in a DRP1-dependent manner. Conversely, depletion of FIS1 by RNAi or microinjection with function-blocking anti-FIS1 antibodies results in an abnormal mitochondrial morphology phenotype that is identical to that induced by downregulation of DRP1 and can be partially rescued by expression of $DRP1^{K38A}$ (James *et al.*, 2003; Yoon *et al.*, 2003).

Fis1p/FIS1 localises completely to mitochondria and is uniformly distributed throughout the mitochondrial compartment. It is a small 17 kDa protein embedded in the OM by a single transmembrane (TM) domain at its C-terminal end such that the bulk of the molecule is exposed to the cytosol (James *et al.*, 2003; Mozdy *et al.*, 2000). The TM domain is necessary and sufficient for mitochondrial localisation (Yoon *et al.*, 2003). Structural analysis of FIS1 revealed that the N-terminal cytosolic domain forms six α-helices and that α2-α3 and α4-α5 adopt tetratricopeptide repeat (TPR) folds known to mediate protein-protein interactions (Dohm *et al.*, 2004; Suzuki *et al.*, 2003). There is significant evidence to suggest that FIS1 recruits DRP1 from

the cytosol to mitochondria for the fission reaction (Mozdy *et al.*, 2000; Yoon *et al.*, 2003; Yu *et al.*, 2005).

Fluorescence recovering after photobleaching (FRET) and co-immunoprecipitation studies demonstrated that DRP1 interacts with the TPR region of FIS1 but suggested that the interaction is transient (Yoon *et al.*, 2003; Yu *et al.*, 2005). Truncation analysis and the introduction of helix-breaking point-mutations in the TPR domain suggested that this interaction is essential for the ability of FIS1 to induce fission (Yu *et al.*, 2005). FIS1 had no effect on GTP hydrolysis by DRP1 *in vitro*, suggesting that the primary function of FIS1 is to recruit DRP1 to mitochondria and that FIS1 is a limiting factor in mitochondrial fission (Yoon *et al.*, 2003). This may explain why overexpression of Drp1 has been reported to have no effect on mitochondrial morphology in mammalian cells (Pitts *et al.*, 1999).

The α1 helix of FIS1 negatively regulates the FIS1-DRP1 interaction and this is important for the mechanism of mitochondrial fission. Co-immunoprecipitation experiments showed that deletion of the α1 helix increases the interaction between FIS1 and DRP1, suggesting that the α1 helix normally inhibits this interaction. Overexpression of $FIS1^{\Delta\alpha1}$ resulted in the formation of swollen mitochondria, suggesting a dominant negative effect on fission, but this was prevented by the introduction of helix-breaking point mutations into the $FIS1^{\Delta\alpha1}$ TPR domain. Overexpression of $DRP1^{K38A}$ had no effect on the formation of swollen mitochondria induced by $FIS1^{\Delta\alpha1}$, indicating that the FIS1-DRP1 interaction is independent of DRP1 GTPase activity (Yu *et al.*, 2005). Taken together, these results suggest that DRP1 is recruited to the OM by binding to the FIS1 TPR domain, resulting in a local DRP1 concentration high enough for self-assembly. The FIS1 α1 helix destabilises this interaction, either to allow DRP1-mediated constriction and membrane scission to take place or to release DRP1 to the cytosol after fission has occurred.

FIS1 oligomerisation may play a role in DRP1 binding. FIS1 forms homodimers via self-interaction of its N-terminal domain and this is essential for its ability to mediate mitochondrial fission (Yu *et al.*, 2005). Deletion of the α1 helix greatly increases the formation of dimeric and multiple oligomeric forms of FIS1, whereas further deletions decrease them, indicating that the α1 helix functions as a negative regulator of the FIS1 self-interaction (Yu *et al.*, 2005). Y87 in the α5 helix and the linker between the α3 and α4 helices participate in FIS1 oligomerization; mutations in these regions greatly reduce the ability of wild-type FIS1 to induce mitochondrial fragmentation and also the ability of $FIS1^{\Delta\alpha1}$ to induce the formation of swollen mitochondria (Yu *et al.*, 2005). Furthermore, DRP1 recruitment to mitochondria is dramatically reduced in cells overexpressing oligomerisation-defective $FIS1^{\Delta\alpha1}$ (Yu *et al.*, 2005).

Very little is known about fission of the IM. It is conceivable that the activity of Dnm1p/DRP1 is sufficient to sever both OM and IM simultaneously. However, the diameter of tubular mitochondria is 300-400 nm whereas the diameter of Dnm1p spirals is only 100 nm (Ingerman *et al.*, 2005). It has been suggested that Dnm1p assembly on mitochondria results in successful division of the organelle only when it coincides with a prior constriction event, i.e. IM fission (Legesse-Miller *et al.*, 2003). Labelling of the IM and OM with different fluorescent markers and fluorescence loss in photobleaching (FLIP) studies using mitochondrial matrix-targeted GFP (mtGFP) showed that IM fission can cause separation of matrix compartments in the absence of OM fission in *C. elegans* (Labrousse *et al.*, 1999). It is therefore likely that a separate IM fission machinery exists, although this has not been identified to date.

Two unrelated proteins that are integral to the IM have been proposed to contribute to IM fission: Mdm33p in yeast and MTP18 in mammals. Overexpression of Mdm33p induces fragmentation of mitochondria, with septation and subsequent vesiculation of the IM, possibly due to enhanced IM fission activity; in contrast, mutants lacking Mdm33p contain giant ring-shaped mitochondria (Messerschmitt *et al.*, 2003). Overexpression of MTP18 causes extensive

DRP1-dependent mitochondrial fragmentation, whereas downregulation of MTP18 by RNAi results in the formation of highly fused mitochondrial tubules that cluster around the nucleus (Tondera *et al.*, 2004, 2005); the latter phenotype cannot be suppressed by overexpression of FIS1, suggesting that MTP18 is essential for mitochondrial fission prior to or in conjunction with FIS1-mediated recruitment of DRP1 (Tondera *et al.*, 2005). The identification of mammalian homologues of Mdm33p, and further investigation into the structure and function of MTP18, may provide insights into the mechanism of IM fission.

1.2.1.2 Mitochondrial fusion

The first protein to be identified as a component of the mitochondrial fusion apparatus was that encoded by the *fuzzy onions* gene (*Fzo*), which was isolated from a screen for genes involved in *Drosophila* spermatogenesis (Hales and Fuller, 1997). Homologous proteins with similar function were later identified in other organisms, namely Fzo1p in yeast (Hermann *et al.*, 1998; Rapaport *et al.*, 1998) and mitofusin 1 and 2 (Mfn1 and Mfn2) in mammals (Rojo *et al.*, 2002; Santel and Fuller, 2001). Depletion or loss of function of these proteins results in fragmentation of mitochondria and loss of mtDNA (Chen *et al.*, 2003, 2005; Hermann *et al.*, 1998). In mammalian cells, overexpression of either mitofusin results in a variety of abnormal mitochondrial morphology phenotypes, including mitochondrial tubulation, perinuclear clustering of mitochondria and the formation of swollen, spherical mitochondria, sometimes with crescent-shaped or ring-shaped structures (Legros *et al.*, 2002; Rojo *et al.*, 2002; Santel and Fuller, 2001). Electron microscopy showed that swollen mitochondria exhibit swelling and/or rarefaction of cristae, with the IM closely apposed to the OM (Rojo *et al.*, 2002).

Mfn1 and Mfn2 have distinct but partially redundant roles in mitochondrial fusion in mammalian cells. *Mfn1*$^{-/-}$ and *Mfn2*$^{-/-}$ mouse embryonic fibroblasts (MEFs) have greatly reduced levels of mitochondrial fusion but either mitofusin can functionally replace the other, and either mitofusin

can correct mitochondrial morphology in *Mfn1*$^{-/-}$*Mfn2*$^{-/-}$ MEFs, indicating some degree of functional redundancy (Chen *et al.*, 2003, 2005). However, expression of Mfn2 in *Mfn1*$^{-/-}$ MEFs only partially rescues the abnormal mitochondrial morphology phenotype, suggesting differing roles for Mfn1 and Mfn2 in mitochondrial fusion. Consistent with this theory, *Mfn1*$^{-/-}$ and *Mfn2*$^{-/-}$ mitochondrial morphology phenotypes are slightly different: *Mfn1*$^{-/-}$ MEFs have very short mitochondrial tubules and very small, spherical mitochondria that are uniform in size, with a diameter no larger than that of the tubules, whereas *Mfn2*$^{-/-}$ MEFs have tubular and spherical mitochondria of widely varying sizes (Chen *et al.*, 2003, 2005).

Mfn1 and Mfn2 also have different roles in development. Although both *Mfn1*$^{-/-}$ and *Mfn2*$^{-/-}$ mice show early embryonic lethality due to a placental defect (Chen *et al.*, 2003), conditional loss of Mfn1 outside of the placenta leads to no detectable abnormalities, whereas similar non-placental loss of Mfn2 causes severe multisystem defects and early postnatal death (Chen *et al.*, 2007). The different roles of the mitofusins in different tissues and throughout development may reflect differences in their relative expression levels and/or biochemical differences between them, as discussed below.

Mfn1 and Mfn2 are anchored in the OM via a bi-partite TM domain, which spans the membrane twice, such that both the N-terminus and the C-terminus are exposed to the cytosol in each case. Both TM and C-terminal domains are necessary and sufficient for targeting of the proteins to the OM (Rojo *et al.*, 2002). The N-terminus contains a GTPase domain with four canonical GTPase motifs (G1-G4) (Santel and Fuller, 2001). In addition, there are two 4,3 hydrophobic heptad repeat regions (HR1 and HR2) that flank the bi-partite TM domain (Koshiba *et al.*, 2004; Rojo *et al.*, 2002).

Polyethylene glycol (PEG)-mediated cell fusion assays and *in vitro* membrane tethering assays showed that Mfn1 and Mfn2 can form homotypic and heterotypic complexes *in trans* to mediate

mitochondrial fusion (Chen *et al.*, 2005; Ishihara *et al.*, 2004; Koshiba *et al.*, 2004). Co-immunoprecipitation experiments showed that isolated HR2 domains can form homotypic and heterotypic complexes *in vitro* and the crystal structure of Mfn1/HR2$_{660-735}$ at 2.5 Å resolution showed a dimeric, antiparallel coiled coil (Koshiba *et al.*, 2004). Introducing proline substitutions into recombinant Mfn1/HR2$_{660-735}$ at positions 691 and 705 significantly reduced the stability of the coiled coil and this correlated with a reduced ability of the full-length mutant protein to mediate mitochondrial fusion, as shown by expression in *Mfn1*$^{-/-}$*Mfn2*$^{-/-}$ MEFs and by PEG-mediated cell fusion assays (Koshiba *et al.*, 2004). Taken together, these results suggest that Mfn1 and Mfn2 form homotypic and heterotypic complexes via interactions between their HR domains to tether apposing mitochondrial membranes prior to fusion.

GTP hydrolysis is required for membrane fusion but not membrane tethering. *In vitro* membrane tethering assays showed that GTP hydrolysis is required for mitochondrial fusion (Ishihara *et al.*, 2004). Expression of Mfn1$_{331-741}$ (lacking the N-terminal GTPase domain) in NIH 3T3 cells resulted in mitochondrial aggregation, but this was abolished by the introduction of mutations that destabilise the HR2 coiled-coil domain (Koshiba *et al.*, 2004). Electron microscopy revealed that the mitochondria were densely packed and separated by a uniform gap between apposing outer membranes (Koshiba *et al.*, 2004). Taken together, these results suggest that, in the absence of the GTPase domain, Mfn1 forms tethered intermediates that cannot complete fusion, seen as mitochondrial aggregates by fluorescence microscopy.

The differing roles played by Mfn1 and Mfn2 in mitochondrial fusion can be explained by their biochemical properties. *In vitro* membrane tethering assays showed that Mfn1-Mfn1 interactions are relatively strong, Mfn2-Mfn2 interactions are relatively weak, and Mfn1-Mfn2 interactions are of intermediate strength (Ishihara *et al.*, 2004). Furthermore, Mfn1 has higher GTPase activity (Ishihara *et al.*, 2004). This suggests that, whilst Mfn2 can mediate mitochondrial fusion when

expressed at high levels in the absence of Mfn1, Mfn1 is better able to facilitate fusion than Mfn2 and is predominantly responsible for mitochondrial fusion in most mammalian tissues.

OM and IM fusion events are coupled *in vivo* but separable and mechanistically distinct *in vitro*, indicating that separate fusion machineries exist in each membrane (Malka *et al.*, 2005; Meeusen *et al.*, 2004). The dynamin-like GTPase optic atrophy 1 (OPA1) is situated in the IMS, tightly bound to the IM, and is a prime candidate for mediating IM fusion in mammalian cells (Griparic *et al.*, 2004; Olichon *et al.*, 2003). OPA1 is the mammalian orthologue of yeast Mgm1p. This protein was first identified as being necessary for mtDNA maintenance in *S. cerevisiae* (Jones and Fangman, 1992) and it was later shown that loss of mtDNA in *mgm1* mutants was a secondary effect of ongoing mitochondrial fragmentation in the absence of mitochondrial fusion (Sesaki *et al.*, 2003; Wong *et al.*, 2000, 2003). Downregulation of OPA1 results in mitochondrial fragmentation in MEFs, whereas overexpression results in extensive mitochondrial tubulation (Cipolat *et al.*, 2004). Furthermore, overexpression of OPA1 promotes mitochondrial fusion in *Mfn2*$^{-/-}$ MEFs but not in *Mfn1*$^{-/-}$ MEFs, which display mainly fragmented mitochondria (Cipolat *et al.*, 2004). This suggests that Mfn1 and OPA1 are functionally interdependent, presumably in the co-ordination of OM and IM fusion.

Both OPA1 and Mgm1p are members of the dynamin-related protein family. They consist of an N-terminal mitochondrial targeting sequence, two consecutive hydrophobic segments (that may be involved in IM binding), a coiled-coil domain, a GTPase domain, a “middle” domain and a C-terminal coiled-coil domain that may correspond to a GED domain (Griparic *et al.*, 2004; Olichon *et al.*, 2003). Both OPA1 and Mgm1p exist in multiple isoforms, which are important for mitochondrial fusion activity. Mgm1p exists in a long form, l-Mgm1p, and a short form, s-Mgm1p, which is generated from l-Mgm1p by the mitochondrial rhomboid protease, Rbd1p/Pcp1p (Herlan *et al.*, 2003; McQuibban *et al.*, 2003). OPA1 exists in at least 8 different splice variants, and multiple long and short protein isoforms (L-OPA1 and S-OPA1 respectively),

and is extensively post-translationally processed by regulated proteolysis in a manner that is still poorly understood (Cipolat *et al.*, 2006; Delettre *et al.*, 2001; Guillery *et al.*, 2008b; Ishihara *et al.*, 2006).

There is significant evidence to suggest that Mgm1p/OPA1 controls biogenesis of the cristae in addition to IM fusion (Meeusen *et al.*, 2006) and regulates the cristae remodelling pathway during apoptosis (Cipolat *et al.*, 2006; Frezza *et al.*, 2006; Meeusen *et al.*, 2006; Pellegrini and Scorrano, 2007). An emerging hypothesis is that IM topology is a parameter that is regulated by the cell to optimise mitochondrial performance and response to stimuli. Different mitochondrial morphologies associated with various osmotic, metabolic, and disease states suggest that IM topology represents a balance between fission and fusion, with defects (such as vesiculation of cristae) corresponding to an imbalance in this process (Mannella, 2006, 2008).

1.2.2 Mitochondrial transport

Transport of mitochondria throughout the cell is essential for correct inheritance of the organelles upon cell division and for localisation of the organelles to regions of the cell where energy demands or oxygen supplies are greatest. It is particularly important in neurons because mitochondria have to travel long distances down axons to synapses, where exocytosis of neurotransmitter vesicles depends on local ATP and Ca^{2+} concentrations. Most of what is currently known about mitochondrial transport in mammals comes from studies in neurons, since long neuronal processes are robust models for characterising motility properties such as direction, duration and persistence of movement. In non-neuronal cells such as fibroblasts, in which mitochondria are transported over relatively short distances and exist primarily as a reticulum rather than as individual organelles, the importance of mitochondrial transport remains unclear.

Both microtubules and microfilaments are involved in mitochondrial transport in neurons (Morris and Hollenbeck, 1995). It has been postulated that long distance transport of mitochondria occurs along microtubules whereas movement along microfilaments may provide a localised transport system within axons to localise organelles in one region, move organelles that have become dissociated from microtubules back onto microtubules, and improve the efficiency of organelle transport in regions of the cell in which microtubules are few or absent, such as axonal growth cones.

1.2.2.1 Long-distance transport of mitochondria along the microtubule cytoskeleton

Approximately 80 % of mitochondrial movement during axonal transport is dependent upon microtubules, which are arranged in parallel arrays that are polarised with their plus ends towards the nerve terminal and their minus ends towards the cell body (Ligon and Steward, 2000). Axonal mitochondria display bi-directional motion, whereby individual mitochondria stop, start, and often change direction (Hollenbeck and Saxton, 2005; Overly *et al.*, 1996; Pilling *et al.*, 2006). Transport of mitochondria along microtubules is primarily dependent on plus-end-directed kinesins for anterograde transport (away from the nucleus) and minus-end-directed dyneins for retrograde transport (towards the nucleus) (Deacon *et al.*, 2003; Habermann *et al.*, 2001; Tanaka *et al.*, 1998; Varadi *et al.*, 2004).

Assuming that mitochondria are attached to two opposing motors, net movement in one direction may be determined by the motor with the overall highest activity or, alternatively, only one of the motors may be engaged with the microtubule track (De Vos *et al.*, 2003; Welte, 2004). Both motors may be components of the same complex and inhibition of one motor may disrupt the function of the other. The molecular mechanisms involved in co-ordination of anterograde *versus* retrograde transport remain poorly understood and will not be discussed here. These motors transport multiple cargoes along cytoskeletal tracks therefore it is presumed

that organelle-specific adaptor proteins exist to allow specificity of binding to occur. The components of the anterograde mitochondrial transport machinery are the most well-characterised to date.

The first protein to be identified as a crucial component of the mitochondrial anterograde transport machinery was *Drosophila* Milton (Stowers *et al.*, 2002). This protein was found to be required for mitochondrial transport within *Drosophila* photoreceptors. Photoreceptors mutant for the *milton* (*milt*) gene showed aberrant synaptic transmission despite normal phototransduction. Mitochondria were clustered in the cell bodies and absent from axons and synaptic termini, which were otherwise normal in their general architecture, suggesting a mitochondria-specific transport defect. Consistent with this hypothesis, Milton was associated with mitochondria and co-immunoprecipitated with kinesin heavy chain (Khc) in extracts from fly heads.

Milton transcripts are broadly expressed in *Drosophila* and flies that were homozygous for *milt* mutations died as second instar larvae, suggesting a wider role for Milton than its reported function in photoreceptors. Glater *et al.* (2006) expressed mtGFP in neurons of the central nervous system (CNS) in first instar larvae homozygous for a null allele of *milt* and showed that the selective loss of mitochondria from axons and synapses occurs in sensory and motor neurons as well. Co-immunoprecipitation assays demonstrated that Milton associates with Khc in the absence of a light chain, raising the possibility that Milton functions as a mitochondria-specific light chain and mitochondrial adaptor for the anterograde transport machinery (Brickley *et al.*, 2005; Glater *et al.*, 2006; Smith *et al.*, 2006).

The mitochondrial Rho (Miro) proteins were the next proteins to be identified as crucial components of the mitochondrial anterograde transport machinery. These proteins are present in yeast (Gem1p; Frederick *et al.*, 2004), *Drosophila* (dMiro; Guo *et al.*, 2005) and mammals (Miro1 and Miro2; Fransson *et al.*, 2003). They constitute an evolutionarily conserved family of

Rho GTPases, with atypical domain organisation and unique cellular properties. Each member of the family contains an N-terminal GTPase domain, similar to that found in other Rho GTPases, together with two EF-hand motifs and a C-terminal GTPase domain, which are atypical. Miro proteins are anchored at their C-terminus to the OM, with all functional domains exposed to the cytosol (Fransson *et al.*, 2003, Frederick *et al.*, 2004). Genetic studies in yeast indicated that both GTPase domains and both EF-hand motifs are required for Miro function (Frederick *et al.*, 2004).

Drosophila miro mutants phenocopy *milt* mutants and immunofluorescence analysis of cultured neurons and subcellular fractionation of *Drosophila* head extracts showed that dMiro associates with mitochondria and with Milton (Fransson *et al.*, 2006; Glater *et al.*, 2006; Guo *et al.*, 2005). This evidence suggests that dMiro functions as a mitochondrial receptor for the anterograde transport machinery and that Milton functions as a mitochondria-specific adaptor linking dMiro with Khc on microtubules. However, the situation in mammalian cells is more complex.

Two Milton homologues, trafficking protein, kinesin-binding 1 and 2 (TRAK1 and TRAK2), have been identified in mammalian cells and shown to interact with kinesin-1 heavy chain isoforms (KIF5 isoforms) and mitochondria (Brickley *et al.*, 2005). Both Miro1 and Miro2 interact with TRAK1 and TRAK2 (Fransson *et al.*, 2006) but the Miro1-TRAK2 interaction seems to be the most important for mitochondrial transport *in vivo* (MacAskill *et al.*, 2009a,b). Miro1 recruits TRAK2 to mitochondria, consistent with a role for TRAK2 as a mitochondria-specific adaptor (MacAskill *et al.*, 2009a). However, Miro1 also directly interacts with KIF5 in a Ca^{2+}-dependent manner (MacAskill *et al.*, 2009b; Saotome *et al.*, 2008). In short, the degree of functional redundancy between Miro1 and Miro2, and between TRAK1 and TRAK2, and the precise functions of these proteins in mitochondrial transport in mammalian cells remain unclear.

In mammalian cells, physiological increases in Ca^{2+} concentration ($[Ca^{2+}]$) have an inhibitory effect on microtubule-based mitochondrial mobility, with maximal movement at resting cytosolic $[Ca^{2+}]$ and complete arrest during agonist-induced cytosolic $[Ca^{2+}]$ spikes and oscillations (Yi *et al.*, 2004). This results in the positioning of mitochondria at intracellular sites with high cytosolic $[Ca^{2+}]$, in order to enhance local Ca^{2+} buffering and the production of ATP, which promotes re-uptake of Ca^{2+} by the endoplasmic reticulum (ER). The effects of cytosolic $[Ca^{2+}]$ on mitochondrial mobility appear to be independent of $\Delta\psi_m$, mitochondrial Ca^{2+} uptake and the activity of Ca^{2+}/calmodulin-dependent kinases and calcineurin (Yi *et al.*, 2004). Furthermore, the molecular structures of kinesin and dynein show no evidence of a binding site for Ca^{2+} or calmodulin (Vale, 2003). This suggests the existence of a cytosolic Ca^{2+}-dependent sensor molecule capable of inhibiting the mitochondrial transport machinery in the presence of Ca^{2+}.

There is significant evidence to suggest that Miro fulfils this role. Saotome *et al.* (2008) reported that, in resting H9c2 cells, overexpression of Miro1 or Miro2 resulted in an increase in mitochondrial motility whereas RNAi depletion of either protein resulted in a decrease in mitochondrial motility. These effects were independent of the presence of the EF-hand motifs, since Miro EF-hand mutants had the same effect. Increasing cytosolic $[Ca^{2+}]$ led to inhibition of basal mitochondrial motility as expected, the extent of which showed a sigmoid function of $[Ca^{2+}]$. However, overexpression of Miro1 or Miro2 shifted the Ca^{2+} sensitivity curve to the left, indicating increased sensitivity, and overexpression of Miro EF-hand mutants or RNAi depletion of Miro proteins shifted the Ca^{2+} sensitivity curve to the right, indicating reduced sensitivity. Overexpression of $Miro1^{N18}$ or $Miro2^{N18}$, dominant negative GTPase mutants of Miro, also reduced the extent of mitochondrial mobility inhibition in response to cytosolic $[Ca^{2+}]$, indicating that both EF-hand motifs and GTPase domains of Miro are required. Finally, MacAskill *et al.* (2009a,b) reported that Miro1 binds directly to KIF5 in a Ca^{2+}-dependent manner, strongly supporting a role for Miro in the Ca^{2+}-dependent inhibition of mitochondrial transport.

Perinuclear mitochondrial aggregates are indicative of an impairment of the microtubule-based anterograde transport machinery. This is often accompanied by the formation of long, thin, thread-like mitochondria, depending on the cell type and the nature of the transport defect, most probably due to the effects of abnormal transport on mitochondrial fission/fusion. Disruption of microtubules by nocodazol in human umbilical vein endothelial cells (HUVEC) resulted in collapse of mitochondria around the nucleus and the formation of very long, folded mitochondria, with some ring structures (Bereiter-Hahn *et al.*, 2008). Similar results were obtained in HeLa cells, but to a much lesser degree (Varadi *et al.*, 2004). Inactivation of KIF5 resulted in perinuclear clustering of mitochondria in undifferentiated extra-embryonic cells from mice (*kif5B*$^{-/-}$ cells; Tanaka *et al.*, 1998), in human fibroblasts (by microinjection of function-blocking anti-KIF5 antibodies; Rodionov *et al.*, 1993) and in HeLa cells (by transfection with the dominant negative mutant KIF5^{T93N}; Varadi *et al.*, 2002). Perinuclear accumulations of mitochondria were also seen in *Drosophila* mutants of Milton and dMiro (Guo *et al.*, 2005; Stowers *et al.*, 2002).

Several interesting studies reveal that there is a complex interdependent relationship between mitochondrial transport and fission/fusion. The shape and connectivity of mitochondria are likely to impinge on the ability of relevant motors to attach to and/or transport the organelle. Consistent with this theory, mutations in *Drosophila* Drp1 led to dramatic defects in synaptic localisation of mitochondria in motor neurons, whereby mitochondria clustered in cell bodies, consistent with a mitochondrial transport defect (Verstreken *et al.*, 2005). Conversely, proteins involved in mitochondrial transport have been shown to play additional roles in the regulation of mitochondrial fission. In H9c2 cells, the Miro proteins were shown to promote mitochondrial tubulation at resting cytosolic [Ca^{2+}] and mitochondrial fragmentation at high cytosolic [Ca^{2+}], by inhibition and activation of Drp1 respectively (Saotome *et al.*, 2008). Furthermore, the dynein/dynactin complex was shown to be involved in recruitment of DRP1 to mitochondria in HeLa cells and disruption of dynein function resulted in reduced association of DRP1 with

mitochondria and an abnormal mitochondrial morphology phenotype consistent with an imbalance in mitochondrial fission/fusion in favour of fusion (Varadi *et al.*, 2004).

Importantly, a recent study by Misko *et al.* (2010) reported that Mfn2 interacts directly with the microtubule-based mitochondrial transport machinery and is essential for the regulation of mitochondrial transport, independent of its role in mitochondrial fusion. Co-immunoprecipitation experiments demonstrated that both Mfn1 and Mfn2 can interact with Miro1 and Miro2 when exogenously expressed in HEK293T cells, with an apparently stronger interaction observed for Mfn2:Miro2 than for Mfn2:Miro1. Both mitofusins were also found to interact with TRAK1 and TRAK2. Pathogenic $MFN2^{R94Q}$ and $MFN2^{H361Y}$ mutants maintained the ability to interact with Miro and TRAK proteins and did not dissociate these proteins from each other or from kinesin, suggesting that Mfn2 regulates the mitochondrial transport machinery but is not required for complex formation between its component proteins. Finally, RNAi knockdown of Miro2 in cultured mouse sensory neurons produced mitochondrial transport deficits identical to those caused by loss of Mfn2, and overexpression of Miro2 in $Mfn2^{-/-}$ cultures did not rescue transport deficits, suggesting that both Mfn2 and Miro2 are required to co-operatively mediate mitochondrial transport.

1.2.2.2 Short-distance transport of mitochondria along the actin cytoskeleton

Short-distance transport of mitochondria is thought to be mediated by myosin motor proteins along actin filaments. In the absence of microtubules, actin filaments can support mitochondrial transport in axons to some degree, although axons contain actin filaments concentrated near the plasma membrane in a meshwork with no obvious polarity (Morris and Hollenbeck, 1995). Dendritic spines and presynaptic terminals contain few, if any, microtubules but they do contain actin filaments and transport of vesicles and organelles in these regions of the neuron is thought to be myosin-based. Several families of myosins (I, II, V and VI) have been implicated in

organelle and vesicle transport in axons, but only myosin V has been found to be present in dendritic spines and presynaptic terminals (Bridgman, 2004). However, no direct association of myosins with mitochondria has been reported until recently.

Quintero *et al.* (2009) characterised myosin-XIX (Myo19), the founding member of a novel class of myosin that associates with mitochondria and is involved in short-distance actin-based mitochondrial dynamics. Clear orthologues of human Myo19 are present in multiple vertebrate species including mouse, chicken, *X. laevis* and zebrafish, and Myo19 is widely expressed in vertebrate tissues. Immunocytochemical staining of Myo19 in A549, HeLa and COS7 cells revealed a clear and striking localisation of endogenous Myo19 to mitochondria. Expression of GFP-tagged truncation mutants of Myo19 in these cells showed that the C-terminal tail domain is necessary and sufficient for localisation of Myo19 to mitochondria. Interestingly, this domain has no obvious sequence homology with other proteins in the databases.

Time-lapse imaging of A549 cells and COS7 cells transfected with GFP-Myo19 and mtDsRed showed that Myo19 dramatically increases mitochondrial dynamics (Quintero *et al.*, 2009). In 40% of cells transfected with GFP-Myo19, the mitochondria moved continuously in a non-linear fashion for several micrometers, with average velocities more than 80 % greater than those of mitochondria in control cells. This movement was dependent on the Myo19 motor domain, since expression of the GFP-Myo19 tail had no effect on mitochondrial movements. It was also dependent on actin filaments, since movement ceased on destabilisation of the actin cytoskeleton with latrunculin B (Quintero *et al.*, 2009). However, the importance of Myo19 in regulating actin-based mitochondrial transport and mitochondrial morphology in neurons, and in mammalian cells in general, remains to be determined.

1.2.3 Anchoring of mitochondria to the microtubule and/or actin cytoskeleton

Together, movement and anchoring ultimately determine the distribution of mitochondria throughout the cell. In neurons, mitochondria are synthesised in the cell body then transported to and retained at sites of high ATP utilisation including the synapse, active growth cones, nodes of Ranvier, myelination boundaries and sites of axonal protein synthesis. Furthermore, axonal mitochondria spend long periods of time persistently stationary, suggesting that they have static docking interactions with the cytoskeleton (Hollenbeck, 1996; Morris and Hollenbeck, 1993). However, little is known about the proteins used to anchor mitochondria at particular subcellular sites or which elements of the cytoskeleton are involved. The importance of mitochondrial anchoring in non-neuronal cells such as fibroblasts, in which mitochondria travel relatively short distances to their destinations, also remains unclear.

Studies by Chada and Hollenbeck (2003, 2004) suggest that anchoring of mitochondria at active neuronal growth cones depends on the actin cytoskeleton. Placing a bead coated in nerve growth factor (NGF), which specifically promotes axonal outgrowth, on the axon of a cultured chick sensory neuron resulted in TrkA receptor-mediated accumulation of mitochondria at that site. This was dependent on the actin cytoskeleton, since it was abolished by treatment with latrunculin B, although mitochondria were still motile and distributed throughout axons. Time-lapse imaging of mitochondrial movements in a 100 µm region of the axon centred on a point of bead contact showed that mitochondria entered more frequently and exited less frequently from the region of contact with an NGF-bead compared to that of a control bead and the percentage of moving mitochondria decreased as they moved into the immediate vicinity of the NGF-bead. It seems, therefore, that the accumulation of mitochondria in regions of NGF stimulation is the result of both modulation of motor protein activities and upregulation of docking interactions with the actin cytoskeleton, although the proteins involved are yet to be identified.

Numerous ultrastructural studies have shown the presence of cross-links between mitochondria and microtubules in axons, although it is not known what fraction of these represents transient interactions between mitochondria and motor proteins as opposed to more static interactions with docking proteins (Benshalom and Reese, 1985; Hirokawa, 1982; Pannese *et al.*, 1986; Price *et al.*, 1991; Schnapp and Reese, 1982). However, Kang *et al.* (2008) recently identified syntaphilin (SNPH) as a protein that anchors mitochondria to microtubules in axons thoughout the CNS. SNPH was initially identified as a putative regulator of SNARE complex formation between neurotransmitter vesicles and the presynaptic membrane, a crucial step in exocytosis of neurotransmitter vesicles at synapses (Lao *et al.*, 2000). Immunocytochemical analysis of cultured rat hippocampal neurons showed that SNPH is absent from dendritic processes but enriched in axons, where it colocalises with more than 60 % of mitochondria (Kang *et al.*, 2008). Localisation analysis of GFP-SNPH truncation mutants revealed that residues 381-469 constitute the axon-sorting sequence and the C-terminal bi-partite TM domain targets the protein to the OM (Kang *et al.*, 2008).

The motility of SNPH-labelled and non-SNPH-labelled mitochondria in axons was analysed by time-lapse confocal imaging of cultured rat hippocampal neurons expressing mtDsRed and GFP-SNPH, using kymograph analysis to identify mobile and stationary mitochondria (Kang *et al.*, 2008). Almost all GFP-SNPH-labelled mitochondria were stationary in all axons analysed. In contrast, deletion of the SNPH microtubule-binding domain dramatically increased the proportion of mobile mitochondria (Kang *et al.*, 2008). Furthermore, in cultured hippocampal neurons from *snph*$^{-/-}$ mice, mitochondria showed dramatically increased mobility and reduced density in axons, although the velocities of mobile mitochondria and the ratio of anterograde to retrograde movements were not significantly different from those in control neurons. The observed phenotype was fully rescued with the reintroduction of the *snph* gene into the mutant neurons (Kang *et al.*, 2008). Taken together, these observations strongly support a role for SNPH in microtubule-based anchoring of mitochondria in neurons.

1.2.4 Mitophagy

Mitochondrial abundance is regulated by organelle formation, half-life, and autophagic degradation. Autophagy is the process by which intracellular components are sequestered and subsequently degraded by the lysosomal machinery. Autophagy is ongoing in nucleated cells, helping to maintain the correct balance between synthesis, degradation and subsequent recycling of cellular products. It is typically activated in response to starvation *in vivo* or nutrient deprivation *in vitro*, when it breaks down non-essential cellular components to release nutrients to maintain cellular processes. Autophagy also removes toxic protein aggregates and unwanted or dysfunctional organelles. Whether autophagy is selective or non-selective is controversial, although there is evidence to suggest that selective degradation of mitochondria occurs by autophagy, a process termed “mitophagy”.

Autophagy occurs via a variety of different mechanisms, although the final stage in the process is always hydrolytic digestion by lysosomes. Macroautophagy, the predominant and most well-defined mechanism of autophagy, involves the surrounding of cytoplasmic constituents by a crescent-shaped isolation membrane, called a phagophore, which forms a closed double membrane-bound structure, called an autophagosome; the autophagosome then fuses with a lysosome to become an autolysosome, its contents are degraded by acidic lysosomal hydrolases, and the resulting macromolecules are released into the cytosol via lysosomal membrane permeases (Mizushima *et al.*, 2002; Xie and Klionsky, 2007). Only macroautophagy, hereafter referred to as autophagy, will be discussed in the context of mitochondrial degradation in mammalian cells.

A crucial event in the formation of autophagosomes in mammalian cells is the post-translational processing of the ubiquitin-like Atg8 family of proteins, which includes GATE-16, GABARAP and LC3 (Ichimura *et al.*, 2000; Kabeya *et al.*, 2000, 2004; Kirisako *et al.*, 2000; Tanida *et al.*, 2003).

These proteins are conjugated to phosphatidyl ethanolamine in newly forming autophagosomal membranes. After fusion of autophagosomes with lysosomes, they are degraded by lysosomal hydrolases or delipidated and recycled. The lipidated form of these proteins is known as “form II”. LC3-II proteins selectively localise to forming and newly-formed autophagosomes, making them useful autophagosomal markers, and fluorescently-labelled LC3 has been used to study autophagy in cultured mammalian cells.

The degradation of mitochondria by autophagy under starvation conditions has been monitored in mammalian cells using a variety of experimental techniques. Rat hepatocytes or hepatocytes from GFP-LC3 transgenic mice (Mizushima *et al.*, 2004) were loaded with different organelle-specific fluorescent dyes, subjected to nutrient deprivation and glucagon, and monitored using time-lapse confocal imaging (Elmore *et al.*, 2001; Kim *et al.*, 2004; Rodriguez-Enriquez *et al.*, 2006). MitoTracker Green and/or tetramethylrhodamine methylester (TMRM) were used to label mitochondria; both dyes accumulate in polarised mitochondria but TMRM is released on depolarisation; TMRM quenches MitoTracker Green fluorescence by FRET, so in cells labelled with both TMRM and MitoTracker, green fluorescence uniquely identifies depolarised mitochondria. LysoTracker Red, which accumulates in acidic organelles, was used to label fully-formed autophagosomes, lysosomes and autolysosomes. GFP-LC3 fluorescence was used to monitor autophagosome formation. After induction of starvation conditions, GFP-LC3-positive structures were seen to surround and completely sequester individual mitochondria. This was inhibited by 3-methyladenine (3MA), which inhibits the class III PI 3-kinases involved in sequestration (Petiot *et al.*, 2000). Sequestered mitochondria depolarised after a few more minutes, shown by release of TMRM, and then acidification occurred, shown by uptake of LysoTracker Red. This was followed by dissipation of GFP-LC3 fluorescence, representing degradation or recycling of LC3-II.

Using the same experimental techniques, it was shown that damaged mitochondria can be destroyed by mitophagy under nutrient-rich conditions. Selected mitochondria inside hepatocytes from GFP-LC3 transgenic mice were subjected to laser-induced photodamage and monitored using time-lapse confocal imaging (Kim *et al.*, 2006). Portions of hepatocytes containing 5-10 mitochondria were exposed to a pulse of light from an argon laser and mitochondrial depolarisation occurred in a light dose-dependent fashion, as shown by loss of TMRM fluorescence. At lower doses of light, mitochondria depolarised transiently but subsequently recovered TMRM fluorescence within a few minutes. After a greater exposure, mitochondrial depolarisation became irreversible. After irreversible but not reversible photodamage, GFP-LC3 fluorescence began to envelop and completely encircle depolarised mitochondria. After formation of these autophagosomes, acidification occurred, as shown by uptake of LysoTracker Red.

Mitochondrial fission is involved in the segregation of damaged or dysfunctional mitochondria from the rest of the mitochondrial population, but it is unclear whether it is *per se* a trigger of mitophagy. The relationship between mitochondrial fission, fusion and autophagy is poorly defined. It is not clear how individual dysfunctional mitochondria are partitioned and eliminated when mitochondria exist in a continuous network and all parts of that network are equipotential, nor is it clear how the fate of dysfunctional mitochondria is determined, i.e. whether they are rescued by fusion with the rest of the network or degraded by autophagy. Mitochondrial fission and fusion events, matrix lumen continuity and $\Delta\psi_m$ have been studied in cells stained with tetramethylrhodamine ethylester (TMRE) and transfected with mitochondrial matrix-targeted photoactivatable GFP (mtPA-GFP) by time-lapse confocal imaging after laser-mediated photoactivation of mtPA-GFP in a small area of the network (Twig *et al.*, 2006). Using this technique, a subpopulation of mitochondria with low fusion ability and low $\Delta\psi_m$ was identified. Photoactivation of mtPA-GFP in individual mitochondria stained with TMRE allowed temporal

mapping of individual fission and fusion events and associated variations in $\Delta\psi_m$ and allowed the fate of fusing and non-fusing mitochondria to be investigated (Twig *et al.*, 2008a).

Twig *et al.* (2008a) found that mitochondria undergo continuous cycles of fusion and fission, in which fission is triggered by fusion, as shown by cumulative probability analysis. 85 % of fission events observed generated daughter mitochondria with equal and opposite differences in $\Delta\psi_m$: one daughter was hyperpolarised (-6 mV relative to baseline) and the other was depolarised (+6 mV relative to baseline). It was postulated that this occurred by either random or selective segregation of dysfunctional mitochondrial components into one daughter but not the other. Single mitochondria with low $\Delta\psi_m$ generated by a recent fission event were less likely to re-fuse with the mitochondrial network and more likely to undergo autophagy. Furthermore, non-fusing mitochondria with low $\Delta\psi_m$ had 50 % less OPA1 protein relative to fusing mitochondria and were preferentially segregated into GFP-LC3-labelled autophagosomes. This study was the first to measure the metabolic consequence of a single fission event, to show that mitochondrial fusion occurs preferentially between mitochondria with higher $\Delta\psi_m$, and to show that fission followed by selective fusion generates an isolated subpopulation of non-fusing mitochondria that are then degraded by mitophagy.

It was hypothesised that mitochondrial fusion, fission and autophagy operate a quality control system, whereby fission followed by selective fusion segregates dysfunctional mitochondria from the rest of the mitochondrial network and permits their removal by mitophagy (Twig *et al.*, 2008b). In line with this hypothesis, increased fusion, caused by overexpression of OPA1, and decreased fission, caused by overexpression of $DRP1^{K38A}$ or RNAi knockdown of FIS1, reduced mitophagy without affecting non-selective autophagy and resulted in reduced OXPHOS and increased mitochondrial oxidative damage, consistent with the accumulation of dysfunctional mitochondria (Twig *et al.*, 2008a). It seems therefore that mitochondrial fission is essential for mitophagy but is not itself the trigger for mitophagy. Non-fusing mitochondria depolarised long

before the onset of mitophagy, as shown by pulse-labelling with MitoTracker Red at various timepoints before the onset of mitophagy, suggesting that low $\Delta\psi_m$ could be the signal targeting dysfunctional mitochondria for mitophagy (Twig *et al.*, 2008a).

Further evidence that mitochondrial membrane depolarisation targets mitochondria for mitophagy came from experiments in which the effects of different mutants of FIS1 on mitochondrial morphology and function were investigated (Gomes and Scorrano, 2008). Co-expression of wild-type FIS1 and mitochondrial matrix-targeted red fluorescent protein (mtRFP) in both HeLa cells and MEFs resulted in extensive fragmentation of the mitochondrial network and induction of mitophagy. Overexpression of $FIS1^{K148R}$, which retains mitochondrial fission ability but is unable to cause mitochondrial dysfunction, did not induce mitophagy. However, overexpression of $FIS1^{\Delta\alpha1}$, which acts as a dominant negative for mitochondrial fusion and causes extensive mitochondrial dysfunction, was at least as efficient as wild-type FIS1 in promoting mitophagy (Gomes and Scorrano, 2008). This suggests that loss of $\Delta\psi_m$ is the common feature enabling wild-type FIS1 and $FIS1^{\Delta\alpha1}$ to induce mitophagy.

Surprisingly, Parkin can signal mitophagy in mammalian cells (Narendra *et al.*, 2008). Parkin is an ubiquitin ligase encoded by the *PARK2* gene, loss-of-function mutations in which are associated with a familial juvenile form of Parkinson's disease (Kitada *et al.*, 1998). Treatment of HEK293 cells with the mitochondrial uncoupler CCCP resulted in collapse of $\Delta\psi_m$ and mitochondrial fission, followed by recruitment of endogenous Parkin from the cytosol to the mitochondria. Within 48 hours, all mitochondria had disappeared, leaving other organelles, including peroxisomes, undisturbed (Narendra *et al.*, 2008). The same effects were observed in HeLa cells expressing exogenous Parkin tagged with yellow fluorescent protein (YFP) (Narendra *et al.*, 2008). Elimination of YFP-Parkin-labelled mitochondria was blocked in CCCP-treated HeLa cells by treatment with 3MA. Furthermore, in CCCP-treated HeLa cells lacking Parkin, mitochondrial membrane depolarisation and fragmentation occurred but mitochondria

underwent little other morphological change over the next 48 hours (Narendra *et al.*, 2008). Taken together, these results indicate that Parkin plays an essential role in the mechanism of mitophagy in mammalian cells.

Several observations suggest that loss of $\Delta\psi_m$ is the signal for recruitment of Parkin to mitochondria. In *Mfn1*$^{-/-}$*Mfn2*$^{-/-}$ MEFs, in which the mitochondrial network is completely fragmented into small spherical organelles, YFP-Parkin co-localised with a subset of mitochondria that showed lower MitoTracker staining, suggesting that Parkin is selectively recruited to dysfunctional mitochondrial with low $\Delta\psi_m$. In CCCP-treated HeLa cells expressing DRP1^{K38A}, in which the mitochondrial network is highly fused, Parkin still accumulated along elongated mitochondria, indicating that mitochondrial fission is not necessary for Parkin recruitment (Narendra *et al.*, 2008). These observations support the theory that mitochondrial membrane depolarisation, and not mitochondrial fission, signals mitochondria for destruction by mitophagy and suggests that Parkin may play an essential role in the mechanism of mitophagy, downstream of mitochondrial membrane depolarisation.

Defective or insufficient mitophagy results in the formation of “giant mitochondria” with disorganisation and rarefaction of cristae. Several studies have reported the accumulation of giant mitochondria in aging post-mitotic tissues, such as skeletal muscle, the myocardium and the brain, and in cultured myoblasts at higher passage numbers (Beregi *et al.*, 1988; Coleman *et al.*, 1987; Navratil *et al.*, 2008; Vanneste and van den Bosch de Aguilar, 1981). This is believed to be the result of insufficient autophagy, according to the mitochondrial-lysosomal axis theory of aging (Brunk and Terman, 2002; Terman *et al.*, 2004). Furthermore, giant mitochondria appear after treatment of cultured cells with 3MA (Navratil *et al.*, 2008; Stroikin *et al.*, 2004; Terman *et al.*, 2003). Giant mitochondria vary dramatically in length but are typically 1-5 µm wide, approximately 3-fold to 10-fold thicker than normal mitochondria. They have low mtDNA content, low $\Delta\psi_m$ and 50 % less OPA1 protein than normal mitochondria. PEG-

mediated cell fusions between populations of 3MA-treated cells labelled with spectrally separated mitochondrially-targeted fluorescent dyes suggest that giant mitochondria are unable to fuse with each other or with the rest of the mitochondrial population (Navratil *et al.*, 2008), consistent with the observations made by Twig *et al.* (2008a) about the properties of mitochondria degraded by mitophagy.

The *Drosophila* homologue of Parkin is encoded by the *parkin* gene. Interestingly, *parkin*-null *Drosophila* exhibit a severe phenotype, with loss of dopaminergic neurons, disrupted spermatogenesis resulting in male sterility, and giant mitochondria with severe disruption and rarefaction of the cristae in the flight muscles; this leads to degeneration of the flight muscles and concomitant locomotor defects (Greene *et al.*, 2003; Whitworth *et al.*, 2005). These results support the theory that Parkin plays an essential role in the mechanism of mitophagy and that defective mitophagy, due to the absence of Parkin, results in the formation of giant mitochondria.

1.2.5 Mitochondria and the endoplasmic reticulum

The ER is a eukaryotic organelle consisting of a dynamic, interconnected network of membrane-bound cisternae arranged in stacks. The ER is arranged into subcompartments: the rough ER, which is responsible for protein synthesis, and the smooth ER, which is responsible for synthesis of lipids and steroids. Importantly, the ER is the main intracellular store of Ca^{2+} ions and, in response to extracellular stimuli, releases Ca^{2+} to the cytosol in characteristic spatial and temporal patterns to control a wide variety of cellular processes. Mitochondria absorb Ca^{2+} released from the ER and modulate the size and duration of intracellular Ca^{2+} signals. In mammalian cells, juxtaposition between mitochondria and the ER is a well-known phenomenon. The molecular basis of this juxtaposition remained unknown until recently, when de Brito and Scorrano (2008) showed that mitochondria are directly tethered to the ER via transorganellar

homo- and heterodimers of Mfn2. Mfn2-mediated ER-mitochondria tethering is essential for efficient mitochondrial Ca^{2+} uptake after ER Ca^{2+} release and therefore plays a crucial role in intracellular Ca^{2+} signalling and homeostasis. It is therefore possible that a relationship exists between ER-mitochondria tethering and mitochondrial fusion and/or transport.

Studies using centrifugation, electron microscopy and high resolution 3D electron tomography have provided significant evidence for the close association between mitochondria and the ER in mammalian cells (Csordás *et al.*, 2006; Mannella *et al.*, 1998; Marsh *et al.*, 2001; Meier *et al.*, 1981; Rizzuto *et al.*, 1998; Shore and Tata, 1977). It is estimated that up to 20 % of the mitochondrial surface is in direct contact with the ER (Rizzuto *et al.*, 1998). The region of close contact between the two organelles is known as the mitochondria-associated ER membrane (MAM). Physical links between the ER and mitochondria were visualised using electron tomography and found to be approximately 10 nm long at the smooth ER and 25 nm long at the rough ER, the greater length at the rough ER reflecting the need to accommodate ribosomes on the ER surface (Csordás *et al.*, 2006). These tethers were thought to be proteinaceous, because they were destroyed by limited proteolysis (Csordás *et al.*, 2006).

Several ER- or mitochondria-bound proteins have been implicated as possible linking elements due to their enrichment in MAMs and/or their ability to change the spatial relationship between the two organelles. The most notable examples are the phosphor-acidic cluster sorting protein 2 (PACS-2), which localises to both the ER and mitochondria, the ER Ca^{2+} release channel inositol 1,4,5-triphosphate receptor (IP_3R), the voltage-dependent anion channel (VDAC) of the OM, and the molecular chaperone glucose-regulated protein 75 (grp75) (Beckenridge *et al.*, 2003; Köttgen *et al.*, 2005; Rizzuto *et al.*, 1998; Simmen *et al.*, 2005; Szabadkai *et al.*, 2006). However, no evidence for a direct role of these proteins in ER-mitochondria tethering has been found to date. Interestingly, overexpression of DRP1 results in mitochondrial fragmentation and uncoupling from the ER (Pitts *et al.*, 1999; Szabadkai *et al.*, 2004) and the effects of PACS-2 on

ER-mitochondria coupling are due to modulation of DRP1 activity (Beckenridge *et al.*, 2003; Simmen *et al.*, 2005). This suggests that changes in the balance of mitochondria fission/fusion may influence ER-mitochondria tethering, and perhaps *vice versa*.

The only protein found to be directly involved in ER-mitochondria tethering to date is one that is also involved in mitochondrial fusion and transport. De Brito and Scorrano (2008) showed that Mfn2 controls the morphology of both the ER and mitochondria, that Mfn2 is enriched in MAMs, and that Mfn2 on the ER engages in homotypic and heterotypic complexes with Mfn2 or Mfn1 on mitochondria respectively to tether the two organelles. Immunofluorescence and subcellular fractionation experiments showed that Mfn2 is present in both ER and mitochondrial membranes and is enriched 14-fold in MAMs relative to mitochondria. 3D confocal fluorescence microscopy showed that *Mfn2*$^{-/-}$ MEFs and *Mfn1*$^{-/-}$*Mfn2*$^{-/-}$ MEFs, but not *Mfn1*$^{-/-}$ MEFs, have fragmented mitochondrial and ER networks and a 40 % reduction in the ER-mitochondria interface. Expression of ER-targeted Mfn2 corrected both ER morphology and ER-mitochondria tethering in *Mfn2*$^{-/-}$ MEFs but only ER morphology in *Mfn1*$^{-/-}$*Mfn2*$^{-/-}$ MEFs, unless it was expressed with Mfn1 or mitochondrially-targeted Mfn2, in which case tethering was also restored. Conversely, mitochondrially-targeted Mfn2 corrected mitochondrial morphology only in *Mfn2*$^{-/-}$ MEFs and did not correct any defects in *Mfn1*$^{-/-}$*Mfn2*$^{-/-}$ MEFs, unless it was expressed with ER-targeted Mfn2, in which case both ER morphology and tethering were restored.

The ability of Mfn2 to regulate ER morphology and ER-mitochondria tethering is not necessarily independent of its ability to regulate mitochondrial fusion and transport. Mfn2 has a p21-Ras-binding domain immediately upstream of its GTPase domain (Chen *et al.*, 2004). The ability of Mfn2 to regulate ER morphology and ER-mitochondria tethering resides in the p21-Ras-binding domain, since Mfn2$^{\Delta Ras}$ completely corrected mitochondrial morphology in *Mfn2*$^{-/-}$ MEFs but failed to restore ER-morphology and ER-mitochondria tethering (de Brito and Scorrano, 2008). However, Mfn2 mutant proteins, which are incompetent for mitochondrial fusion in

Mfn1$^{-/-}$*Mfn2*$^{-/-}$ MEFs, are competent for fusion in *Mfn2*$^{-/-}$ MEFs because they can form fusion-competent complexes in trans with Mfn1 (Detmer and Chan, 2007). Until the effects on mitochondrial morphology of the Mfn2$^{\Delta Ras}$ mutant are studied in the absence of Mfn1, its mitochondrial fusion ability remains unclear. The ability of Mfn2$^{\Delta Ras}$ to regulate mitochondrial transport has also not been investigated.

There are still many unanswered questions. What is the sorting mechanism ensuring localisation of Mfn2 to both the ER and mitochondrial compartments? If Mfn2$^{\Delta Ras}$ can correct mitochondrial morphology but not ER morphology in *Mfn2*$^{-/-}$ MEFs, what is the mechanism by which wild-type Mfn2 mediates fusion of ER membranes? What is the regulatory mechanism that prevents fusion of ER and mitochondrial membranes after tethering? There is significant heterogeneity in the length of ER-mitochondria tethers observed by electron tomography (Csordás *et al.*, 2006) and ER-mitochondria contact zones are still formed in mitofusin-deficient cells (de Brito and Scorrano, 2008), so what other proteins are involved? Until these questions are answered, it will not be clear to what extent abnormalities in ER morphology and ER-mitochondria tethering can affect mitochondrial morphology and *vice versa*.

Juxtaposition of the ER with mitochondria is essential for efficient mitochondrial Ca^{2+} uptake after ER Ca^{2+} release in response to extracellular signals. Binding of extracellular agonists to receptors in the plasma membrane results in the formation of inositol 1,4,5-triphosphate (IP_3), which binds and activates IP_3R Ca^{2+} channels in the ER membrane, resulting in rapid Ca^{2+} release. Mitochondria absorb Ca^{2+} via VDAC in the OM and the Ca^{2+} uniporter in the IM. However, the affinity of the uniporter for Ca^{2+} is too low to account for the rapid mitochondrial uptake of Ca^{2+} after IP_3-induced Ca^{2+} release, based on the observed increase in cytosolic [Ca^{2+}] (Carafoli, 2003; Rizzuto *et al.*, 2009). The calcium microdomains hypothesis, also known as the “hotspot hypothesis”, states that juxtaposition of the ER with mitochondria results in [Ca^{2+}] microdomains at close contacts between the two organelles, where the [Ca^{2+}] is much

greater than that of the bulk cytosol, and that this facilitates rapid uptake of Ca^{2+} by the mitochondria (Rizzuto *et al.*, 1992, 1993, 2004).

An extension of the calcium microdomains hypothesis states that the proportion of the ER apposed to mitochondria and the distance between the two organelles are inversely correlated with the rate of mitochondrial Ca^{2+} uptake. In support of this theory, mitochondrial Ca^{2+} uptake was reported to be lower and slower in *Mfn2*$^{-/-}$ MEFs than in wild-type cells (de Brito and Scorrano, 2008). Furthermore, increased levels of apoptosis were observed after overexpression of Mfn2 in rat vascular smooth muscle cells (Guo *et al.*, 2007) and after expression of a "synthetic linker" (RFP fused to an OM targeting sequence at the N-terminus and an ER targeting sequence at the C-terminus) that led to shorter ER-mitochondria tethers in RBL-2H3 cells (Csordás *et al.*, 2006); this is presumably due to excessive mitochondrial Ca^{2+} uptake in each case, leading to induction of the mitochondrial permeability transition (MPT) (Szalai *et al.*, 1999).

Mitochondrial Ca^{2+} uptake after IP_3-induced ER Ca^{2+} release affects mitochondrial metabolism and shapes the size and duration of the Ca^{2+} signal. In the mitochondrial matrix, Ca^{2+} activates three key metabolic enzymes, the pyruvate, α-ketoglutarate and isocitrate dehydrogenases, resulting in increased OXPHOS (McCormack *et al.*, 1990). Removal of Ca^{2+} from high [Ca^{2+}] microdomains between the ER and mitochondria reduces the local positive feedback effects of Ca^{2+} on IP_3Rs, resulting in subcellular heterogeneity in IP_3R excitability (Rizzuto *et al.*, 2009). Spatial clustering of mitochondria in a defined portion of the cell limits the propagation of cytoplasmic Ca^{2+} waves to/from that region; for example, in pancreatic acinar cells, clustering of mitochondria around the apical pole prevents the spread of IP_3-evoked Ca^{2+} waves from that region to the basal part of the cell containing the nucleus (Tinel *et al.*, 1999).

ER-mitochondria tethering is therefore crucial for intracellular Ca^{2+} signalling and homeostasis. Abnormalities in ER-mitochondrial tethering may have an inhibitory effect on mitochondrial metabolism and may disrupt normal microtubule-based mitochondrial transport and subcellular distribution, since binding of Miro proteins to kinesin is Ca^{2+}-dependent. Furthermore, ER-mitochondria tethering may be crucial for neuronal function. Mironov and Symonchuk (2006) showed that, in mouse respiratory neurons, exocytosis of neurotransmitter vesicles at dendritic synapses is dependent on the presence of functional ER vesicles and mitochondria and the efficiency of Ca^{2+} exchange between these organelles, which in turn is dependent on the distance between them. However, little is known about the distribution of the ER in neuronal axons and studies on exocytosis in the absence of ER-mitochondria tethering have been conducted on dendrites only, so the global effects of abnormal ER-mitochondria tethering on neuronal function remain unclear. In any case, it seems that the effects of ER-mitochondria tethering on mitochondrial morphology and function and the function of the cell as a whole are potentially significant and wide-ranging and worthy of further investigation.

1.2.6 Mitochondria and peroxisomes

Peroxisomes are single membrane-bound organelles present in most eukaryotic cells. They are devoid of DNA, a protein translation machinery or a respiratory chain. They oxidise a wide variety of cellular substrates coupled with reduction of O_2 to H_2O_2, which is degraded by catalase, and in so doing protect the cell against oxidative stress and the accumulation of toxic lipid derivatives, such as bile acid intermediates. Peroxisomes fulfil a number of essential cellular functions, including β-oxidation of fatty acids, α-oxidation of phytanic acid, biosynthesis of lipids such as plasmalogens, bile acids and cholesterol, and metabolism of reactive oxygen species (ROS) and amino acids. There is growing evidence to suggest that mitochondria and peroxisomes exhibit a close inter-relationship that includes metabolic co-operations and cross-talk, a novel putative mitochondria-to-peroxisome vesicular trafficking pathway, and an overlap

in key components of their fission machinery (Camões *et al.*, 2009). It seems therefore that alterations in peroxisomal metabolism, biogenesis and dynamics may influence mitochondrial morphology and function, and *vice versa*.

Manipulation of peroxisomal metabolism has effects on mitochondrial function and *vice versa*, supporting the existence of a close functional relationship between the two organelles. It has been shown that elevating peroxisomal catalase levels in late-passage human fibroblasts restores $\Delta\psi_m$ (Koepke *et al.*, 2007) whereas inhibition of peroxisomal catalase activity in early-passage human fibroblasts has the opposite effect, reducing $\Delta\psi_m$ and increasing mitochondrial ROS production, indicative of age-related mitochondrial dysfunction (Koepke *et al.*, 2008).

Peroxisomes and mitochondria co-operate in fatty acid β-oxidation: saturated unbranched very-long-chain fatty acids (VLCFAs; $C_{>22:0}$) and certain branched-chain fatty acids are chain-shortened in peroxisomes then the resulting long-chain fatty acids (LCFAs; $C_{>12:0}$) are oxidised to completion in mitochondria. There appears to be a relationship between VLCFA β-oxidation in peroxisomes and LCFA β-oxidation in mitochondria, suggesting that metabolic cross-talk exists between the two organelles (McGuinness *et al.*, 2003). Mutations in genes involved in mitochondrial LCFA β-oxidation, such as carnitine palmitoyltransferase 1 (CPT1), involved in the import of LCFAs, or mitochondrial long-chain fatty acyl-CoA dehydrogenase (LCAD), involved in the β-oxidation pathway itself, significantly reduce peroxisomal VLCFA β-oxidation in human fibroblasts (McGuinness *et al.*, 2003). Conversely, drugs that induce mitochondrial LCFA β-oxidation, such as 4-phenylbutyrate (4PBA), increase peroxisomal VLCFA β-oxidation and correct VLCFA levels in fibroblasts from patients with X-linked adrenoleukodystrophy (X-ALD) and mouse models of this disease (Kemp *et al.*, 1998; McGuinness *et al.*, 2001, 2003).

X-ALD is a peroxisomal disorder characterised by elevated levels of VLCFAs in plasma and tissues, particularly in the brain white matter and the adrenal cortex (Aubourg, 2007). The

primary genetic defect occurs in the *ABCD1* gene that encodes adrenoleukodystrophy protein (ALDP), a member of the ABC transporter superfamily situated in the peroxisomal membrane, although its function is unknown (Mosser *et al.*, 1993, 1994). Several studies have shown that there is only partially reduced peroxisomal VLCFA β-oxidation activity in human and mouse X-ALD fibroblasts, demonstrating that ALDP is not necessary for VLCFA β-oxidation (Forss-Petter *et al.*, 1997; Kobayashi *et al.*, 1997; Lu *et al.*, 1997; McGuinness *et al.*, 2003). It is thought that ALDP facilitates the metabolic interaction between mitochondria and peroxisomes, perhaps by transporting VLCFAs and/or LCFAs across the peroxisomal membrane, although the nature of this interaction remains unclear. The absence of ALDP and the disruption of this interaction in X-ALD may result in mitochondrial dysfunction, with reduced peroxisomal VLCFA β-oxidation and elevated VLCFAs levels as a secondary effect, or *vice versa*. Interestingly, ultrastructural abnormalities were observed in mitochondria of adrenocortical cells from X-ALD mice and 4PBA treatment of these mice reduced these abnormalities, as well as increasing mitochondrial LCFA β-oxidation and correcting VLCFA levels (McGuinness *et al.*, 2003). This demonstrates that peroxisomes can influence mitochondrial morphology as well as function and clearly implicates mitochondria in the pathogenesis of peroxisomal disorders.

Ultrastructural and functional changes in mitochondria have also been observed in patients with other peroxisomal disorders and in mouse models of these diseases. Two classes of peroxisomal disorders have been described: single peroxisomal enzyme deficiencies (PEDs), typified by X-ALD, and peroxisomal biogenesis disorders (PBDs) caused by mutations in *PEX* genes, which encode proteins called peroxins that are involved in the biogenesis of peroxisomes (Camões *et al.*, 2009). The most severe PBD is the cerebro-hepato-renal syndrome known as Zellweger syndrome, resulting in death within 1 year of age. In human Zellweger patients and in *Pex5*$^{-/-}$ mice, severe alterations in mitochondrial ultrastructure and in the expression, distribution and activities of the respiratory chain complexes have been

observed in peroxisome-rich tissues, the liver being the organ most severely affected (Baumgart *et al.*, 2001; Dirkx *et al.*, 2005; Goldfischer *et al.*, 1973).

In the original report on Zellweger syndrome (Goldfischer *et al.*, 1973), mitochondrial abnormalities consisted of irregular and twisted cristae and dilatation of the intracristate space. In several subsequent studies on Zellweger patients, mitochondrial alterations of varying types and severity were reported and in a few cases no alterations were observed (Aubourg *et al.*, 1985; Lazarow *et al.*, 1985). However, in *Pex5*$^{-/-}$ mice, ultrastructural alterations affect every subcompartment of the mitochondria (the OM, the IM and the cristae) and are extremely heterogeneous, both within and between cells of the same tissue as well as between different tissues and organs (Baumgart *et al.*, 2001).

In tissues of *Pex5*$^{-/-}$ mice, large aggregates of pleomorphic mitochondria were observed, together with swollen mitochondria, in which there was very little internal structure, and "megamitochondria", in which the matrix was densely packed with cristae (Baumgart *et al.*, 2001). Indeed, many mitochondria showed rarefaction of cristae, circularisation of cristae, and arrangement of cristae into parallel stacks. The most significant biochemical abnormality was a marked reduction in the activity of complex I, reduced by more than 50 % in hepatocytes (Baumgart *et al.*, 2001). In a mouse model with hepatocyte-selective elimination of peroxisomes, in addition to ultrastructural abnormalities of mitochondria like those described above and a severe reduction in the activity of complex I, the activity of citrate synthase was increased 2- to 3-fold (Dirkx *et al.*, 2005). These observations indicate the existence of complex and widespread mitochondrial dysfunction in the absence of functional peroxisomes.

There are several theories to explain abnormalities of mitochondria associated with the absence of functional peroxisomes. The abnormalities are suggestive of oxidative stress caused by increased ROS production. Indeed, similar ultrastructural alterations in mitochondria have been

described in other diseases associated with oxidative stress, such as Reye's syndrome (Iancu *et al.*, 1977). An alternative theory is that toxic lipid derivatives normally degraded by peroxisomal β-oxidation, such as bile acid intermediates, accumulate in mitochondria and bring about changes in their ultrastructure. Lipidic inclusions associated with ultrastructural alterations have been found in skeletal muscle mitochondria in patients with Zellweger syndrome (Sarnat *et al.*, 1983) and in mitochondria of patients with adrenomyeloneuropathy (AMN), the adult form of X-ALD (Powers *et al.*, 2001). However, regardless of the nature of the metabolic connection between mitochondria and peroxisomes, it is clear that the absence of functional peroxisomes can have marked effects on mitochondrial ultrastructure and function.

There may even be a direct morphological connection between mitochondria and peroxisomes, since a novel DRP1-independent vesicular transport pathway from mitochondria to peroxisomes has very recently been described (Neuspiel *et al.*, 2008). In searching for proteins involved in the regulation of mitochondrial morphology, Neuspiel *et al.* (2008) identified a new OM protein, mitochondria-anchored protein ligase (MAPL), containing a novel RING-finger domain. Overexpression of MAPL in HeLa or COS7 cells resulted in DRP1-dependent mitochondrial fragmentation and required the intact RING-finger domain. Interestingly, however, confocal microscopy of cells expressing fluorescently-labelled MAPL and DRP1^{K38A} highlighted the existence of a pool of MAPL-positive vesicular structures within the otherwise highly interconnected mitochondrial reticulum. Further confocal and electron microscopy analysis of these vesicles revealed that they are 70-100 nm in diameter, emanate from the sides of mitochondria in a DRP1-independent manner, and are enriched with either MAPL or another OM marker, translocase of outer membrane 20 kDa subunit (TOM20).

The dynamics of these mitochondria-derived vesicles (MDVs) were studied using time-lapse confocal microscopy. Enrichment of MAPL along tubular mitochondria was observed before this region was seen to pinch off from the side of the organelle, liberating a spherical vesicle. MAPL-

positive MDVs were seen to fuse with a small subset of peroxisomes, representing a novel vesicular transport pathway from mitochondria to peroxisomes. TOM20-positive MDVs did not fuse with peroxisomes, however, and their fate is unknown. They may contribute to the removal of damaged, misfolded, or mistargeted proteins from mitochondria, and transport them to the lysosomes for degradation. Conversely, MAPL-positive MDVs may function in the transport of metabolites, lipids or proteins from mitochondria to a subpopulation of peroxisomes or they may be involved in the retrieval of peroxisomal membrane proteins that have been mistargeted to mitochondria (Schrader and Fahimi 2008). A reciprocal vesicular transport pathway (from peroxisomes to mitochondria) has not been identified but remains a possibility.

Mitochondria and peroxisomes also share key components of their fission machinery, namely Drp1 and Fis1 (Schrader, 2006). Growth and division of peroxisomes in mammalian cells is a multistep process including (i) elongation, mediated by Pex11βp, (ii) constriction, by an as yet unknown mechanism, and (iii) final scission, mediated by Drp1 and Fis1 (Kobayashi *et al.*, 2007; Koch *et al.*, 2003, 2004, 2005; Li and Gould, 2003; Schrader *et al.*, 1998). Although the mechanism of peroxisomal constriction is currently unknown, a novel mitochondrial and peroxisomal fission protein, mitochondrial fission factor (Mff), has recently been identified, which may play a role in this process (Gandre-Babbe and van der Bliek, 2008). Mff is anchored in the OM and in the peroxisomal membrane via a C-terminal TM domain, with the bulk of the molecule exposed to the cytosol. Loss of Mff function inhibits mitochondrial and peroxisomal fission, and results in elongation of both organelles, in a way that is indistinguishable from the effects of loss of function of Drp1 or Fis1. However, Mff exists in a complex different from the one containing Fis1. It is therefore plausible that Mff functions as a novel adaptor protein to assemble a protein complex involved in constriction of the organelle membranes prior to final scission (Gandre-Babbe and van der Bliek, 2008).

1.2.7 Localisation of nuclear mRNAs encoding mitochondrial proteins to the mitochondrial outer membrane: a putative role for AKAP149

Localisation of mRNAs to specific subcellular regions is an important mechanism of regulation of post-transcriptional gene expression in higher eukaryotes, particularly in the context of organelle biosynthesis because the majority of proteins destined for organelles, including mitochondria, are encoded in nuclear genes (Corral-Debrinski, 2007). In *S. cerevisiae*, subcellular fractionation and whole-genome oligonucleotide array analyses showed that approximately one third of all transcripts coding for mitochondrial proteins preferentially localise to the organelle surface (Sylvestre *et al.*, 2003a). This phenomenon is conserved in human cells and the mitochondrial targeting sequence lies in the 3'UTR of these mRNAs (Russo *et al.*, 2006; Sylvestre *et al.*, 2003b). Rogne *et al.* (2009) recently demonstrated that an OM protein called A kinase-anchoring protein 149 kDa (AKAP149) binds RNA *in vivo* and that this is required for maintenance of normal mitochondrial morphology in human cells. One possible explanation for this is that AKAP149 regulates the expression of nuclear-encoded proteins involved in mitochondrial fission, fusion or transport by localising their mRNAs to the mitochondrial surface.

A kinase-anchoring proteins (AKAPs) are membrane-bound scaffolding molecules localised to different subcellular compartments that mediate the spatial and temporal organisation of protein phosphorylation by cAMP-dependent protein kinase A (PKA) (Beene and Scott, 2007). AKAP149 is encoded by the *AKAP1* gene and is widely expressed in human tissues (Trendelenburg *et al.*, 1996). The alternative splice product of the *AKAP1* gene, S-AKAP84, is a C-terminally truncated form of the protein that is only expressed in the testes (Lin *et al.*, 1995; Trendelenburg *et al.*, 1996). AKAP149 has an N-terminal targeting/TM domain that anchors it in the OM and ER-nuclear envelope compartments, exposing the rest of the molecule to the cytosol (Steen *et al.*, 2000; Trendelenburg *et al.*, 1996). In addition to the canonical PKA-binding

domain, AKAP149 also contains a C-terminal RNA-binding K homology (KH) domain, which is absent from S-AKAP84 (Rogne *et al.*, 2006; Trendelenburg *et al.*, 1996).

Phosphorylation-dependent RNA binding by the KH domain of AKAP149 is required for maintenance of normal mitochondrial morphology. Co-immunoprecipitation experiments using 293T cell lysates showed that AKAP149 binds RNA *in vivo* through a conserved RVXF motif, ^{627}RYVSF^{631}, in its KH domain but only when S630 is phosphorylated (Rogne *et al.*, 2009). It is likely that S630 is phosphorylated by PKA, since ^{627}RYVS^{630} is a consensus PKA phosphorylation site. Expression of RNA-binding-deficient mutants AKAP149^{V629E} and AKAP149^{S630A} in HeLa cells resulted in perinuclear clustering of mitochondria and the formation of large mitochondrial aggregates in 30-50 % of cells (Rogne *et al.*, 2009). This abnormal mitochondrial morphology phenotype is similar to that associated with an imbalance in mitochondrial fission/fusion in favour of fusion or a defect in microtubule-based mitochondrial transport. Only one theory has been put forward to explain these observations.

AKAP149 may regulate the expression of nuclear-encoded proteins involved in mitochondrial fission, fusion or transport by localising their mRNAs to the OM, via an interaction between the KH domain and the 3'UTR of the mRNAs. KH domains are found in proteins associated with mRNA stabilisation, subcellular localisation and translational regulation (Valverde *et al.*, 2008). AKAP121, the mouse homologue of AKAP149 (Chen *et al.*, 1997), binds the 3'UTR of two transcripts encoding mitochondrial proteins, manganese superoxide dismutase (MnSOD) and the Fo-f subunit of mitochondrial ATP synthase, via its KH domain *in vitro* (Ginsberg *et al.*, 2003). Binding of these transcripts to the KH domain depends on the stem-loop secondary structure of the 3'UTR and is stimulated by PKA phosphorylation of the KH domain (Ginsberg *et al.*, 2003). Interestingly, the Fo-f subunit of mitochondrial ATP synthase lacks a typical N-terminal mitochondrial import sequence (Collinson *et al.*, 1994), so binding of the transcript to

AKAP121 on mitochondria may be crucial for targeting of the protein. No mRNA targets of AKAP149 have been identified to date but this is a subject worthy of investigation in the future.

1.3 MITOCHONDRIAL DYNAMICS AND RESPIRATORY CHAIN FUNCTION

A bi-directional relationship exists between mitochondrial morphology and respiratory chain function, although the nature of this relationship remains unclear. Mutations in mitochondrial or nuclear genes encoding subunits of the respiratory complexes, and mutations in mitochondrial tRNA genes, are associated with a wide variety of mitochondrial morphology phenotypes, from fragmented networks with swollen organelles to apparently normal tubular networks. Conversely, mutations in genes encoding components of the mitochondrial fission and fusion machineries can result in large reductions in glucose oxidation, oxygen consumption, ATP synthesis and $\Delta\psi_m$, and deficiencies in the activities of one or more of the respiratory complexes, or have no detectable effect on any bioenergetic parameter. The reason for these discrepancies is unknown.

1.3.1 Secondary effects on mitochondrial morphology resulting from genetic defects in oxidative phosphorylation

Skin fibroblasts from patients with severe defects in OXPHOS, as a result of mutations in mitochondrial or nuclear genes encoding subunits of the respiratory complexes, exhibit mild alterations in $\Delta\psi_m$ and apparently normal mitochondrial morphology under basal culture conditions (Guilllery *et al.*, 2008a; Morán *et al.*, 2010). In each case, mitochondria fragment upon treatment with CCCP and recover their tubular morphology after removal of the drug, indicating that they are capable of normal fission and fusion, although small alterations in fission and/or fusion rate were observed in the cells of some patients. These findings differ from previous reports describing a high proportion of fragmented and/or swollen mitochondria in cells

from patients with other well-defined OXPHOS defects (Bernard *et al.*, 2007; Koopman *et al.*, 2007; Pham *et al.*, 2004). In short, there appears to be no obvious relationship between mitochondrial morphology and OXPHOS function. It is likely that the nature of the genetic defect, the severity of the metabolic deficit, and the genetic background in each patient all play a role in determining the phenotype.

The mitochondrial morphology phenotypes associated with complex I deficiency are particularly heterogeneous. Mutations in genes encoding different subunits, and even mutations in the same gene, have been reported to have opposite effects on mitochondrial length and branching. In particular, different mutations in the nuclear gene *NDUFS4*, encoding an accessory subunit of complex I, have been associated with an increase in mitochondrial length and branching, a decrease in mitochondrial length and branching, or normal mitochondrial morphology (Koopman *et al.*, 2007; Willems *et al.*, 2009). There seems to be no correlation between mitochondrial morphology and the affected complex I subunit. However, there does seem to be a linear correlation between complex I activity and the morphological complexity of mitochondria, with lower complex I activity associated with more fragmented mitochondria (Koopman *et al.*, 2007; Willems *et al.*, 2009).

A large reduction in cellular ATP levels has been observed in patient fibroblasts with severe OXPHOS defects but only mild perturbations in $\Delta\psi_m$ and normal mitochondrial morphology (Guillery *et al.*, 2008a; Morán *et al.*, 2010). For this reason, and due to the differing effects of CCCP and deoxyglucose on mitochondrial morphology in control cells and OXPHOS-deficient cells, it is thought that it is $\Delta\psi_m$ rather than OXPHOS that is tightly linked with mitochondrial morphology. Treatment with CCCP dissipates $\Delta\psi_m$ and results in extensive mitochondrial fragmentation in all cells, regardless of the presence of defects in OXPHOS (Guillery *et al.*, 2008a; Morán *et al.*, 2010). Treatment with deoxyglucose, which inhibits glycolysis and thus forces cells to rely on OXPHOS for ATP synthesis, has no effect on mitochondrial morphology in

control cells but results in extensive mitochondrial fragmentation in OXPHOS-deficient cells (Guillery *et al.*, 2008a). It has been hypothesised that glycolysis-derived ATP powers the reverse operation of ATP synthase to maintain $\Delta\psi_m$ in OXPHOS-deficient cells and that this is responsible for maintenance of normal mitochondrial morphology (Morán *et al.*, 2010). In cells with severe metabolic dysfunction, glycolysis-derived ATP may not be sufficient to maintain $\Delta\psi_m$, and this may account for the mitochondrial fragmentation observed in some patients with OXPHOS defects.

The link between metabolic dysfunction and modulation of mitochondrial morphology may be $\Delta\psi_m$-sensitive proteolytic processing of OPA1. In HeLa cells and fibroblasts, CCCP-induced loss of $\Delta\psi_m$ results in rapid and complete processing of L-OPA1 to S-OPA1 and concomitant fragmentation of mitochondria (Duvezin-Caubet *et al.*, 2006; Guillery *et al.*, 2008b). CCCP-induced OPA1 processing is inhibited by the metalloprotease inhibitor *o*-phenanthroline and recovery of L-OPA1 levels after CCCP treatment is inhibited by cycloheximide, suggesting that OPA1 processing involves irreversible proteolytic cleavage of L-OPA1 (Duvezin-Caubet *et al.*, 2006; Guillery *et al.*, 2008b). CCCP-induced mitochondrial fragmentation is prevented by overexpression of OPA1, which slows down OPA1 processing, or overexpression of $DRP1^{K38E}$, which has no effect on OPA1 processing but inhibits mitochondrial fission (Duvezin-Caubet *et al.*, 2006). Taken together, these observations suggest that severe metabolic dysfunction may result in loss of $\Delta\psi_m$, which in turn results in proteolytic processing of L-OPA1 to S-OPA1, inhibition of OPA1-mediated mitochondrial fusion and concomitant mitochondrial fragmentation due to ongoing mitochondrial fission.

Generalised defects in mitochondrial protein synthesis, due to point mutations in mitochondrial tRNA genes, result in deficiencies in the activities of the OXPHOS complexes and severe abnormalities in mitochondrial morphology, but only when the percentage of mutant mtDNA exceeds a certain threshold in cells of affected tissues (Chomyn *et al.*, 1992; Hayashi *et al.*,

1994). In order to assess the pathogenicity of different mitochondrial tRNA mutations, mutant mtDNA from patient fibroblasts was transferred to ρ0 HeLa cells with a normal nuclear genetic background. This was achieved by enucleation of patient fibroblasts and PEG-mediated fusion of those cells with ρ0 HeLa cells to make “cybrid cells”. In cybrid clones containing >95 % mtDNA with either the m.3243A>G mutation in the $tRNA^{Leu(UUR)}$ gene or the m.4269A>G mutation in the $tRNA^{Ile}$ gene, translation of all 13 mtDNA-encoded proteins was dramatically reduced, the activities of complexes I and IV were dramatically reduced, and the mitochondria had completely lost their tubular morphology and instead consisted of clusters of large, swollen organelles. In cybrid clones with <95 % mutant mtDNA, no defects were observed, indicating a threshold effect (Chomyn *et al.*, 1992; Hayashi *et al.*, 1994). However, in patients with the m.3243A>G mutation, the percentage of mutant mtDNA differs vastly amongst different tissues, with the majority of tissues containing 60-90 % mutant mtDNA, suggesting that a lower threshold may exist *in vivo* (Finsterer, 2007).

Severe abnormalities in mitochondrial morphology have also been associated with deficiency of heat shock protein 60 kDa (HSP60), a mitochondrial chaperone which is required for the correct folding of multiple mitochondrial proteins, including key metabolic enzymes. Skin fibroblasts from two patients with partial HSP60 deficiency, in which levels of the protein were 60-80 % reduced relative to those of control cells, showed multiple mitochondrial enzyme deficiencies and severe abnormalities in mitochondrial morphology (Agsteribbe *et al.*, 1993; Briones *et al.*, 1997; Huckriede and Agsteribbe, 1994; Huckriede *et al.*, 1995). The mitochondrial network was sparse and fragmented at regular intervals into short tubules, with many large, swollen organelles clustered around the nucleus. Electron microscopy showed disorganisation and rarefaction of cristae and even arrangement of cristae into concentric rings. Sequence variants found in the promoter, coding region and intron/exon boundaries of the nuclear gene *HSPD1*, which encodes HSP60, were not responsible for the disease phenotype in either patient and the primary genetic defect was never identified (Bross *et al.*, 2007). Deficiency of HSP60 may be a

secondary effect of a defect in another process, for example, a defect in mitochondrial protein import or mitochondrial dynamics.

1.3.2 Secondary effects on mitochondrial metabolism resulting from genetic defects in mitochondrial dynamics

A relatively small number of studies have investigated the metabolic consequences of genetic defects in components of the mitochondrial fission and fusion machineries, namely Drp1, Mfn1, Mfn2 and OPA1, in mammalian cells.

Drp1 deficiency results in extensive mitochondrial tubulation in all cell types analysed but this is not always accompanied by defects in OXPHOS. RNAi knockdown of DRP1 in HeLa cells resulted in a significant reduction in basal respiration rate and a large reduction in the rate of ATP synthesis; DRP1-deficient cells grew slowly in glucose medium and died after 3 days in galactose medium, indicating severe defects in OXPHOS (Bernard *et al.*, 2007). In contrast, fibroblasts from a patient with a pathogenic point mutation in DRP1, A395D, showed no defects in OXPHOS despite a similar mitochondrial morphology phenotype (Waterham *et al.*, 2007).

Deficiency of either mitofusin in MEFs results in fragmentation of mitochondria but seems to have little or no effect on mitochondrial metabolism. In contrast, fibroblasts from patients with pathogenic point mutations in MFN2 have normal mitochondrial morphology and metabolic defects in some cases. Fragmented mitochondria in *Mfn1*$^{-/-}$ MEFs and *Mfn2*$^{-/-}$ MEFs did not show any significant abnormalities in respiration rate, $\Delta\psi_m$ or mtDNA copy number (Chen *et al.*, 2003, 2005). Fibroblasts from patients with pathogenic point mutations in MFN2 showed no abnormalities in mitochondrial morphology, mtDNA content or the activities of the OXPHOS complexes, although M21V, A166T and R364Q mutants showed low $\Delta\psi_m$ and low coupling efficiency (Amiott *et al.*, 2008; Loiseau *et al.*, 2007).

Mfn2 plays a role in the regulation of mitochondrial metabolism, separate from its role in mitochondrial fusion, via upregulating the expression of a subset of nuclear genes encoding subunits of the respiratory complexes. RNAi knockdown of Mfn2 in L6E9 myotubes resulted in a marked reduction in $\Delta\psi_m$, a reduction in oxygen consumption and in the oxidation of glucose, pyruvate and fatty acids, and an increase in lactate production (Bach *et al.*, 2003; Pich *et al.*, 2005). This was associated with a marked repression in the expression of nuclear genes encoding selected subunits of complexes I, II, III and V and a measurable reduction in the activities of complexes I, II and III (Pich *et al.*, 2005). Conversely, overexpression of Mfn2 in L6E9 myoblasts was associated with increased expression of several subunits of complexes I, IV and V and overexpression of Mfn2 in HeLa cells resulted in a marked enhancement of $\Delta\psi_m$ and increased glucose oxidation (Pich *et al.*, 2005). Overexpression of MFN2Δ602-757, a C-terminally truncated form of the protein that lacks the ability to mediate mitochondrial fusion, also resulted in enhanced $\Delta\psi_m$ and glucose oxidation in HeLa cells (Pich *et al.*, 2005), suggesting that the stimulatory effects of Mfn2 on mitochondrial metabolism are independent of its mitochondrial fusion activity. It remains to be determined whether Mfn2-mediated regulation of OXPHOS subunit expression exists in all mammalian cells.

Loss of OPA1 results in severe abnormalities in mitochondrial morphology and OXPHOS, whereas pathogenic point mutations in OPA1 have varying effects on metabolism in a way which does not seem to relate to their effects on mitochondrial morphology. RNAi knockdown of OPA1 in MEFs and HeLa cells results in complete fragmentation of mitochondria and dissipation of $\Delta\psi_m$ and in MEFs this is associated with slow growth rates and a dramatic reduction in basal and maximal (uncoupled) respiration rates, indicative of a severe metabolic defect (Chen *et al.*, 2005; Olichon *et al.*, 2003). Pathogenic point mutations in OPA1, which induce fragmentation of mitochondria to varying degrees, have previously been reported to reduce ATP synthesis or have no effect on mitochondrial metabolism whatsoever in patient fibroblasts (Mayorov *et al.*, 2008; Spinazzi *et al.*, 2008; Zanna *et al.*, 2008), although a recent

study of skeletal muscle biopsies from patients with mutant OPA1 reported deficiency of complex IV activity associated with multiple deletions in mtDNA (Yu-Wai-Man *et al.*, 2010).

1.4 MITOCHONDRIAL DYNAMICS IN DISEASE

Several diseases have already been characterised as resulting from mutations in nuclear genes encoding proteins involved in mitochondrial fission, fusion or transport.

1.4.1 Mutations in *MFN2* cause Charcot-Marie-Tooth disease type 2A

Mutations in the *MFN2* gene cause Charcot-Marie-Tooth disease type 2A (CMT2A), a peripheral neuropathy characterised by abnormal transport of mitochondria in axons of the longest sensory and motor neurons (Baloh *et al.*, 2007; Cartoni and Martinou, 2009; Detmer *et al.*, 2008; Misko *et al.*, 2010; Züchner *et al.*, 2004). The disease has an autosomal dominant pattern of inheritance. Onset occurs in infancy to the sixth decade of life, but usually in the first or second decade of life. Symptoms include progressive muscle wasting, foot drop/structural foot deformities, loss of manual dexterity, sensory loss and hearing impairment. Some severe cases also include optic atrophy (Chung *et al.*, 2006; Züchner *et al.*, 2006). Approximately 60 different pathogenic *MFN2* mutations have been found to date but the molecular mechanism underlying pathogenesis remains unclear (Cartoni and Martinou, 2009).

The cellular phenotype of CMT2A was characterised by studying mitochondrial morphology and transport in dorsal root ganglion (DRG) neurons from *Mfn2*$^{-/-}$ mice and in cultured mouse and rat DRG neurons expressing Mfn2 with different CMT2A mutations (Baloh *et al.*, 2007; Detmer *et al.*, 2008; Misko *et al.*, 2010). The cellular phenotype was identical in every case. Neuronal cell bodies showed perinuclear aggregation of mitochondria, with large areas lacking mitochondria altogether. Axons also showed aggregation of mitochondria, with uneven

clustering of mitochondria along their length. Time-lapse confocal imaging and kymograph analysis showed that axonal mitochondria spent more time paused and travelled at slower velocities in both the anterograde and retrograde directions. These transport defects were specific to mitochondria and occurred in the presence of normal OXPHOS, ATP levels and $\Delta\psi_m$. Mutant Mfn2 proteins showed normal expression levels, stability, GTP-binding and mitochondrial localisation, suggesting that pathogenicity is due to a dominant negative or toxic gain-of-function effect. Overexpression of wild-type Mfn1 or Mfn2 completely corrected the mitochondrial morphology and transport defects. However, Mfn2 is expressed at higher levels than Mfn1 in neurons, so it is likely that levels of endogenous Mfn1 are not sufficient to compensate for loss of Mfn2 in these cells *in vivo*.

Several theories have been put forward to explain the pathogenesis of CMT2A. Some *MFN2* mutations abolish the mitochondrial fusion activity of the protein, resulting in mitochondrial fragmentation (Baloh *et al.*, 2007; Detmer and Chan, 2007), but it is unclear how this could cause defects in mitochondrial transport, since it is assumed that smaller mitochondria are easier to transport. Overexpression of some CMT2A mutants results in aggregation of mitochondria (Detmer and Chan, 2007; Detmer *et al.*, 2008), which could impede mitochondrial transport, although no aggregation is seen when these mutants are expressed at physiological levels. The most common pathogenic mutation in MFN2, R94Q, is located just downstream of the p21-Ras-binding domain and abolishes the ability of MFN2 to regulate ER morphology and ER-mitochondria tethering (de Brito and Scorrano, 2008). Uncoupling of mitochondria from the ER perturbs Ca^{2+} homeostasis and may affect Ca^{2+}-dependent binding of Miro proteins to the microtubule-based transport apparatus (Saotome *et al.*, 2008).

However, some CMT2A MFN2 mutants are fully competent for fusion even in the absence of MFN1, do not induce mitochondrial aggregation even when expressed at high levels, and do not affect ER morphology or ER-mitochondria tethering, yet result in identical defects in

mitochondrial transport when expressed in mouse DRG neurons (Baloh *et al.*, 2007). This suggests that there is an alternative explanation for how mutations in *MFN2* result in mitochondrial transport defects in neurons. The recent study by Misko *et al.* (2010) may provide the answer: MFN2 interacts directly with the microtubule-based mitochondrial transport machinery and is essential for the regulation of mitochondrial transport, independent of its role in mitochondrial fusion, as described in Section 1.2.2.1.

1.4.2 Mutations in *GDAP1* cause Charcot-Marie-Tooth disease type 4A

Mutations in the ganglioside-induced differentiation-associated protein 1 (*GDAP1*) gene cause Charcot-Marie-Tooth disease type 4A (CMT4A), a severe form of peripheral neuropathy associated with demyelinating, axonal or intermediate phenotypes (Baxter *et al.*, 2002; Claramunt *et al.*, 2005; Cuesta *et al.*, 2002; Senderek *et al.*, 2003). Both autosomal recessive and autosomal dominant traits have been reported. Onset occurs in infancy to early childhood. Symptoms include progressive muscle weakness, foot and hand wasting, vocal cord paresis, sensory loss, and disability within the first or second decade of life, leading to wheelchair use. *GDAP1* is widely expressed in the large neurons that constitute the grey matter of the CNS, although CMT4A only affects neurons with peripheral myelinated fibres (Pedrola *et al.*, 2008). The function of GDAP1 and the molecular mechanism underlying the pathogenesis of CMT4A remain unclear.

GDAP1 is located in the OM and is thought to be involved in mitochondrial fission (Niemann *et al.*, 2005). Overexpression of the wild-type protein in COS7 cells resulted in mitochondrial fragmentation, which was inhibited by co-expression with MFN1, MFN2 or DRP^{K38A} and was not associated with apoptosis or collapse of $\Delta\psi_m$. Conversely, RNAi knockdown of *GDAP1* in neuroblastoma cells, which endogenously express *GDAP1*, resulted in an increase in mitochondrial tubulation (Niemann *et al.*, 2005). PEG-mediated cell fusion experiments showed

that HeLa cells overexpressing *GDAP1* are competent for mitochondrial fusion, suggesting that the effects of GDAP1 on mitochondrial morphology are due to promotion of mitochondrial fission rather than inhibition of mitochondrial fusion (Niemann *et al.*, 2005).

The effects of pathogenic *GDAP1* mutations on mitochondrial morphology have been studied in COS7 cells (Niemann *et al.*, 2005; Pedrola *et al.*, 2008). Pathogenic nonsense mutations resulted in C-terminally truncated proteins that had lost their mitochondrial targeting and were unable to induce mitochondrial fragmentation. Most pathogenic missense mutations resulted in proteins that correctly localised to mitochondria and induced mitochondrial fragmentation to varying degrees, although there was some controversy as to whether their ability to promote mitochondrial fission was reduced relative to that of the wild-type protein. One pathogenic missense mutation, T157P, resulted in perinuclear aggregation of mitochondria, suggesting a dominant negative effect on fission. Based on these observations, it seems likely that an imbalance in mitochondrial fission/fusion in the large neurons of the CNS underlies the pathogenesis of CMT4A, but how this results in neuropathy and why only a subset of these neurons are affected remains a mystery.

1.4.3 Mutations in *DNM1L* result in a combined defect in mitochondrial and peroxisomal fission

DRP1 is encoded by the dynamin 1-like (*DNM1L*) gene in humans. DRP1 deficiency results in a combined defect in mitochondrial and peroxisomal fission. Only one case has been reported to date (Waterham *et al.*, 2007). A newborn girl presented with microcephaly, abnormal brain development, optic atrophy and hypoplasia, with persistent lactic acidemia and mildly elevated plasma concentration of VLCFAs. She died suddenly at age 37 days. Biochemical investigations of skin fibroblasts and skeletal muscle biopsies revealed no abnormalities in mitochondrial OXPHOS or peroxisomal β-oxidation. Patient fibroblasts showed very elongated tangled

mitochondrial tubules concentrated predominantly around the nucleus and fewer peroxisomes that were also abnormally arranged in rows. The child was found to be heterozygous for a *de novo* mutation, A395D, in the middle domain of DRP1, which had dominant negative effects on DRP1 function.

1.4.4 Mutations in *OPA1* cause autosomal dominant optic atrophy

Mutations in the *OPA1* gene cause autosomal dominant optic atrophy (ADOA), an hereditary optic neuropathy affecting the retinal ganglion cells and axons that form the optic nerve (Alexander *et al.*, 2000; Amati-Bonneau *et al.*, 2009; Delettre *et al.*, 2000). Onset occurs in the first two decades of life. Symptoms of the disease include progressive vision loss, scotomas, impaired colour vision and temporal pallor/excavation of the optic disc. However, the disease is associated with a very broad spectrum of clinical phenotypes. More than 200 different pathogenic mutations have been identified to date, distributed throughout the entire gene, as shown in the eOPA1 online database (http://lbbma.univ-angers.fr/eOPA1/). The pathogenesis of the disease remains unclear, and seems to vary from case to case, but mtDNA instability and reduced OXPHOS associated with mitochondrial fusion defects are common features.

1.5 THE PROJECT

Mitochondrial encephalopathies are a clinically, biochemically and genetically heterogeneous group of disorders (Tucker *et al.*, 2010). Mitochondrial defects can be restricted to certain organs/tissues, usually brain, heart and skeletal muscle, or can be systemic. Clinical symptoms can include seizures, ataxia, myopathy, cognitive impairment, blindness and stroke. Pathogenic mutations have been found in more than 100 genes, including nuclear and mitochondrial genes encoding OXPHOS subunits or assembly factors, mitochondrial tRNA genes, nuclear genes encoding proteins involved in mtDNA maintenance, and nuclear genes encoding proteins

involved in mitochondrial protein import and folding. Single or combined deficiencies in enzymes of pyruvate metabolism, the citric acid cycle and OXPHOS have been observed.

In those cases where multiple enzymes are affected, including those encoded by both mtDNA and nuclear DNA, it is very difficult to identify the primary genetic defect and less than 50 % of all patients receive a molecular diagnosis. Genetic defects in mitochondrial dynamics result in metabolic deficits in cultured mammalian cells and neurological and/or metabolic disease in humans and model organisms, as discussed in Sections 1.3 and 1.4 respectively. It is therefore possible that, in at least some patients with undiagnosed mitochondrial encephalopathy, the primary defect lies in a gene controlling mitochondrial dynamics.

1.5.1 Introduction to patients studied in the project

The project was based around four patients with undiagnosed early-onset mitochondrial disease. Key common symptoms were lactic acidosis and acute encephalopathy. In each case, skin fibroblasts showed deficiencies in the activities of multiple mitochondrial enzymes and severe abnormalities in mitochondrial morphology.

1.5.2 Hypothesis

It was proposed that the clinical symptoms in each patient were the result of the generalised mitochondrial dysfunction, which in turn was the result of a defect in mitochondrial dynamics.

1.5.3 Aim

The aim of the project was first to characterise fully the cellular phenotype in each patient, including the activities and distributions of key mitochondrial enzymes, mitochondrial

morphology, $\Delta\psi_m$, and the amount and distribution of mtDNA, and second to identify the nuclear gene(s) responsible for the abnormal mitochondrial morphology.

CHAPTER 2: MATERIALS AND METHODS

2.1 CLINICAL PRESENTATIONS OF THE PATIENTS

Patient 1 (P1) was male and presented with early-onset lactic acidosis, renal anomalies, hypertrophic cardiomyopathy and hypotonia. This was accompanied by developmental delay and visual and hearing impairment. A brain MRI scan was abnormal. Information regarding parental consanguinity was not available.

Patient 2 (P2) was female and presented with early-onset lactic acidosis and hyperammonaemia. A brain MRI scan showed periventricular cysts. She was born to consanguineous parents and her sibling died aged 2 days of a possible cerebral haemorrhage.

Patient 3 (P3) was male. He was healthy at birth but presented at 4 months of age with failure to thrive, vomiting, hypotonia and respiratory abnormalities. He died at age 15 months. Levels of lactate in blood and cerebrospinal fluid (CSF) were raised (4 and 3.8 mmol/L respectively). A brain MRI scan did not show any intracerebral lesions and post-mortem neuropathology was not performed. There was no family history of consanguinity.

Patient 4 (P4) was male. He presented with early onset lactic acidosis and abnormal fatty acid oxidation. Information regarding the results of a brain MRI scan was not available. Parents were consanguineous.

2.2 TISSUE CULTURE

2.2.1 Media and reagents

All media and reagents for cell culture were from Sigma-Aldrich, unless otherwise stated.

2.2.1.1 Culture medium

Cells were cultured in Dulbecco's Modified Eagle's Medium/Nutrient Mixture F-12 Ham (DMEM/F-12 Ham) with 15 mM HEPES, pyridoxine and $NaHCO_3$, supplemented with 10 % v/v HyClone fetal bovine serum (FBS; Perbio), 2.5 mM L-glutamine, 100 U/ml penicillin and 100 µg/ml streptomycin.

2.2.1.2 Dulbecco's Phosphate Buffered Saline

Dulbecco's Phosphate Buffered Saline (PBS) did not contain $CaCl_2$, $MgCl_2$ or phenol red.

2.2.1.3 Trypsin-EDTA solution

Trypsin-EDTA solution contained 0.05 % w/v porcine trypsin and 0.02 % w/v EDTA in Hank's Balanced Salt Solution (HBSS) with phenol red.

2.2.1.4 Hoechst 33258 staining

Hoechst 33258 was dissolved in dH_2O to make 10 µg/ml and 1 µg/ml stock solutions, which were filter-sterilised and stored at -20°C. For staining, a solution of 0.05 µg/ml Hoechst 33258 in Hank's buffer pH 7.0 was made immediately before use.

Two buffers were used in Hoechst 33258 staining: Hank's buffer pH 7.0 and M^{c}Ilvaine buffer pH 5.5. Hank's buffer pH 7.0 contained 80 g/L NaCl, 4 g/L KCl, 1.4 g/L $CaCl_2$•$2H_2O$, 2 g/L $MgSO_4$•$7H_2O$, 0.5 g/L Na_2HPO_4 (anhydrous), 0.6 g/L KH_2PO_4 (anhydrous) and 10 g/L glucose. M^{c}Ilvaine buffer pH 5.5 contained 8.3 g/L citric acid and 16 g/L Na_2HPO_4 (anhydrous). Both buffers were stored at -20°C.

2.2.1.5 Emetine

Emetine dihydrochloride hydrate was dissolved in absolute ethanol to give a 10 mg/ml stock solution, which was stored at 4°C.

2.2.2 Culture of human skin fibroblasts

Primary fibroblast cultures established from patient skin biopsies at referring hospitals were used for biochemical and genetic analyses.

2.2.2.1 Culture conditions

Fibroblasts were cultured at 37°C in a humidified incubator with 5 % v/v CO_2 in air. Table 2.1 shows the volume of culture medium used in culture vessels of different sizes. Medium changes were carried out every 3-4 days. Cultures were maintained at less than 80 % confluence. Fibroblast cultures from patients under study were grown alongside those from a control (C1). Fibroblasts from P1 and P2 grew at a similar rate to those from C1 and did not require additional care. Fibroblasts from P3 grew very slowly relative to those from C1 and were therefore cultured in medium supplemented with 10 % v/v AmnioMAX^{TM} II Complete Medium (Invitrogen). Fibroblasts from P4 grew very quickly relative to those from C1 and turned the medium acidic; these cultures were given fresh medium every 1-2 days and were subcultured every 3 days.

Size of culture vessel	Volume of medium (for culture)	Volume of PBS (for rinsing)	Volume of Trypsin-EDTA solution (for rinsing)	Volume of Trypsin-EDTA solution (for trypsinisation)
80 cm^2 flask	15 ml	7 ml	1-2 ml	1 ml
25 cm^2 flask	7 ml	2 ml	0.5 ml	0.5 ml
35 mm diameter Petri dish	2 ml	1 ml	0.3 ml	0.3 ml

Table 2.1 Volumes of media for culture and trypsinisation of cells in culture vessels of different sizes.

2.2.2.2 Trypsinisation

Cells were liberated from the culture surface by trypsinisation prior to subculturing or harvesting. The culture vessel was drained of medium and rinsed twice at room temperature, first with PBS and then with Trypsin-EDTA solution. Cells were then incubated in fresh Trypsin-EDTA solution at 37°C for 3 min or until they begin to lift off the culture surface. Table 2.1 shows the volumes of PBS and Trypsin-EDTA solution required for culture vessels of different sizes.

2.2.2.3 Subculture

Cells were subcultured after reaching 80-100 % confluence. Cells were trypsinised, two thirds by volume were removed and fresh medium was added to the remaining cells. Trypsinised cells were split between additional culture vessels if necessary, such that they covered a third of the culture surface in each case.

2.2.2.4 Harvesting

For harvesting, cells were cultured in an 80 cm^2 flask to 70-80 % confluence before being trypsinised, diluted into 10 ml medium and centrifuged at 1000 g for 5 min. The supernatant was discarded and the pellet was resuspended in 5 ml PBS before being spun again as before. The supernatant was again discarded and the pellet was kept on ice until further processing.

2.2.2.5 Freezing

For storage in liquid nitrogen, cells were harvested as described in Section 2.2.2.4 then resuspended in 1 ml 6 % v/v DMSO in FBS. Cells were stored at -20°C for up to 48 hr before being transferred to liquid nitrogen tanks.

2.2.3 Screening for *Mycoplasma* infection

All cell cultures were systematically screened for *Mycoplasma* infection by staining with Hoechst 33258 (performed by Mrs R. M. Brown, Department of Biochemistry, University of Oxford), based on the technique described by Chen *et al.* (1977). Hoechst 33258 is a fluorophore that binds to AT-rich regions of DNA. In contaminated cell cultures stained with Hoechst 33258, *Mycoplasma* appear as small bright dots on cell membranes and in the spaces between cells.

Cells were cultured in antibiotic-free medium for at least 5 days before being subcultured onto 22 mm x 22 mm glass coverslips in 35 mm diameter Petri dishes. Cells were cultured for a further 48 hr in antibiotic-free medium or until they reached 70-80 % confluence. Cells were rinsed three times in PBS then fixed with a 3:1 mixture of ethanol:acetic acid. Fixation was repeated three times, each time by incubation in 2 ml fixative at room temperature for 2-5 min. Cells were allowed to dry in air overnight before being stained for approximately 15 min by incubation in 1 ml 0.05 µg/ml Hoechst 33258 in Hanks buffer pH 7.0 at room temperature. Cells were then rinsed twice in sterile dH_2O and once in McIlvaine buffer pH 5.5. Coverslips were mounted in M^cIlvaine buffer pH 5.5 and sealed with rubber cement. Cells were visualized using a Zeiss Axioplan 2 Imaging Microscope under UV light with a DAPI filter (see Appendix 1 for Zeiss filter set specifications).

2.2.4 Cell culture in emetine

Emetine inhibits translation by binding to the 40S subunit of the ribosome (Jimenez *et al.*, 1977) and therefore also inhibits translation-dependent processes such as nonsense-mediated decay (NMD). Culture of cells in emetine allows for the subsequent extraction and analysis of aberrantly spliced mRNAs containing premature termination codons that would otherwise be degraded by NMD (Bloethner *et al.*, 2008; Boichard *et al.*, 2008).

Cells were cultured in an 80 cm^2 flask to 80-100 % confluence before incubation in 15 ml medium containing 150 µl stock emetine solution, resulting in a working concentration of 100 µg/ml emetine, at 37°C for approximately 7 hr or until they began to pull away from the culture surface. Cells were then harvested for extraction of messenger RNA (mRNA) as described in Sections 2.2.2.4 and 2.12.4 respectively.

2.3 ASSAY FOR PYRUVATE DEHYDROGENASE ACTIVITY

2.3.1 Buffers and reagents

All reagents were from Sigma-Aldrich, unless otherwise stated.

2.3.1.1 Homogenisation buffer

The homogenisation buffer pH 7.4 was prepared by dissolving the following substances in dH_2O to a final volume of 50 ml: 60.6 mg Tris, 186 mg KCl, 40.7 mg $MgCl_2•6H_20$, 183.2 mg nicotinamide, 7.1 mg Na_2SO_4 (anhydrous) and 18.6 mg $Na_2EDTA•2H_20$. Finally, 5 µl mercaptoethanol was added. The buffer was stored in 10 ml aliquots at -20°C.

2.3.1.2 [1-^{14}C]-pyruvate

[1-^{14}C]-pyruvate was purchased in 50 µCi batches (sodium salt; PerkinElmer). The specific activity was adjusted to approximately 2000 dpm/nmol by mixing with unlabelled pyruvate. First, 2 ml 25 mM unlabelled pyruvate solution was made and the exact concentration was determined with semicarbazide reagent. To make the semicarbazide reagent, 0.2 g semicarbazide and 0.3 g sodium acetate were dissolved in 2 ml dH_2O. To measure the concentration of unlabelled pyruvate solution, 20 µl unlabelled pyruvate solution was mixed with 50 µl semicarbazide reagent, the volume was adjusted to 1 ml with dH_2O, and the solution was scanned from wavelength 200 to 300 nm, taking the peak OD at 248 nm (mM extinction coefficient 10.2). Second, [1-^{14}C]-pyruvate was mixed with unlabelled pyruvate solution and the amount of pyruvate (calculated from the data supplied by Perkin-Elmer) was added to the total. The radioactivity was determined by counting small aliquots (usually 1 and 2 µl). The total volume was divided into five 500 µl aliquots and stored at -20°C.

2.3.2 Outline of the protocol

The pyruvate dehydrogenase complex (PDH complex) catalyses oxidative decarboxylation of pyruvate to acetyl-CoA and CO_2 in the mitochondrial matrix, in a reaction commonly referred to as the link reaction. Acetyl-CoA is the carbon source for the citric acid cycle, making this reaction a key step in the pathway of aerobic respiration:

$$\text{pyruvate} + \text{CoA-SH} + NAD^+ \rightarrow \text{acetyl-CoA} + CO_2 + \text{NADH} + H^+$$

The protocol in brief is as follows. Cells were incubated with dichloroacetate (DCA) to inhibit pyruvate dehydrogenase kinase (PDK), which would otherwise phosphorylate and inhibit the

E1α subunit of the PDH complex. Cells were then sonicated to break open cell membranes and mitochondria and release the PDH complex from the mitochondrial matrix. Cell extracts were incubated with [1-^{14}C]-pyruvate in a gas-tight scintillation vial containing an inner tube of hydroxide of hyamine, which absorbed [^{14}C]-CO_2 produced by the reaction. Acetic acid was injected through the gas-tight seal to stop the reaction and convert aqueous [^{14}C]-HCO_3^-/H^+ to gaseous [^{14}C]-CO_2. The inner tube containing [^{14}C]-CO_2 was removed, non-aqueous scintillant was added, and the amount of [^{14}C]-CO_2 was measured using a scintillation counter.

2.3.3 Preparation of cell extracts

Cells were cultured in 80 cm^2 flasks to 70-80 % confluence and harvested as described in Section 2.2.2.4. The pellet was resuspended in 480 µl PBS and 20 µl 125 mM DCA in 0.5 M KP_i buffer pH 7.4 and incubated in a shaking waterbath at 37ºC for 15 min. The suspension of cells was then centrifuged at 1000 g for 5 min and the supernatant was discarded. The pellet was resuspended in 370-450 µl homogenisation buffer and 400 µl cell suspension was transferred to a 1.5 ml microcentrifuge tube for sonication. Cells were sonicated in ice-cold water in a Misonix 3000 Cup Sonicator with 8 pulses of 1 sec each, a frequency of 2 sec and amplitude setting 0.5. Cell extracts were kept on ice until further processing and vortexed immediately before use.

2.3.4 PDH assay

Cell extracts from patients under investigation were assayed alongside cell extract from C1. All cell extracts were assayed relative to a blank, containing heat-denatured cell extract from C1. Two samples for assay were prepared for each patient, one sample containing 30 µl cell extract (duplicate 1) and one sample containing 60 µl cell extract (duplicate 2). Samples for assay were prepared in glass scintillation vials, as shown in Table 2.2.

Solution/suspension added to scintillation vial	Volume added to scintillation vial		
	Blank	Patient X (duplicate 1)	Patient X (duplicate 2)
dH_20	195 µl	225 µl	195 µl
0.5 M KP_i buffer pH 7.4	40 µl	40 µl	40 µl
100 mg/ml BSA	40 µl	40 µl	40 µl
125 mM DCA in 0.5 M KP_i buffer pH 7.4	20 µl	20 µl	20 µl
6.5 mM CoA-SH	20 µl	20 µl	20 µl
32.5 mM EDTA	20 µl	20 µl	20 µl
0.25 M mercaptoethanol	20 µl	20 µl	20 µl
62.5 mM $MgCl_2$	20 µl	20 µl	20 µl
25 mM Na_2SO_3	20 µl	20 µl	20 µl
40 mM NAD^+	20 µl	20 µl	20 µl
25 mM TPP	20 µl	20 µl	20 µl
Cell extract	60 µl (C1)	30 µl	60 µl
[1-^{14}C]-pyruvate (~2000 dpm/nmol)	5 µl	5 µl	5 µl
Hydroxide of hyamine 10x (in Durham tube)	100 µl	100 µl	100 µl

Table 2.2 Preparation of samples for the PDH assay. Patient X represents C1 or any patient under study.

The blank was prepared by adding 195 µl dH_2O, 40 µl 0.5 M KP_i buffer pH 7.4 and 60 µl C1 cell extract to a scintillation vial, which was then boiled for 3 min and subsequently cooled on ice. 40 µl 100 mg/ml bovine serum albumin (BSA) was then added together with 20 µl of each of the following substrates/cofactors: 125 mM DCA in 0.5 M KP_i buffer pH 7.4, 6.5 mM CoA-SH, 32.5 mM EDTA, 0.25 M mercaptoethanol, 62.5 mM $MgCl_2$, 25 mM Na_2SO_3, 40 mM NAD^+ and 25 mM thiamine pyrophosphate (TPP).

Duplicates 1 and 2 for each patient were prepared by adding 225 µl and 195 µl dH_2O to two scintillation vials respectively. This was followed by the addition of 40 µl 0.5 M KP_i buffer pH 7.4, 40 µl 100 mg/ml BSA and 20 µl of each substrate/cofactor to each scintillation vial, together with 30 µl and 60 µl cell extract respectively.

A Durham tube containing 100 µl hydroxide of hyamine 10x (PerkinElmer) was placed inside each scintillation vial (each Durham tube was sitting inside a small test tube). Finally, 5 µl [1-^{14}C]-pyruvate (specific activity ~2000 dpm/nmol) was added to the reaction mix and each

scintillation vial was sealed with a gas-tight red rubber Suba-Seal®. Sealed scintillation vials were incubated in a shaking waterbath at 37ºC for 90 min. After this incubation period, 500 µl 50 % v/v acetic acid was injected through the Suba-Seal® and scintillation vials were incubated in the same way for a further 15 min.

The Durham tube was removed from each scintillation vial and placed in a 1.5 ml microcentrifuge tube. 200 µl OptiScint 'Safe' (LKB Scintillation Products) was added to the Durham tube. The microcentrifuge tube with the Durham tube was capped and vortexed before being placed in a fresh scintillation vial, ready for counting. Radioactivity was measured using an LKB Wallac 1209 Rackbeta Liquid Scintillation Counter. The PDH activity for each patient duplicate was calculated using the formula in Figure 2.1.

$$\text{Enzyme activity (nmol/min/mg)} = \frac{\text{dpm (patient duplicate)} - \text{dpm (blank)}}{\text{Specific activity of } [^{14}C]\text{-pyruvate (dpm/nmol)} \times \text{Incubation time (90 min)} \times \text{Volume of cell extract (µl)} \times \text{Protein concentration of cell extract (mg/µl)}}$$

Figure 2.1 Formula to calculate enzyme activity measured using the PDH assay.

2.4 ASSAYS FOR CITRATE SYNTHASE AND CYTOCHROME C OXIDASE ACTIVITY

2.4.1 Buffers and reagents

All reagents were from Sigma-Aldrich, unless otherwise stated.

2.4.1.1 MOPS/EDTA/sucrose buffer and MES buffer

MOPS/EDTA/sucrose (M/E/S) buffer pH 7.2 contained 20 mM MOPS, 3 mM EDTA and

0.25 mM sucrose. MES buffer pH 6.0 was made up as a 10x concentrated solution, containing 1 M MES with 0.1 mM EDTA, which was diluted 1:9 in dH_2O immediately before use.

2.4.1.2 Reduced cytochrome c

Cytochrome c was dissolved in MES buffer pH 6.0 to a final concentration of 25 mg/ml cytochrome c. This solution was reduced with an excess of ascorbic acid, separated by size chromatography on a Sephadex G-25 column and assessed by absorption spectrometry. Reduced cytochrome c was used in the assay at a concentration that showed OD_{550} 0.3 in a 1:100 dilution and a ratio of OD_{550}/OD_{565} greater than 14.

2.4.1.3 Potassium ferricyanide

Potassium ferricyanide was dissolved in dH_2O to give a bright yellow solution. The assay simply requires the concentration of potassium ferricyanide to be in excess of that of cytochrome c.

2.4.2 Outline of the protocol

Citrate synthase catalyses the conversion of acetyl-CoA and oxaloacetate to citrate, the first step of the citric acid cycle, in the mitochondrial matrix:

$$\text{acetyl-CoA} + \text{oxaloacetate} + H_2O \rightarrow \text{citrate} + \text{CoA-SH}$$

Cytochrome c oxidase (COX), also known as Complex IV, is situated in the IM, predominantly in that part of the membrane that forms the mitochondrial cristae. It catalyses the last step in the electron transport chain: reduction of molecular oxygen to two molecules of water using one

electron from each of four reduced cytochrome c molecules and four protons from the mitochondrial matrix, at the same time as pumping an additional four protons across the IM from the matrix to the IMS:

$$4\ Fe^{2+}\text{-cyt}\ c_{RED} + 8\ H^{+}_{MATRIX} + O_2 \rightarrow 4\ Fe^{3+}\text{-cyt}\ c_{OX} + 2\ H_2O + 4\ H^{+}_{IMS}$$

Both enzymes were assayed spectrophotometrically, one immediately after the other, using the same cell extract preparations. The protocol in brief is as follows. Cells were lysed by brief exposure to digitonin. Mitochondria were separated from the cell debris by sucrose density gradient centrifugation and sonicated to release the mitochondrial enzymes. Citrate synthase activity was assayed by incubating cell extracts with acetyl CoA, oxaloacetate and dithiobis 2-nitrobenzoic acid (DTNB); CoA-SH produced by the reaction reacted with DTNB to form a coloured product that was detected spectrophotometrically at 412 nm. COX activity was assayed by incubating cell extracts with reduced cytochrome c; the oxidation of cytochrome c was monitored at 550 nm.

2.4.3 Preparation of cell extracts

Cells were cultured in 80 cm^2 flasks to 70-80 % confluence and harvested as described in Section 2.2.2.4. Pelleted cells were resuspended in 400 µl M/E/S buffer pH 7.2 and transferred to a 1.5 ml microcentrifuge tube. 100 µl 5 mg/ml digitonin, pre-chilled to 4°C, was added and the sample was vortexed. Exactly 42 s after adding the digitonin, the sample was centrifuged at 4°C for 1 min at 13000 rpm. The supernatant was discarded and the pellet was resuspended in 600 µl M/E/S buffer pH 7.2, before being centrifuged again at 4°C for 3 min at 13000 rpm. The supernatant was again discarded and the pellet was resuspended in 200 µl M/E/S buffer pH 7.2, ready for sonication. Cell extracts were sonicated in ice-water using an Ultrasonic Processor

with pulse setting 20 s, 20 % duty cycle and microtip output setting 2. Cell extracts were kept on ice until further processing and vortexed immediately before use.

2.4.4 Citrate synthase assay

Cell extracts from patients under investigation were assayed alongside cell extract from C1. All cell extracts were assayed relative to a blank, containing 40 µg/ml DTNB in 60 mM Tris-HCl buffer pH 8.1. Two samples for assay were prepared for each patient, one sample containing 10 µl cell extract (duplicate 1) and one sample containing 20 µl cell extract (duplicate 2). Samples for assay were prepared in 1 ml cuvettes, as shown in Table 2.3.

Solution/suspension added to cuvette	Volume added to cuvette		
	Blank	Patient X (duplicate 1)	Patient X (duplicate 2)
dH_2O	930 µl	900 µl	890 µl
1 M Tris-HCl buffer pH 8.1	60 µl	60 µl	60 µl
4 mg/ml DTNB in 1 M Tris-HCl buffer pH 8.1	10 µl	10 µl	10 µl
25 mM acetyl-CoA	-	10 µl	10 µl
Cell extract	-	10 µl	20 µl
6.8 mg/ml oxaloacetate in 0.1 M Tris-HCl buffer pH 8.1	-	10 µl	10 µl

Table 2.3 Preparation of samples for the citrate synthase assay. Patient X represents C1 or any patient under study.

The blank was prepared by adding 930 µl dH_2O, 60 µl 1 M Tris-HCl buffer pH 8.1 and 10 µl 4 mg/ml DTNB in 1 M Tris-HCl buffer pH 8.1 to a cuvette.

Duplicates 1 and 2 for each patient were prepared by adding 900 µl and 890 µl dH_2O to two cuvettes respectively. This was followed by the addition of 60 µl 1 M Tris-HCl buffer pH 8.1, 10 µl 4 mg/ml DTNB in 1 M Tris-HCl buffer pH 8.1, and 10 µl 25 mM acetyl-CoA to each cuvette, together with 10 µl and 20 µl cell extract respectively.

Absorption at 412 nm was monitored at 37°C by taking readings every 20 sec for 3 min, both before and after the addition of 10 µl 6.8 mg/ml oxaloacetate in 0.1 M Tris-HCl buffer pH 8.1 to each patient duplicate. Citrate synthase activity for each patient duplicate was calculated using the formula in Figure 2.2.

2.4.5 COX assay

Cell extracts from patients under investigation were assayed alongside cell extract from C1. All cell extracts were assayed relative to a blank, containing 100 µg/ml oxidised cytochrome c in MES buffer pH 6.0. Two samples for assay were prepared for each patient, one sample containing 5 µl cell extract (duplicate 1) and one sample containing 10 µl cell extract (duplicate 2). Samples for assay were prepared in 1 ml cuvettes, as shown in Table 2.4.

Solution/suspension added to cuvette	Volume added to cuvette		
	Blank	Patient X (duplicate 1)	Patient X (duplicate 2)
MES buffer pH 6.0	985 µl	985 µl	980 µl
10 mg/ml reduced cytochrome c in MES buffer pH 6.0	10 µl	10 µl	10 µl
Potassium ferricyanide (in excess)	5 µl	-	-
Cell extract	-	5 µl	10 µl

Table 2.4 Preparation of samples for the COX assay. Patient X represents C1 or any patient under study.

The blank was prepared by adding 985 µl MES buffer pH 6.0, 10 µl 10 mg/ml reduced cytochrome c in MES buffer pH 6.0 and 5 µl excess potassium ferricyanide to a cuvette.

Duplicates 1 and 2 for each patient were prepared by adding 985 µl and 980 µl MES buffer pH 6.0 to two cuvettes respectively. This was followed by the addition of 10 µl 10 mg/ml reduced cytochrome c in MES buffer pH 6.0 to each cuvette.

Absorption at 550 nm was monitored at 37°C by taking readings every 10 sec for 2 min, both before and after the addition of 5 µl and 10 µl cell extract to patient duplicates 1 and 2 respectively. The COX activity for each patient duplicate was calculated using the formula in Figure 2.2.

$$\text{Enzyme activity (nmol/min/mg)} = \frac{\text{Final rate (nmol/min)} - \text{Initial rate (nmol/min)}}{\text{Volume of cell extract (µl)} \times \text{Protein concentration of cell extract (mg/µl)}}$$

Figure 2.2 Formula for calculating enzyme activity measured using the citrate synthase and COX assays.

2.5 LOWRY PROTEIN ASSAY

This method for assaying the protein content of a biological sample was first proposed by Lowry *et al.* (1951). The reaction mechanism is not well understood, but involves oxidation of aromatic residues in the protein and reduction of Folin-Ciocalteu Phenol Reagent, which is measured spectrophotometrically by absorption at 750 nm.

Patient cell extracts were assayed alongside six standards, containing 0-50 µg BSA, each in a total reaction volume of 1.3 ml. Two samples for assay were prepared for each patient, one sample containing 5 µl cell extract (duplicate 1) and one sample containing 10 µl cell extract (duplicate 2). Samples for assay were prepared in test tubes, as shown in Table 2.5. Folin & Ciocalteu's Phenol Reagent (BDH) was diluted 1:1 with dH_2O immediately before use. Samples for assay were vortexed after the addition of NaOH solution and again after the addition of Folin-Ciocalteu Phenol Reagent. Test tubes were incubated at room temperature for 45 min before absorption at 750 nm was measured, using air as a blank.

Solution/suspension added to test tube	Volume added to test tube							
	Standards						Patient X (duplicate 1)	Patient X (duplicate 2)
	1	2	3	4	5	6		
dH_2O	200 µl	190 µl	180 µl	170 µl	160 µl	150 µl	195 µl	190 µl
1 mg/ml BSA	0 µl	10 µl	20 µl	30 µl	40 µl	50 µl	-	-
Cell extract	-	-	-	-	-	-	5 µl	10 µl
0.1 M NaOH 20 mg/ml Na_2CO_3 0.02 % w/v sodium tartrate 0.01 % w/v copper sulphate	1 ml	1 ml	1 ml	1 ml	1 ml	1 ml	1 ml	1 ml
Folin & Ciocalteu's Phenol Reagent dil. 1:1 with dH_2O	100 µl	100 µl	100 µl	100 µl	100 µl	100 µl	100 µl	100 µl

Table 2.5 Preparation of samples for the Lowry protein assay. Patient X represents C1 or any patient under study.

The amount of protein (µg) in each patient duplicate was calculated from the standard curve and divided by the volume of cell extract used (µl). A mean average was taken of the two duplicates to give a final value for the protein concentration in cell extract from each patient. Cell extracts prepared according to the protocols described in Sections 2.3.3 and 2.4.3 typically contained protein concentrations of 2-3 µg/µl.

2.6 ANALYSIS OF MITOCHONDRIAL MORPHOLOGY

Mitochondrial morphology was analysed by staining the mitochondrial matrix with MitoTracker® Red CMXRos (Invitrogen Molecular Probes). MitoTracker® probes are mitochondrion-selective fluorescent dyes that accumulate in mitochondria as a result of the $\Delta\psi_m$ but are retained after mitochondrial membrane depolarisation or cell fixation and permeabilisation, preserving the fluorescent staining pattern characteristic of live cells (Poot *et al.*, 1996).

MitoTracker® Red CMXRos was dissolved in DMSO to give a stock solution of 1 mM and stored at -20°C. Cells from patients under investigation were stained alongside cells from C1. Cells were cultured on 22 mm x 22 mm glass coverslips in 35 mm diameter Petri dishes at 70-80 %

confluence. Cells were incubated in 1 ml culture medium containing 100 nM MitoTracker® in the dark at 37°C for 10-15 min. This was followed by two successive 30 min incubations in the dark at 37°C in 2 ml culture medium without MitoTracker®. Cells were then fixed and subjected to ethanol dehydration to remove excess dye from the cytosol, with three washes in 1 ml PBS at room temperature before and after each procedure. Fixation was carried out by incubation in 1 ml 4 % w/v paraformaldehyde in 250 mM HEPES buffer in the dark for 20 min at room temperature. Ethanol dehydration and subsequent rehydration were carried out by five successive 5 min incubations at 4°C in 1 ml 70 %, 90 %, 100 %, 90 % and 70 % v/v ethanol in dH_2O respectively. Coverslips were mounted on glass slides using Mowiol solution and sealed with rubber cement. Cells were visualised using a Zeiss Axioplan 2 Imaging Microscope under UV light using a rhodamine filter (see Appendix 1 for Zeiss filter set specifications).

2.7 ANALYSIS OF THE SUBCELLULAR DISTRIBUTION OF THE PYRUVATE DEHYDROGENASE COMPLEX

The PDH complex has a punctate distribution in the mitochondrial matrix, both in normal and in PDH-deficient cells, which is thought to reflect the structural and metabolic compartmentalisation of mitochondria (Margineantu *et al.*, 2002). The subcellular distribution of the PDH complex was analysed by immunofluorescence with antibodies against the E1α and E2 subunits as follows: mouse anti-PDH E1α subunit monoclonal antibody, unconjugated, clone 9H9AF5 (Invitrogen Molecular Probes); goat anti-mouse IgG conjugated to Alexa Fluor® 594 (Invitrogen Molecular Probes); anti-PDH E2 subunit monoclonal antibody conjugated to Oregon Green®, clone 15D3G9C11 (gift from Dr R. Capaldi and Dr M. Marusich, MitoSciences).

Cells from patients under investigation were stained alongside cells from C1. Cells were cultured on 22 mm x 22 mm glass coverslips in 35 mm diameter Petri dishes to 70-80 %

confluence. All incubation steps in the immunocytochemical staining protocol were carried out at room temperature. Cells were fixed and permeabilised by incubation in 1 ml methanol for 1 min, with three washes in 1 ml PBS before and afterwards, then blocked by incubation in 1 ml 10 % v/v goat serum (GS; Sigma-Aldrich) in PBS for 1 hr. Cells were incubated in 5 µg/ml mouse anti-PDH E1α subunit monoclonal antibody in 1 % v/v GS in PBS for 1 hr. This was followed by four washes in 1 ml 1 % v/v GS in PBS, with 10 min gentle shaking after the second and third washes. Cells were then incubated in 2 µg/ml Alexa Fluor® 594 goat anti-mouse IgG in 1 % v/v GS in PBS in the dark for 1 hr and washed four times in 1 ml 1 % v/v GS in PBS as before. Finally, cells were incubated in 0.3 µg/ml Oregon Green® anti-PDH E2 subunit monoclonal antibody in 1 % v/v GS in PBS in the dark for 1 hr 30 min. Cells were washed three times in 1 ml 1 % v/v GS in PBS, with 10 min gentle shaking after the second and third washes, and then washed once in 1 ml PBS. Coverslips were mounted on glass slides using Mowiol solution and sealed with rubber cement. Cells were visualised using a Zeiss Axioplan 2 Imaging Microscope under UV light using FITC and rhodamine filters (see Appendix 1 for Zeiss filter set specifications).

2.8 ANALYSIS OF TH E SUBCELLULAR DISTRIBUTION OF CYTOCHROME C OXIDASE

The subcellular distribution of COX was analysed by cytochemical staining, based on the technique described by Seligman *et al.* (1968), by incubating cells with exogenous cytochrome c and 3,3'-diaminobenzidine (DAB). Cytochrome c oxidised by COX in turn oxidises DAB, which polymerises on oxidation to form a brown, amorphous, osmiophilic substance. This oxidation product forms non-droplet deposits in the mitochondrial intracristate space and the IMS, which can be visualised using light microscopy. Haematoxylin was used to counterstain nuclei blue so that cells with little or no oxidation product could be identified.

Cells from patients under investigation were stained alongside cells from C1. Cells were cultured on 22 mm x 22 mm glass coverslips in 35 mm diameter Petri dishes to 90-100 % confluence. Cells were washed three times in 1 ml PBS and allowed to dry in air for 45-60 min. Cells were then incubated in 1 ml filter-sterilised enzyme substrate mix, pre-warmed to 37°C, containing 0.5 mg/ml cytochrome c from horse heart (Sigma-Aldrich), 0.5 mg/ml 3,3'-diaminobenzidine tetrahydrochloride (Sigma-Aldrich), 75 mg/ml sucrose and 2 µg/ml catalase in 50 mM sodium phosphate buffer pH 7.4 (39 mM Na_2HPO_4 and 11 mM NaH_2PO_4), in the dark at 37°C for 5 hr. As a negative control, control cells were incubated in 1 ml enzyme substrate mix containing 5 mM NaN_3, which inhibits COX. After the 5 hr incubation, cells were washed three times briefly in dH_2O and allowed to dry in air overnight. Cells were then immersed in filtered Mayer's Haematoxylin Solution (Sigma-Aldrich) for 30 sec at room temperature before being rinsed in tap water and allowed to dry in air for at least 1 hr. Coverslips were mounted on glass slides using Aquamount (BDH) and sealed with rubber cement. Cells were visualised using a Zeiss Axioplan 2 Imaging Microscope under visible light using a CB12 conversion filter.

2.9 ANALYSIS OF THE AMOUNT AND SUBCELLULAR DISTRIBUTION OF MITOCHONDRIAL DNA

PicoGreen® reagent was used to stain mtDNA in live cells, using a technique based on that described by Ashley *et al.* (2005), to analyse the amount and subcellular distribution of mtDNA in nucleoids. PicoGreen® reagent is a green-fluorescent nucleic acid stain used to label dsDNA. It is not specific for dsDNA but its fluorescence is enhanced more than 1000-fold upon binding to dsDNA and much less so upon binding to ssDNA or RNA, making it possible to quantitate dsDNA in the presence of equimolar amounts of ssDNA, RNA or proteins (Singer *et al.*, 1997).

Cells from patients under investigation were stained alongside cells from C1. Cells were cultured on 22 mm x 22 mm glass coverslips in 35 mm diameter Petri dishes to 70-80 %

confluence. Cells were stained with MitoTracker® Red CMXRos, as described in Section 2.6, then incubated in 1 ml culture medium containing 3 µl Quant-iT™ PicoGreen® dsDNA reagent (Invitrogen Molecular Probes) at 37°C for 1 hr 30 min. This was followed by incubation in 2 ml culture medium without PicoGreen® at 37°C for 30 min. Cells were then washed three times in HBSS Modified without phenol red (Sigma-Aldrich) at room temperature before being mounted live. Coverslips were mounted onto Press-to-Seal™ silicone isolators (one well, 20 mm diameter, 0.5 mm deep; Invitrogen Molecular Probes) on glass slides with 200 µl HBSS Modified without phenol red and sealed with rubber cement. Cells were visualised immediately using a Zeiss Axioplan 2 Imaging Microscope under UV light using FITC and rhodamine filters.

2.10 ANALYSIS OF MITOCHONDRIAL MEMBRANE POTENTIAL

5,5',6,6'-tetrachloro-1,1',3,3'-tetraethyl-benzimidazolyl-carbocyanine iodide (JC-1) is a lipophilic cation with a delocalised positive charge. Incubation of cells with JC-1 was used to analyse $\Delta\psi_m$, based on the technique described by Smiley *et al.* (1991). At low concentrations, JC-1 exists as a green monomer, with absorption and emission maxima of 514 and 529 nm respectively. Once a critical concentration is reached, JC-1 monomers aggregate to form red J-aggregates, with absorption and emission maxima of 585 and 590 nm respectively. Incubation of healthy cells with JC-1 results in accumulation of the dye in the mitochondrial matrix due to the negative $\Delta\psi_m$, so the mitochondria are stained red and the cytosol is stained green. In diseased or apoptotic cells, $\Delta\psi_m$ collapses, so JC-1 cannot accumulate in the mitochondria and remains in its green monomeric form (Reers *et al.*, 1991).

JC-1 (Invitrogen Molecular Probes) was dissolved in DMSO to give a stock solution of 1 mg/ml JC-1. Cells from patients under investigation were stained alongside cells from C1. Cells were cultured on 22 mm x 22 mm glass coverslips in 35 mm diameter Petri dishes to 70-80 %

confluence. Culture medium was pre-warmed to 37°C before stock JC-1 solution was added to give a working concentration of 5 µg/ml JC-1. This medium was then vortexed for 15 sec to dissolve JC-1 and centrifuged at 13000 g for 1 min to pellet any undissolved particulate matter, which was discarded. Cells were incubated in 1 ml pre-warmed medium containing 5 µg/ml JC-1 at 37°C for 15 min then washed three times in HBSS Modified without phenol red at room temperature before being mounted live. Coverslips were mounted onto Press-to-Seal™ silicone isolators on glass slides with 200 µl HBSS Modified without phenol red and sealed with rubber cement. Cells were visualised immediately using a Zeiss Axioplan 2 Imaging Microscope under UV light using FITC and rhodamine filters.

2.11 PAIRWISE PATIENT CELL FUSIONS FOR COMPLEMENTATION STUDIES

In an effort to place patients into different categories according to genotype, patient cells were fused together in pairwise combinations by incubation in PEG, based on the technique described by Davidson *et al.* (1976a, 1976b, 1977), and the resulting heterokaryons were stained with MitoTracker® to check for complementation of the mitochondrial morphology defects. Only heterokaryons with three or more nuclei were examined due to the likelihood that a significant proportion of heterokaryons with only two nuclei were the result of fusion of cells from the same patient.

Cells from each of the patients under investigation were fused to each other in pairwise combinations (four patients resulting in six pairwise combinations). For controls, cells from C1 were fused to each other and to cells from each of the patients under investigation. Cells from each patient were grown in 80 cm^2 flasks to 90-100 % confluence before being harvested into 10 ml medium and counted using a Standard Haemocytometer Chamber. 7.5 x 10^5 cells from each of two patients were mixed and split into two 25 cm^2 flasks, a third by volume in one flask

as a control and two thirds by volume in a second flask for fusion, which was carried out the following day. Cells were fused by incubation in 1 ml 50 % w/v PEG 1500 in 75 mM HEPES (Roche) for 2 min at room temperature, with three washes in 5 ml FBS-free culture medium before and afterwards. Cells were then allowed to recover in normal culture medium for 4 days to allow for protein expression, before subculture onto coverslips for MitoTracker® staining. Cells were stained by MitoTracker® Red CMXRos, fixed and dehydrated as described in Section 2.6.

2.12 SEQUENCE ANALYSIS OF CANDIDATE GENES

2.12.1 Selection of candidate genes

Extensive biomedical literature searches were carried out to identify genes that when under- or overexpressed in yeast, *Drosophila* or mammalian cells resulted in abnormalities in mitochondrial morphology similar to those seen in the patients' cells. These findings are summarised in Chapter 1. Based on this research and on the cellular phenotype of each patient, the following genes were selected as candidates for sequence analysis in the patients in order to try to find the primary genetic defect in each case: *AKAP1*, *DNM1L*, *FIS1*, *MFN1*, *MFN2*, *RHOT1*, *RHOT2*, *TRAK1* and *TRAK2*. Gene symbols approved by the Human Genome Organisation (HUGO) were obtained from the HUGO Gene Nomenclature Committee (HGNC) Database, EMBL Outstation - Hinxton, European Bioinformatics Institute, Wellcome Trust Genome Campus, Hinxton, Cambridge, UK, available at www.genenames.org, in May 2010. (See Appendix 2 for gene symbols and their aliases.)

2.12.2 Selection of reference sequences

The genomic DNA (gDNA) and complementary DNA (cDNA) sequences for each gene were obtained from the Ensembl database, available at www.ensembl.org/Homo_sapiens. For the

majority of genes under study, the gDNA sequence was poorly defined and its annotation changed considerably throughout the course of the project, therefore a cDNA sequence was chosen as the reference sequence for each gene. Only those cDNA sequences validated by the collaborative consensus coding sequence (CCDS) project were considered. The CCDS project is a collaboration between the NCBI, Ensembl and UCSC Genome Browsers that tracks identical protein annotations with a stable identifier (CCDS ID) and reviews inconsistent protein annotations between sites, as well as annotations for which new evidence suggests a revision is needed, with the ultimate goal of identifying and accurately annotating all protein-coding genes on the reference mouse and human genomes (Pruit *et al.*, 2009). Of those cDNA sequences with CCDS IDs, the reference sequence was chosen as the cDNA sequence with the greatest number of exons. (See Appendix 3 for a list of reference sequences.)

2.12.3 Oligonucleotide primer design

Oligonucleotide primers for PCR and sequencing were designed using the Primer3 software, developed by the Whitehead Institute for Biomedical Research, Cambridge, MA, USA (Rozen and Skaletsky, 2000), available at http://frodo.wi.mit.edu/primer3/input.htm. (See Appendices 5 and 6 for a list of primers for PCR and sequencing respectively.) Primers were commercially manufactured by Sigma-Genosys and dissolved in 200 µl TE buffer pH 8.0, containing 10 mM Tris and 1 mM EDTA, to give stock solutions of varying concentration. Aliquots were diluted into nuclease-free water to give 10 and 5 µM working stocks, stored at -20°C, for use in PCR and sequencing reactions respectively.

2.12.4 Template preparation

Cells were harvested as described in Section 2.2.2.4. gDNA and mRNA were extracted using the Nucleon® BACC2 Genomic DNA Extraction Kit (Tepnel Life Sciences) and the High Pure

RNA Isolation Kit (Roche) respectively, according to the manufacturer's instructions (see Appendix 4). cDNA was synthesised from mRNA using the AffinityScript^{TM} Multiple Temperature Reverse Transcriptase (Stratagene) according to the manufacturer's instructions (see Appendix 4), using 3 µg mRNA as starting material.

2.12.5 Polymerase chain reaction

The coding region of each gene was amplified by PCR from a cDNA template. Where alternative splicing resulted in transcripts with skipped exons, those exons and adjacent intronic regions were amplified from gDNA. All PCR protocols were designed and optimised *de novo* with the exception of those for *MFN1* and *MFN2* (work carried out by Mrs R. H. Head, Department of Biochemistry, University of Oxford). PCR protocols were optimised using template DNA from two controls (C2 and C3). (See Appendix 5 for a list of PCR protocols for each gene.)

The DNA polymerase enzymes used were Taq (NEB) or TopTaq^{TM} (Qiagen), in each case either with or without Q-Solution^{TM} (Qiagen) in the reaction mix, depending on the optimum conditions determined for amplification of each gene. The PCR reaction mix contained nuclease-free water, DNA polymerase buffer 1x, 0.8 mM PCR Grade dNTPs (0.2 mM each of dATP, dCTP, dGTP and dTTP; sodium salt; Roche), 0.5 µM forward PCR primer, 0.5 µl reverse PCR primer, DNA polymerase (according to the manufacturer's instructions) and 2.0 µl DNA in a total volume of 50.0 µl. Q-Solution^{TM} was used at a concentration of 10 % v/v in the reaction mix, if required. cDNA was used undiluted. gDNA was diluted in nuclease-free water to 100 ng/µl before use. PCR reactions were carried out in PCR Sprint or Px2 Thermal Cyclers (Thermo Scientific).

2.12.6 Gel electrophoresis

PCR products were analysed using gel electrophoresis. PCR products were run alongside DNA Molecular Weight Markers XIV or XVII (Roche) on 1 % w/v agarose gels with 0.5 µg/ml EtBr in TBE buffer pH 8.0 (see Appendix 7) at 100 mV for 30-40 min. Gels were visualised under UV light and photographed using an AlphaImager® HP High Resolution Imaging System (Alpha Innotech).

2.12.7 Purification and quantification

PCR products were purified using the QIAquick® PCR Purification Kit (Qiagen) and a microcentrifuge according to the manufacturer's instructions (see Appendix 8). Purified DNA was quantified by gel electrophoresis, as described in Section 2.12.6, by comparison of bands with those of DNA Molecular Weight Markers XIV or XVII of known concentration.

2.12.8 Sequencing

Purified PCR products were sequenced using BigDye® Terminator v.3.1 (Applied Biosystems). The following solutions were added to a 0.5 ml nuclease-free microcentrifuge tube: 1.0 µl BigDye® Terminator v.3.1, 2.0 µl BigDye® Terminator v.3.1 sequencing buffer 5x, 1.0 µl 5 µM primer, *x* µl PCR product and *y* µl dH_2O, where *x* was the volume containing 1 ng DNA/100 bp DNA to be sequenced and *y* was such that the total volume of the mixture was 10.0 µl. Sequencing was carried out in PCR Sprint or Px2 Thermal Cyclers using one cycle of 96°C for 10 sec followed by 25 cycles of 96°C for 30 sec, 50°C for 15 sec, and 60°C for 2 min. The final products were analysed in an ABI 3730 DNA Analyser (service provided by Source Bioscience – AUTOGEN™ & Geneservice™, Department of Biochemistry, University of Oxford). Sequence

alignments were carried out using the LALIGN software, from the Genestream Resource Centre at “Institut de Génétique Humaine”, Montpellier, France, available at http://vega.igh.cnrs.fr/bin/align-guess.cgi.

2.12.9 Sequence analysis of *TRAK1*

TRAK1 amplified from cDNA from C2 and C3 but not from cDNA from patients under investigation. In each case, it was thought that this could be due to the introduction of a premature termination codon in the *TRAK1* coding sequence, as a result of either a point mutation or aberrant splicing that altered the reading frame downstream, which resulted in degradation of the *TRAK1* transcript by NMD. Cells from C2 and C3 and from the patients under investigation were therefore cultured in emetine, as described in Section 2.2.4, to inhibit NMD. However, it was also not possible to amplify *TRAK1* from cDNA derived from emetine-treated cells from patients under investigation, whereas *TRAK1* amplified well from cDNA derived from emetine-treated control cells. It was thought that the failure to amplify TRAK1 may be due to the quality of the cDNA template so part of *POLG* (c.1044_2506), the housekeeping gene that encodes the catalytic subunit of the mtDNA polymerase, was amplified from patient cDNA to test its quality. The primers and protocol are shown in Table 2.6.

Primer sequence 5’→3’	Product size (bp)	DNA polymerase	PCR		
			Stage 1	Stage 2	Stage 3
(F) GGACATCAGCAGTGTCAACAGTC (R) GGCCTTCCTCATCATAGTCG	1463	TopTaq™	94ºC 3 min 1 cycle	94ºC 30 s 61ºC 30 s 72ºC 2 min 35 cycles	72ºC 10 min 1 cycle

Table 2.6 Primers and protocol for PCR amplification of *POLG* c.1044_2506 from cDNA.

TRAK1 was amplified by nested PCR using PfuUltra™ II Fusion HS (Stratagene) and 2.0 µl of PCR product as template, even though PCR products could not be visualised on agarose gels. The primers and protocol are shown in Table 2.7. Initially, the nested PCR did not amplify the

P1 PCR product; the original PCR was done with 6.0 µl cDNA as template and 50 cycles, then 6.0 µl of the product of this reaction was used as template in the nested PCR.

Primer sequence 5'→3'	Product size (bp)	DNA polymerase	PCR		
			Stage 1	Stage 2	Stage 3
(F) GCTCTCATGGAGGCTCTCTC (R) GTGGACAGAGAAGGGCAGAG	3030	PfuUltra™ II Fusion HS	95°C 1 min 1 cycle	95°C 20 s 61°C 20 s 72°C 2 min 30 cycles	72°C 3 min 1 cycle

Table 2.7 Primers and protocol for nested PCR amplification of *TRAK1*, using PCR product as template.

CHAPTER 3: RESULTS

3.1 MITOCHONDRIAL ENZYME ACTIVITIES

The activities of the PDH complex, citrate synthase and COX were assayed in fibroblasts from a control and from patients under investigation as described in Sections 2.3 and 2.4. Due to time and financial constraints, it was not possible to do multiple repeats of each assay for each patient. However, each assay was carried out at least twice for each patient and the raw data are shown in Table 3.1. The normal range for each assay was as follows: PDH assay, 0.7-1.1 nmol/min/mg; citrate synthase assay, 12-24 nmol/min/mg; COX assay, 30-90 nmol/min/mg (Dr G. K. Brown, personal communication). As expected, enzyme activities assayed in control cells fell within the normal range in each case, although the values for citrate synthase activity varied considerably. All four patients under investigation showed abnormalities in the activities of one or more mitochondrial enzymes.

Patient	Enzyme activity (nmol/min/mg)		
	PDH complex	Citrate synthase	COX
C1	0.86, 0.90, 0.90, 0.91, 0.91	12, 13, 19, 24	56, 62, 69, 69
P1	0.38, 0.48	7, 14	25, 37
P2	0.38, 0.64, 0.81, 1.1	12, 18	44, 51
P3	0.32, 0.37	35, 36	13, 23
P4	0.23, 0.26	10, 15	18, 26

Table 3.1 Activities of the PDH complex, citrate synthase and COX assayed in fibroblasts from C1 and from patients under study. The normal range for each assay was as follows: PDH assay, 0.7-1.1 nmol/min/mg; citrate synthase assay, 12-24 nmol/min/mg; COX assay, 30-90 nmol/min/mg (Dr G. K. Brown, personal communication).

In cells of P1, PDH activity was well below the normal range and approximately 50 % reduced relative to that of control cells; citrate synthase activity was at the lower boundary of the normal range; COX activity was also at the lower boundary of the normal range but approximately 50 % reduced relative to that of control cells.

In cells of P2, values for the PDH activity varied from well below the normal range, similar to values obtained for cells of P1, to the upper boundary of the normal range; both citrate synthase and COX activities were normal.

In cells of P3, PDH and COX activities were well below the normal range in each case and approximately 60-70 % reduced relative to those of control cells; in contrast, citrate synthase activity was well above the normal range and approximately twice that of control cells.

In cells of P4, as in those of P3, PDH and COX activities were well below the normal range in each case and approximately 60-70 % reduced relative to those of control cells; however, unlike in P3 cells, citrate synthase activity was at the lower end of the normal range.

3.2 MITOCHONDRIAL MORPHOLOGY

Mitochondrial morphology was analysed in patient fibroblasts by staining the mitochondrial matrix with MitoTracker® Red CMXRos, as described in Section 2.6. Images are shown in Figure 3.1. Mitochondria were observed as a continuous reticulum of long, interconnected tubules in control cells. However, severe abnormalities in mitochondrial morphology were observed in cells of patients under investigation.

P1, P2 and P4 displayed similar abnormalities in mitochondrial morphology. In each case, the mitochondrial reticulum was fragmented at regular intervals into short tubules, although the length and distribution of these tubules varied considerably between the patients. In cells of P1, the mitochondrial reticulum was fragmented into very short tubules, which were very sparsely distributed, and almost all cells had large areas of cytoplasm without mitochondria. In cells of P2, the reticulum consisted of longer, straighter tubules, which overlapped in a chaotic arrangement, although in many cells the reticulum did not look fragmented at all; only 50-60 %

of cells had large areas of cytoplasm without mitochondria and up to 20 % of cells appeared normal. In cells of P4, tubules of intermediate length relative to those in cells of P1 and P2 were observed, although they were tortuous rather than straight; 50-60 % of cells had large areas of cytoplasm without mitochondria and only 5-10 % of cells appeared normal.

Perinuclear clusters of small mitochondrial “aggregates” were also observed in cells of P1, P2 and P4 (2-5 aggregates per cell), although the proportion of cells containing these aggregates varied amongst the patients: 30-40 % of cells in cultures from P1, 10-20 % of cells in cultures from P2, and 20-30 % of cells in cultures from P4. In each case it was not clear whether these structures were individual swollen mitochondria or aggregates of smaller organelles.

P3 showed a very different mitochondrial morphology phenotype from the other patients. Most notably, there were perinuclear clusters of large mitochondrial “aggregates” in 50 % of cells (5-10 aggregates per cell); interestingly, at least some of these aggregates appeared to be donut-shaped rather than solid, spherical structures. In the majority of cells, the mitochondrial reticulum was highly fused, with skinny, tortuous, long tubules in a dense, chaotic arrangement, concentrated around the nucleus. However, there was massive phenotypic variation between cells, in terms of both the density of the reticulum and the length of tubules (some cells displayed a sparse, highly fragmented reticulum, like that seen in P1). 20-30 % of cells had large areas of cytoplasm without mitochondria. 5-10 % of cells appeared normal.

3.3 SUBCELLULAR DISTRIBUTION OF THE PYRUVATE DEHYDROGENASE COMPLEX

Immunofluorescent staining of the E1α and E2 subunits of the PDH complex was carried out on patient fibroblasts, as described in Section 2.7, in order to investigate the subcellular distribution of the PDH complex. Images are shown in Figure 3.2. The PDH complex had a punctate distribution in cells of all patients, with co-localisation observed between the E1α and E2

subunits in each case. Excess anti-E2 antibody resulted in non-specific background staining and large, fluorescent green puncta in the extracellular space in some images, particularly those of control cells and P4 cells. However, it was still clear that, in control cells, puncta were arranged in long, straight rows that interconnected and spread throughout the entire cytosol, consistent with the morphology of the mitochondrial matrix observed by MitoTracker® staining; it was also clear that the distribution of the PDH complex was very different between control cells and cells of the patients under investigation.

P1, P2 and P4 displayed similar abnormalities in the distribution of the PDH complex, but to varying degrees of severity. P1 had the most severe phenotype: fewer, larger puncta were observed, rows of puncta were sparsely distributed, and there were large areas without puncta in every cell. The phenotype of P4 was very similar, although rows of puncta were shorter and more densely packed, consistent with the morphology of the mitochondrial matrix observed by MitoTracker® staining, and up to 10 % of cells appeared normal. P2 had the mildest phenotype, with upto 50 % of cells showing normal staining.

Once again, P3 showed a very different phenotype from the other patients. PDH puncta were not obviously arranged in rows but densely clustered around the nucleus in many cells. They were smaller than normal at the extremities of cells and larger than normal close to the nucleus. Very large puncta were observed in 50 % of cells, presumably corresponding to the large mitochondrial aggregates observed by MitoTracker® staining. Many cells had large areas of cytosol without puncta. Some cells had very small, sparsely distributed puncta. There were few cells, if any, with normal staining.

3.4 SUBCELLULAR DISTRIBUTION/ACTIVITY OF CYTOCHROME C OXIDASE

The subcellular distribution of COX was analysed by cytochemical staining in patient fibroblasts, as described in Section 2.8. This technique also gave information about the activity of the enzyme, since the intensity of staining is proportional to the activity. Images are shown in Figure 3.3. In control cells, staining revealed long, straight, interconnecting tubules extending throughout the entire cytosol, in a pattern identical to that shown by MitoTracker® staining of the mitochondrial matrix. However, two different patterns of staining were observed in cells of the patients under investigation.

P1 and P2 displayed similar abnormalities in COX staining, although the phenotype in P1 was much more severe. In cells of P1, only sparsely distributed short tubules were stained, staining was very faint and there were large areas without staining in every cell; some cells appeared to be negative, although the proportion of negative cells was difficult to quantify because staining was so faint; furthermore, some perinuclear aggregates of COX were observed, consistent with the mitochondrial aggregates observed by MitoTracker® staining. In P2, some cells appeared normal and very few were negative, although staining was generally faint and uneven, with some distinct aggregates of COX.

Interestingly, staining was mosaic in cultures of cells from P3 and P4, with 95 % of cells negative for staining in cultures from P3 and 20-40 % of cells negative for staining in cultures from P4. In each case, the remaining cells showed very faint, diffuse staining (it was not possible to distinguish tubular structures in most cells) and no normal cells were observed.

3.5 AMOUNT AND SUBCELLULAR DISTRIBUTION OF MITOCHONDRIAL DNA

Patient fibroblasts were stained with PicoGreen® reagent and MitoTracker® Red CMXRos simultaneously, as described in Section 2.9, in order to analyse the mtDNA content and distribution of nucleoids in the mitochondrial matrix. PicoGreen® reagent stains both mtDNA and nuclear DNA, so nuclei appeared bright green in all cells. Images are shown in Figure 3.4. In control cells, nucleoids appeared as hundreds of tiny foci located close together but evenly distributed along every tubule of the mitochondrial reticulum. However, cells of all four patients under investigation displayed abnormalities in the mtDNA content and distribution of nucleoids.

P1 and P2 displayed similar abnormalities in the mtDNA content and distribution of nucleoids, with P1 displaying the more severe phenotype. Patient cells contained fewer, larger foci with large areas of the cytosol lacking foci altogether, particularly at the extremities of cells. No cells with normal PicoGreen® staining were observed.

In cells of P3 and P4, there were fewer, smaller foci and large areas of cytosol without foci in most cells, although some cells appeared normal for PicoGreen® staining. In P3, mtDNA accumulated in the large mitochondrial aggregates clustered around the nucleus.

3.6 MITOCHONDRIAL MEMBRANE POTENTIAL

$\Delta\psi_m$ was analysed in patient fibroblasts by staining the mitochondrial matrix with JC-1, as described in Section 2.10. Images are shown in Figure 3.5. In cells of all patients, the mitochondrial reticulum was stained green with short tubular sections stained red, particularly in the extremities of cells, and mitochondrial morphology was similar to that observed by MitoTracker® staining in each case. However, there was no significant difference in the ratio of

red to green JC-1 fluorescence between cells from the control and those from patients under investigation, indicating that $\Delta\psi_m$ was normal in these patients.

3.7 COMPLEMENTATION ANALYSIS

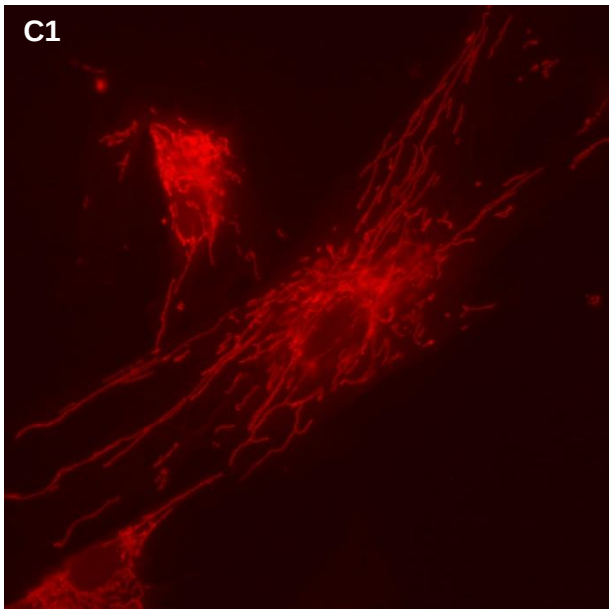
In an effort to place patients into different categories according to genotype, fibroblasts from patients under investigation were fused together in pairwise combinations by incubation in PEG, as described in Section 2.11, and the resulting heterokaryons were stained with MitoTracker® Red CMXRos to check for complementation of the mitochondrial morphology defects. For controls, cells from the control were fused to each other and to cells from each of the four patients. Images are shown in Figures 3.6 and 3.7.

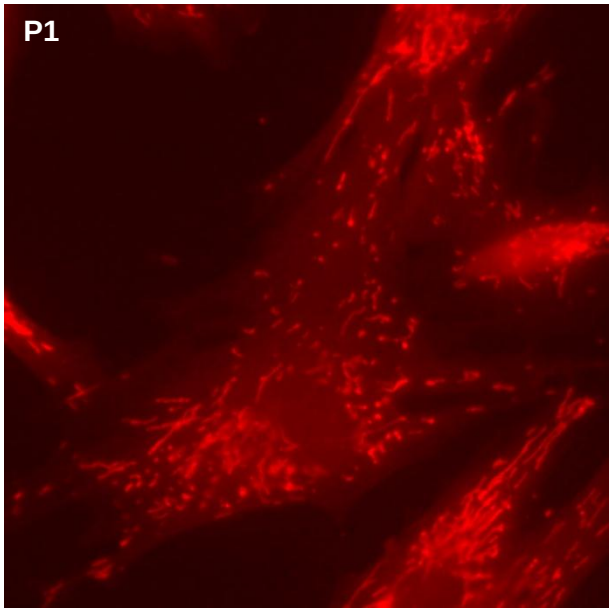
Heterokaryons resulting from fusion of control cells to each other had a mitochondrial network with morphology very similar to that of individual cells (although the reticulum was particularly dense around the nuclei in the centre of the cell), indicating that the fusion process does not affect the morphology of the mitochondria. Furthermore, fusion of control cells to cells from each of the patients under investigation resulted in complementation of the mitochondrial morphology defects in 60-80 % of the resulting heterokaryons; presumably the remaining heterokaryons were the result of fusion of patient cells to themselves and therefore retained the mitochondrial morphology defects observed in the unfused cells.

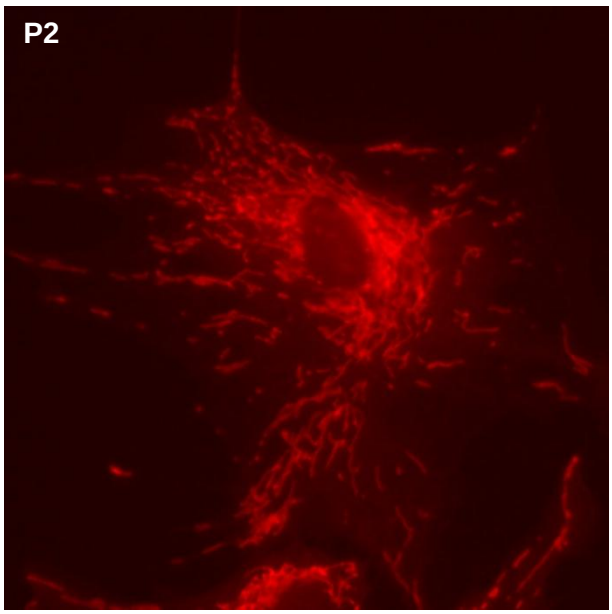
No complementation of mitochondrial morphology defects was observed in heterokaryons resulting from pairwise fusions between cells from P1, P2 and P4. P1/P2 heterokaryons displayed a mitochondrial network that was fragmented at regular intervals into short tubules, which were tortuous, chaotically arranged and particularly dense around the nucleus; small mitochondrial aggregates were also observed, consistent with observations of unfused cells. P1/P4 heterokaryons resembled P1/P2 heterokaryons but the mitochondrial reticulum was more

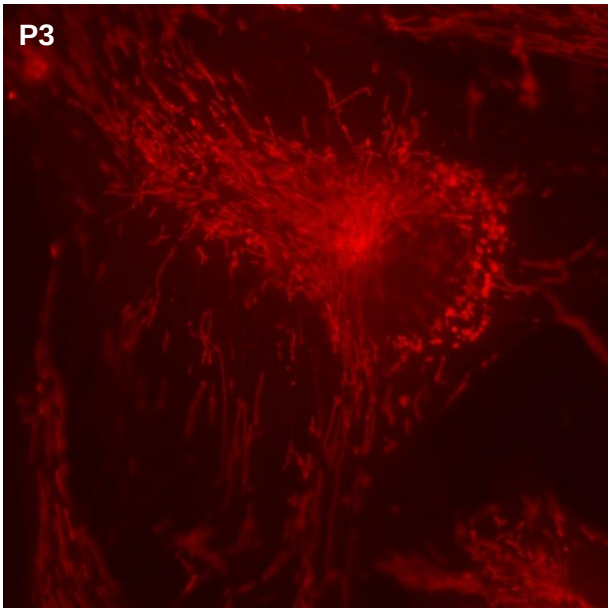
fragmented and less dense, and large areas of cytoplasm had little or no mitochondrial network, consistent with observations of unfused cells. Similarly, P2/P4 heterokaryons resembled patient P1/P2 heterokaryons but showed a mitochondrial reticulum that was denser and less fragmented, consistent with observations of unfused cells.

Interestingly, some degree of complementation was seen in heterokaryons resulting from fusion of cells from P3 with those of P1, P2 and P4, most notably in heterokaryons resulting from fusion of cells from P1 and P3. 60-80 % of P1/P3 heterokaryons had a continuous mitochondrial network with long, straight tubules; of these heterokaryons, approximately half had a network that was still skinny and very dense around the nucleus and half had a network that looked normal. Very few heterokaryons had mitochondrial aggregates and, in those that did, aggregates were small. Less than 5 % of unfused cells showed large mitochondrial aggregates, suggesting that almost all cells from P3 had fused with those from P1, and therefore that the absence of large mitochondrial aggregates in P1/P3 heterokaryons was due to complementation. P2/P3 heterokaryons resembled P1/P3 heterokaryons, except that only 40-60 % of them had a continuous mitochondrial network and very few looked normal. Similarly, 20-40 % of P3/P4 heterokaryons had a continuous network and the remainder had a skinny, fragmented network concentrated around the nucleus, although no mitochondrial aggregates were observed, suggesting partial complementation.


C1


P1


P2



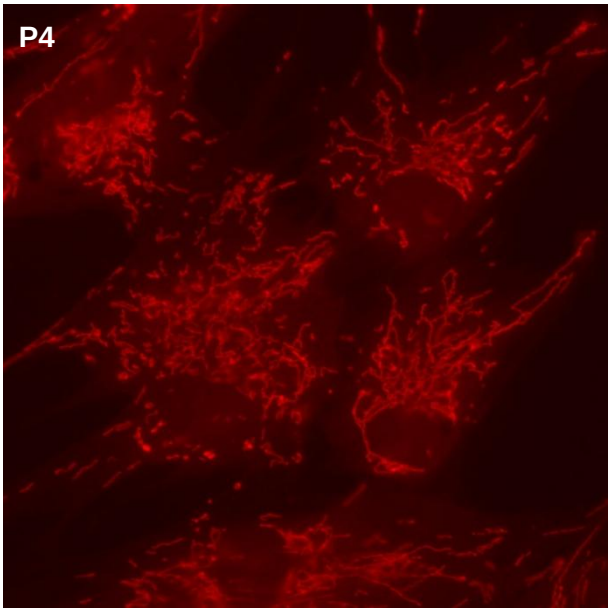
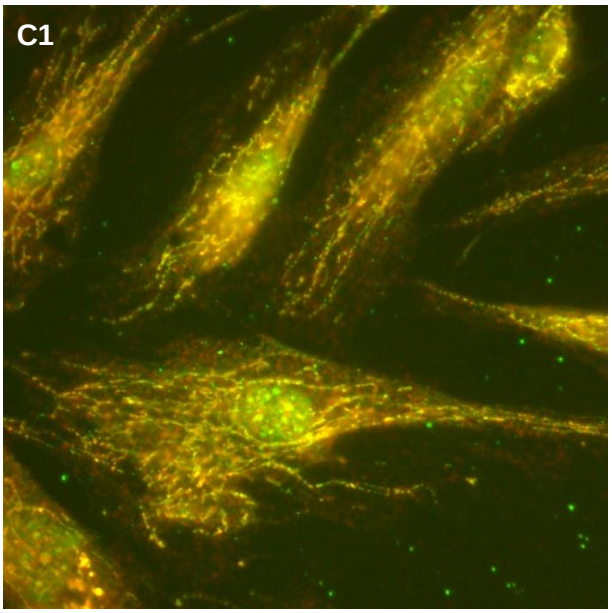
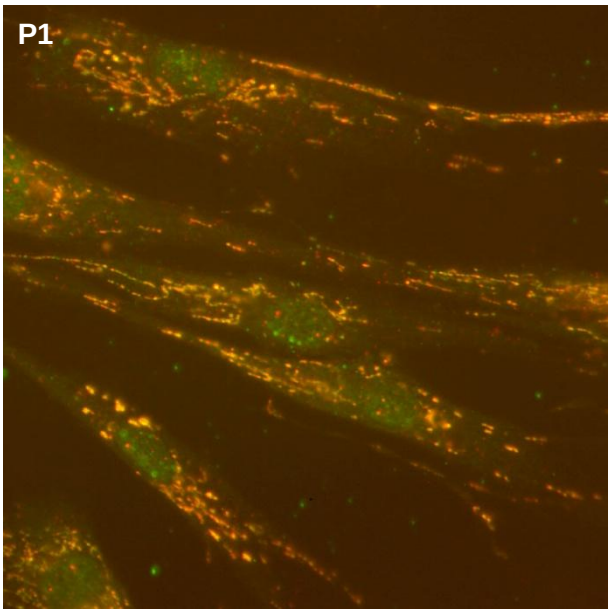
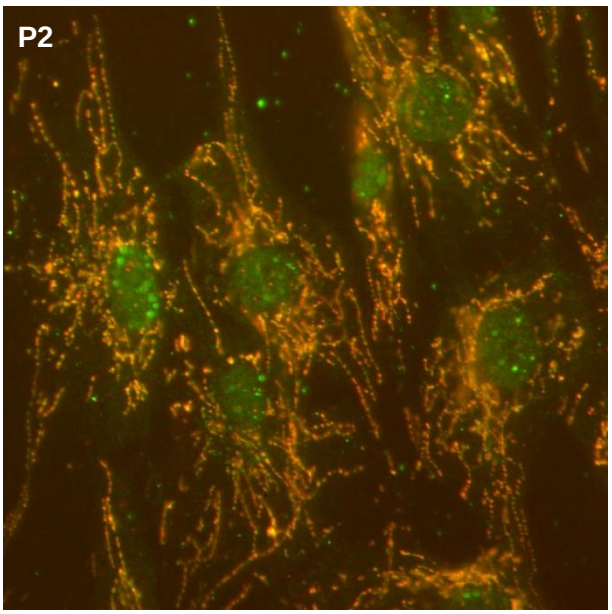


Figure 3.1 Staining of the mitochondrial matrix with MitoTracker® Red CMXRos in fibroblasts from C1 and from patients under investigation. Mitochondria were observed as a continuous reticulum of long, interconnecting tubules in cells of C1. In cells of P1, P2 and P4, the mitochondrial reticulum was fragmented at regular intervals into short tubules, although the length and distribution of tubules varied considerably between the patients. In cells of P3, the mitochondrial reticulum was highly fused and consisted of very long, skinny tubules organized in a dense, chaotic network, concentrated around the nucleus. Most notably, perinuclear clusters of large mitochondrial aggregates were observed in 50 % of cells in cultures from P3.


C1


P1


P2

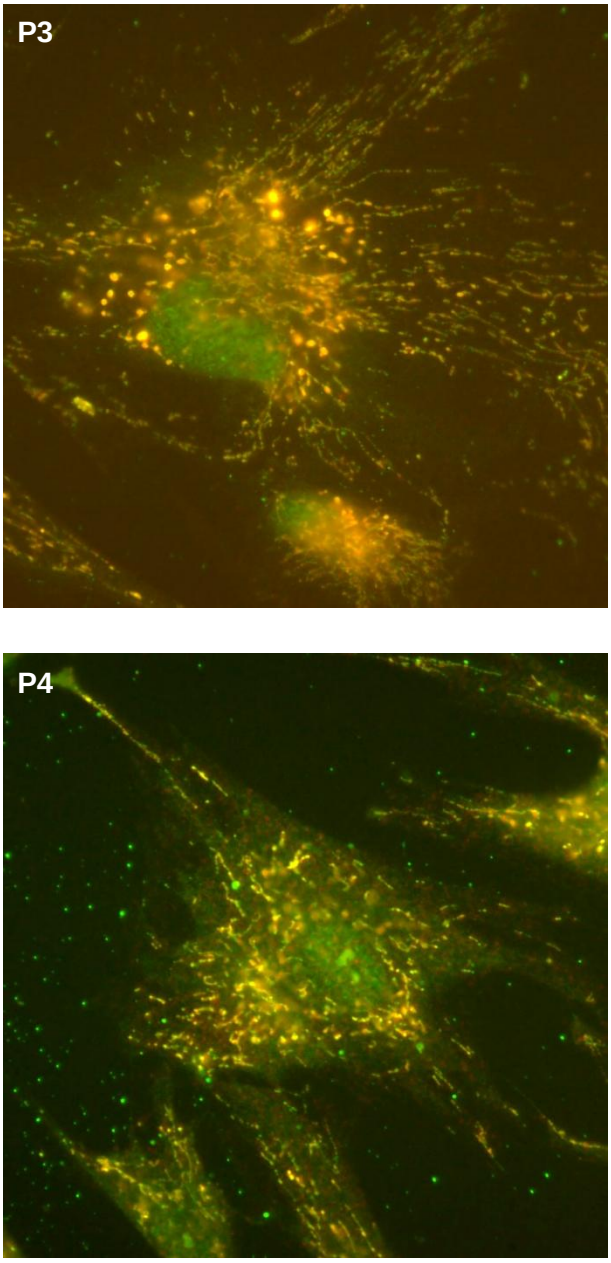
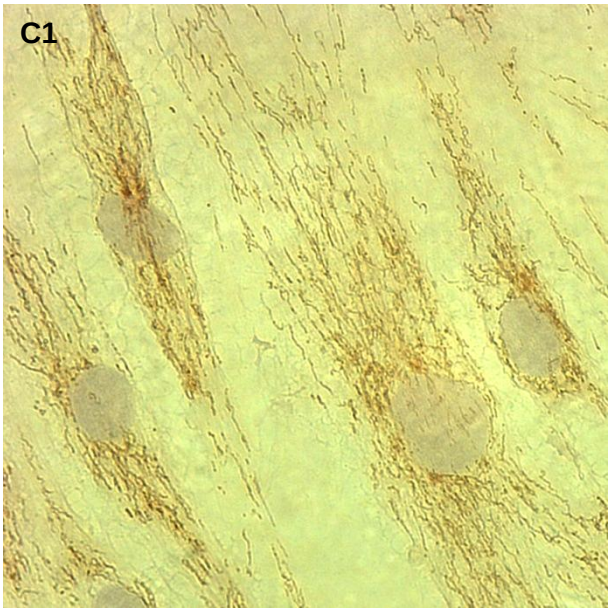
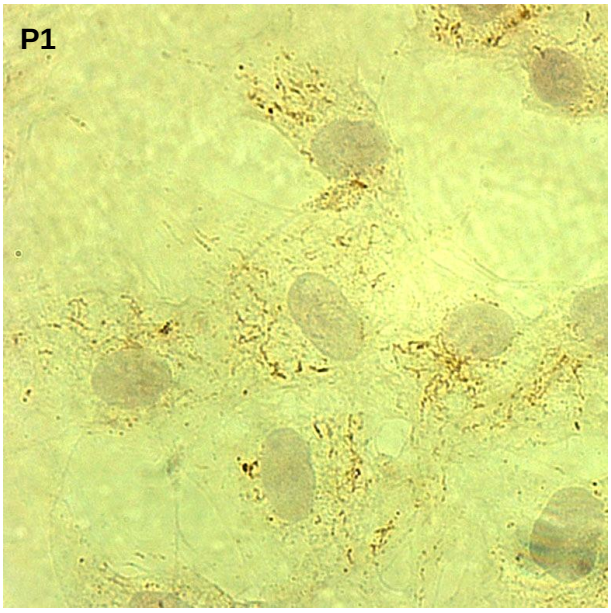
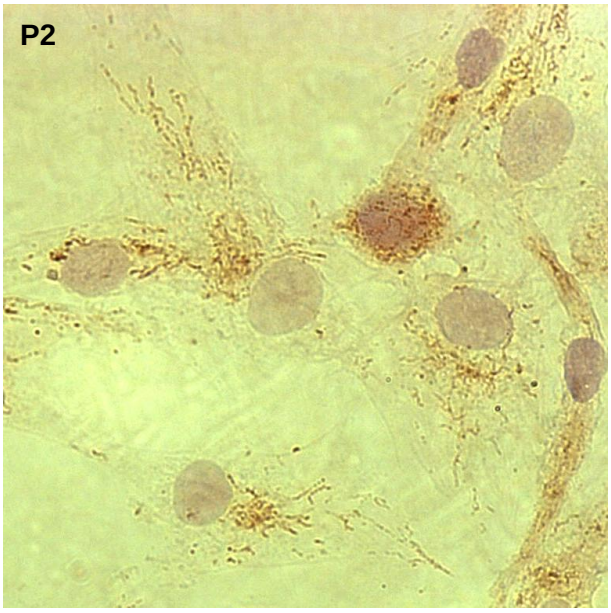


Figure 3.2 Immunofluorescent staining of the PDH complex, using antibodies against the E1α subunit (red, Alexa Fluor® 594) and the E2 subunit (green, Oregon Green®), in fibroblasts from C1 and from patients under investigation. The PDH complex had a punctate distribution in cells of all patients, with co-localisation observed between the E1α and E2 subunits in each case. In C1 cells, puncta were arranged in long, straight rows that interconnected and spread throughout the entire cytosol. In cells of P1, P2 and P4, there were fewer, larger puncta, rows of puncta were more sparsely distributed and there were large areas of the cytosol that lacked puncta altogether. In cells of P3, puncta were smaller than normal at cell extremities and larger than normal close to the nucleus, and the PDH complex was concentrated in large perinuclear aggregates in 50 % of cells.


C1


P1


P2

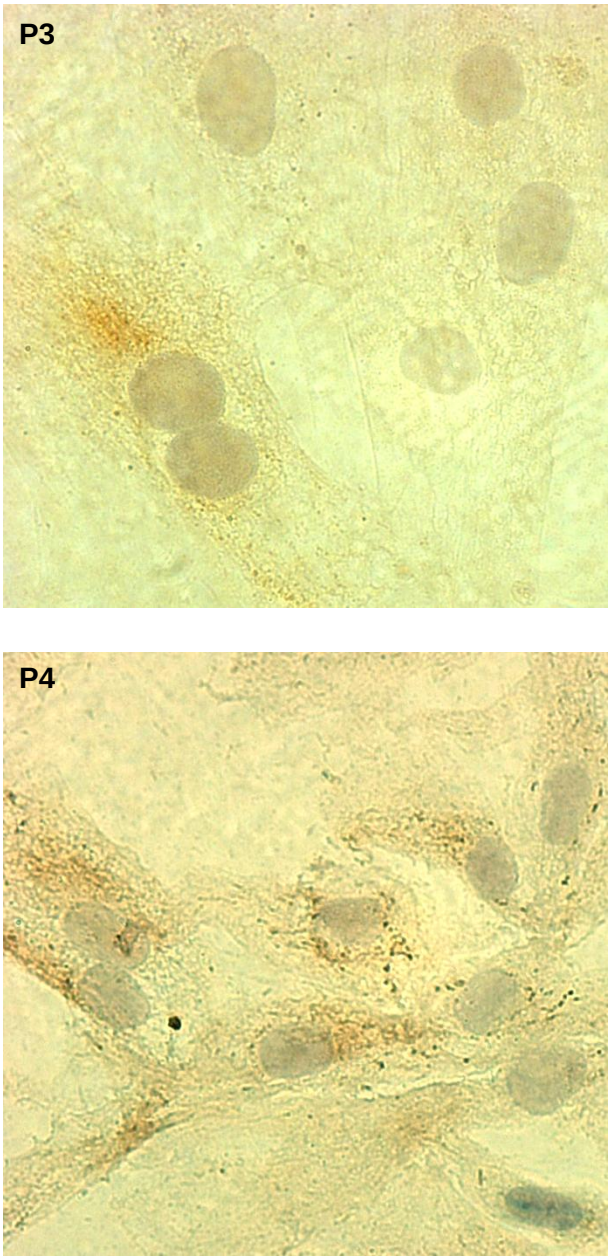
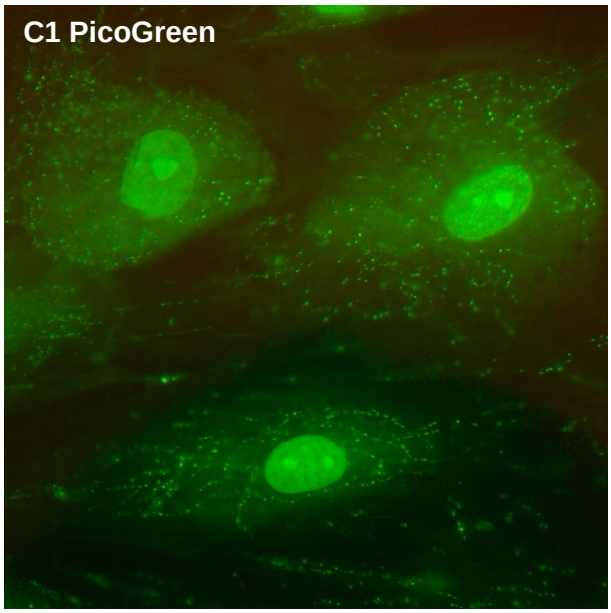
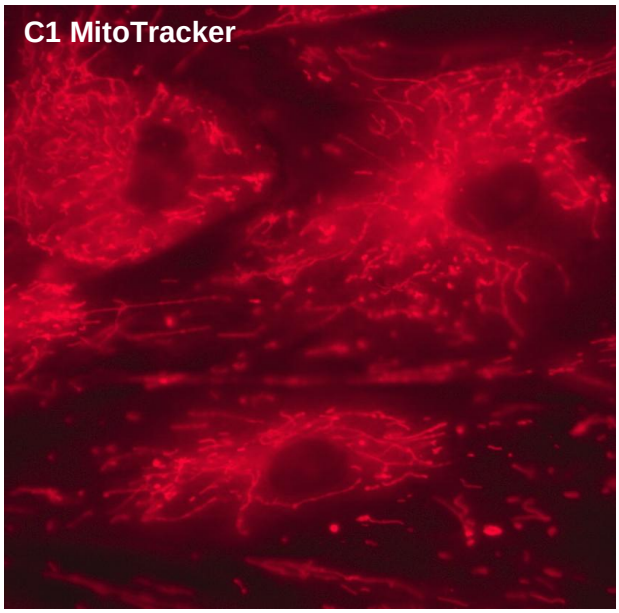
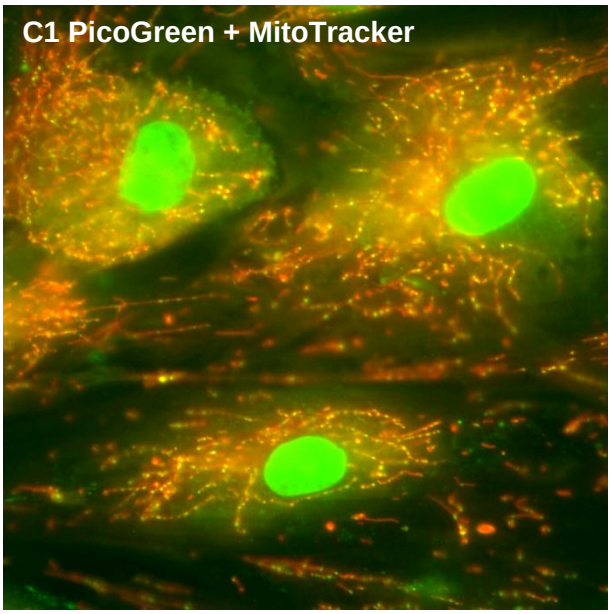
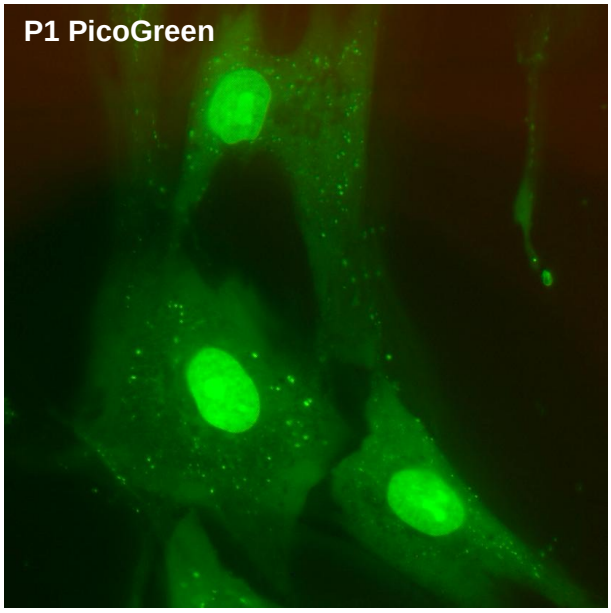


Figure 3.3 Cytochemical staining of COX, using exogenous DAB and cytochrome c, in fibroblasts from C1 and from patients under investigation. Haematoxylin was used to counterstain nuclei blue to enable cells with little or no COX staining to be identified. In cells of C1, staining revealed long, straight, interconnecting tubules extending throughout the entire cytosol. In cells of P1 and P2, only sparsely distributed short tubules were stained, staining was faint and there were large areas of the cytosol without staining altogether. In cells of P3 and P4, staining was mosaic (95 % of cells were negative for staining in cultures from P3 and 20-40 % of cells were negative for staining in cultures from P4) and positive cells had faint, diffuse staining (it was not possible to distinguish tubular structures) in each case.

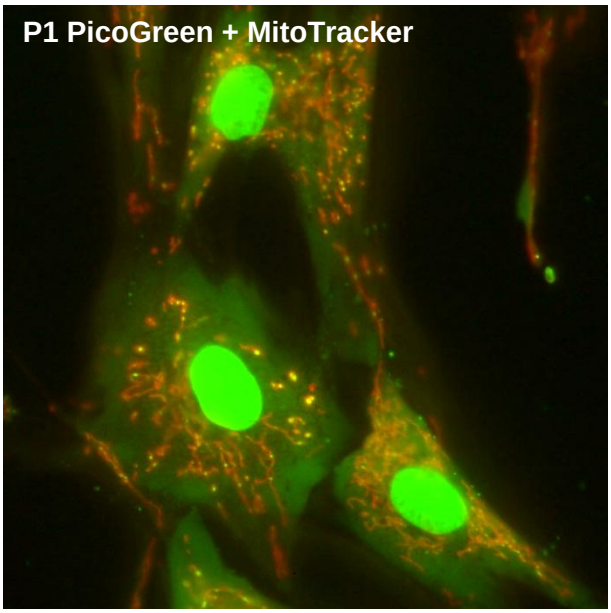

C1 PicoGreen

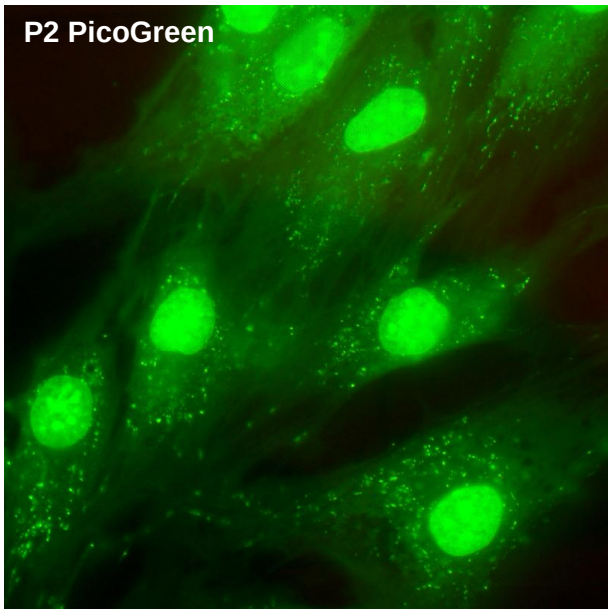

C1 MitoTracker

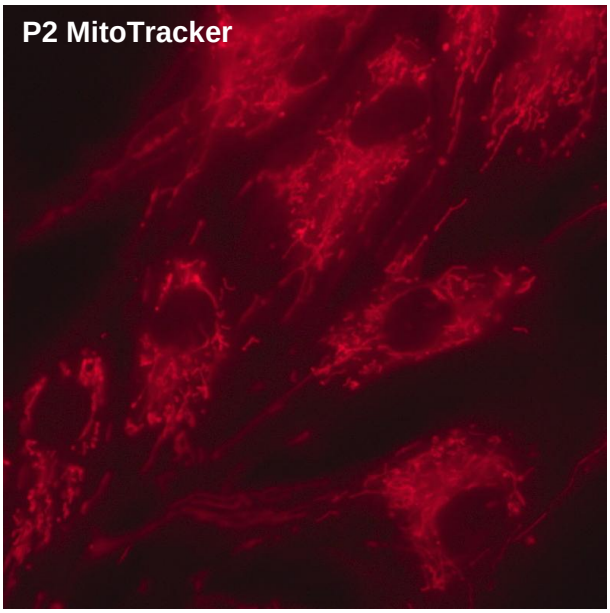

C1 PicoGreen + MitoTracker

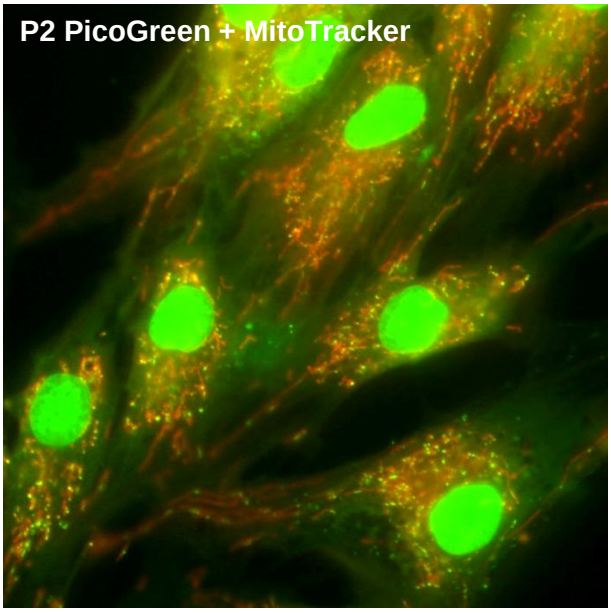

P1 PicoGreen

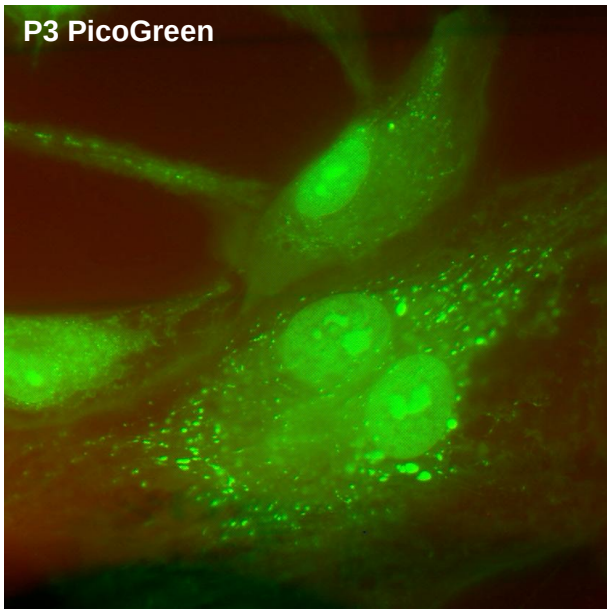

P1 MitoTracker

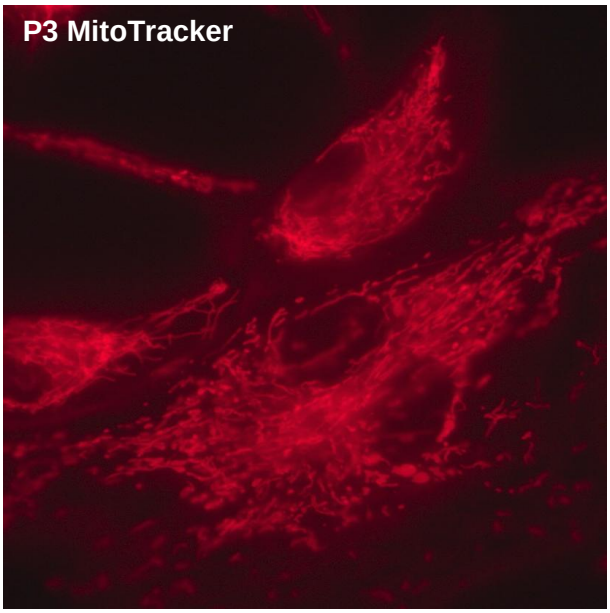

P1 PicoGreen + MitoTracker

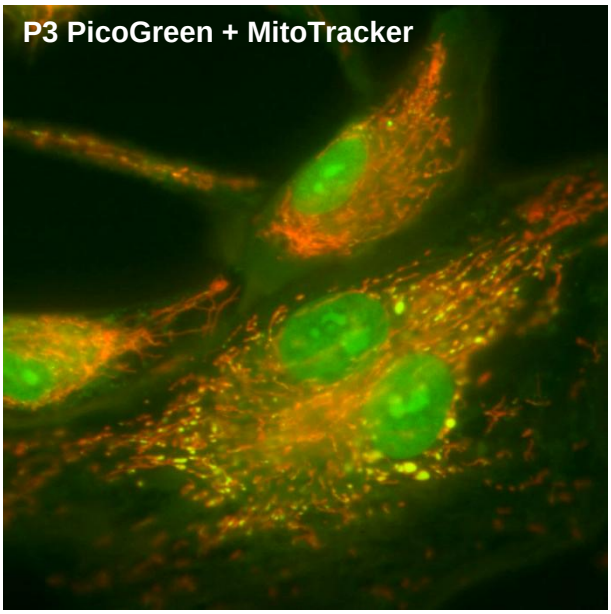

P2 PicoGreen


P2 MitoTracker


P2 PicoGreen + MitoTracker


P3 PicoGreen


P3 MitoTracker


P3 PicoGreen + MitoTracker

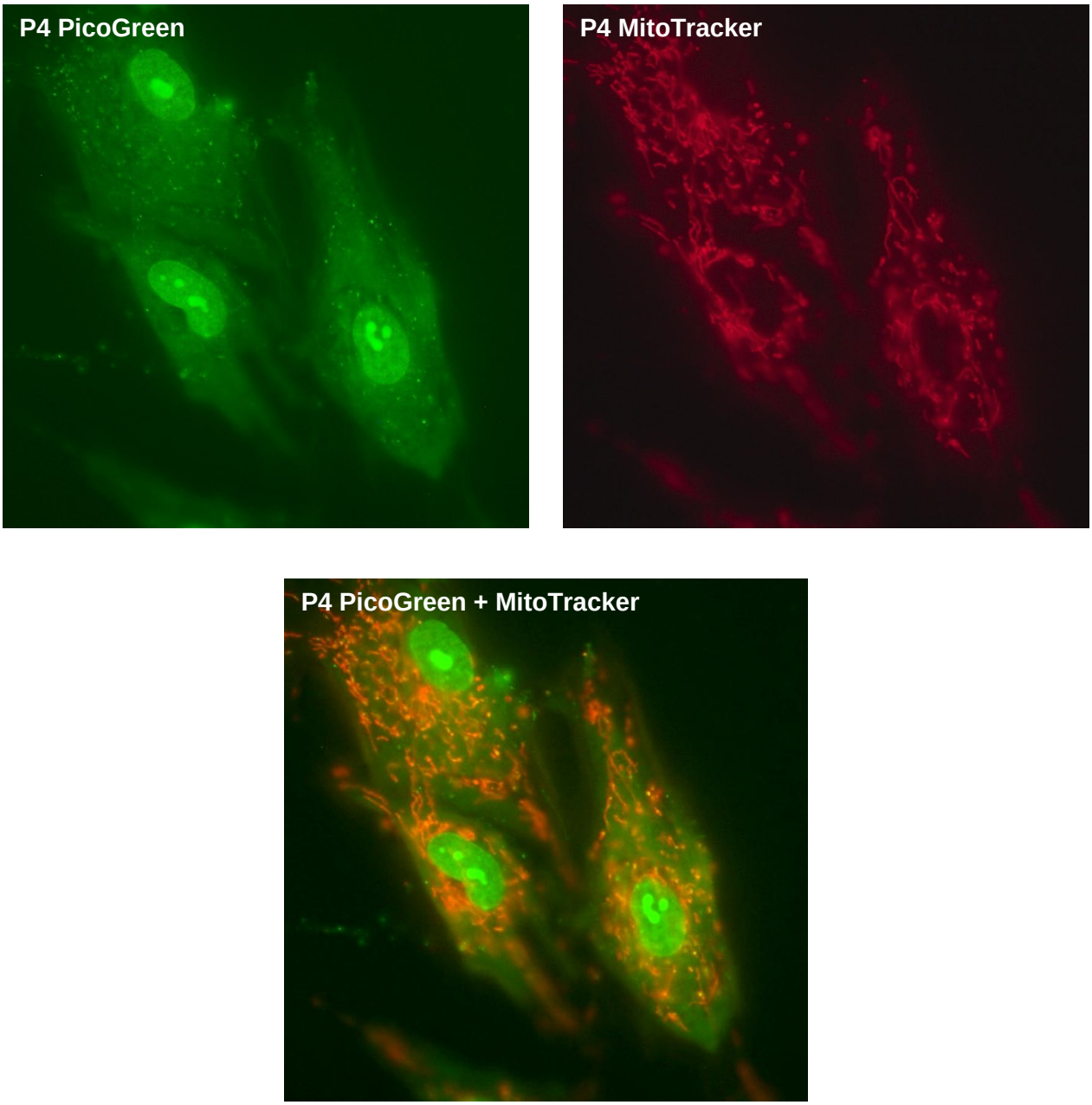
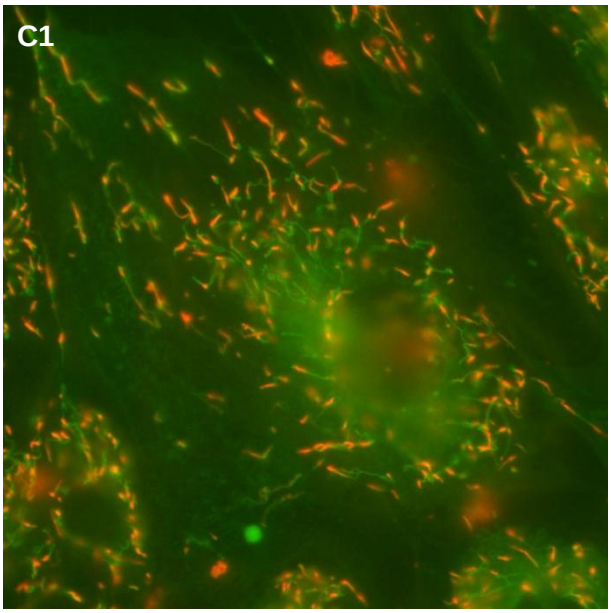
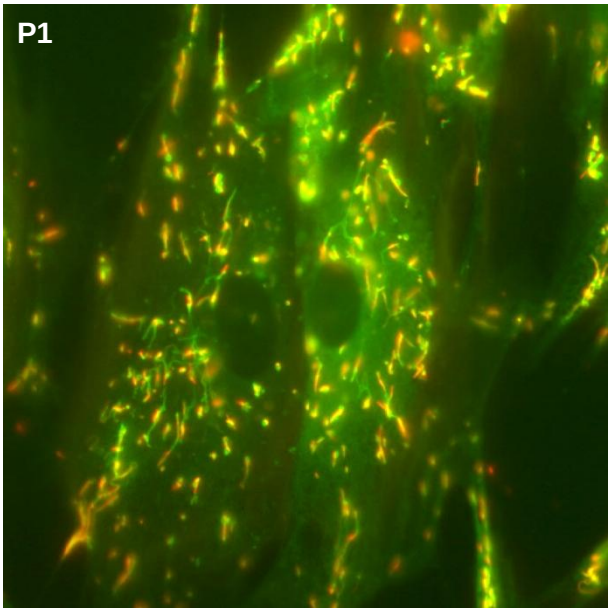
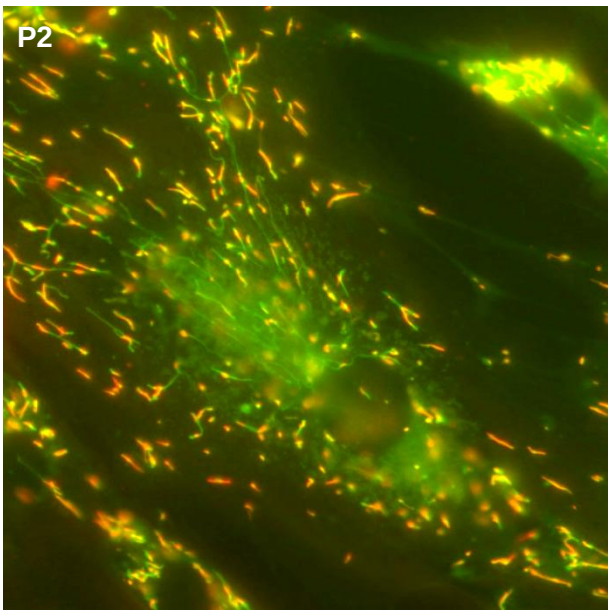


Figure 3.4 Staining of mtDNA and nuclear DNA with PicoGreen® reagent and staining of the mitochondrial matrix with MitoTracker® Red CMXRos in fibroblasts from a control and from patients under investigation. Images taken using both separated and combined colour channels are shown. Co-localisation was observed between mtDNA in nucleoids stained by PicoGreen® reagent and mitochondrial tubules stained by MitoTracker®. In cells of the control, mitochondrial nucleoids appeared as hundreds of tiny foci, evenly distributed throughout the entire mitochondrial matrix. In cells of P1 and P2, there were fewer, larger nucleoids (especially in P1) and large areas of the cytosol lacking nucleoids altogether, particularly at the extremities of cells. In cells of P3 and P4, there were fewer, smaller nucleoids. In P3, mtDNA accumulated in large mitochondrial aggregates, clustered around the nucleus in 50 % of cells.


C1


P1


P2

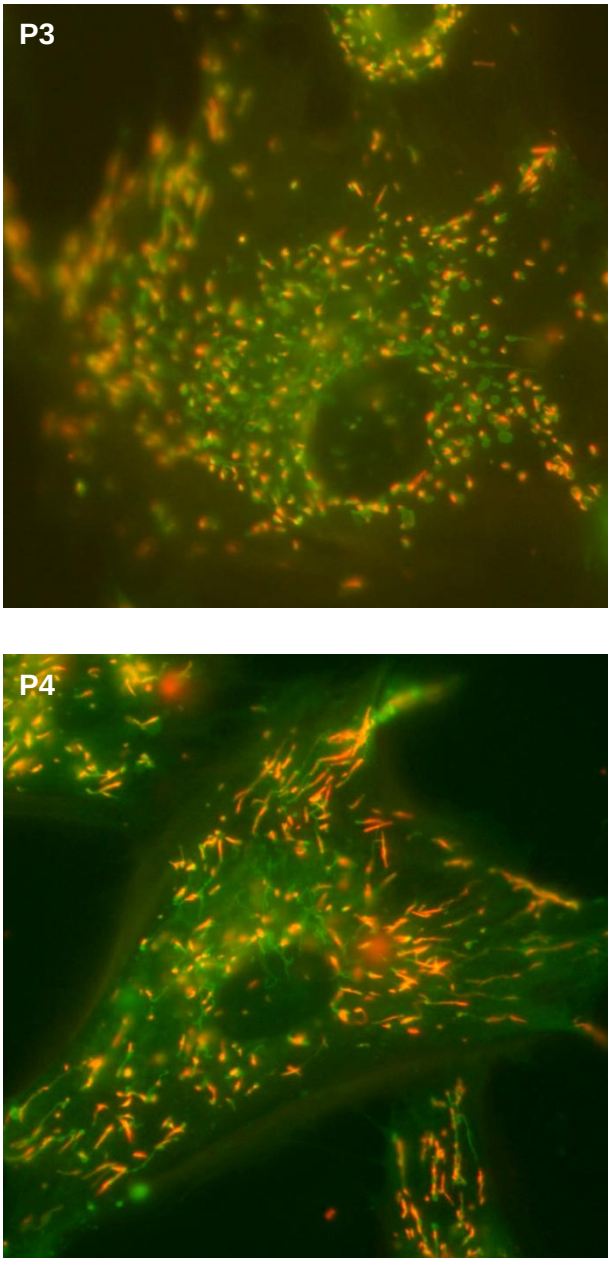
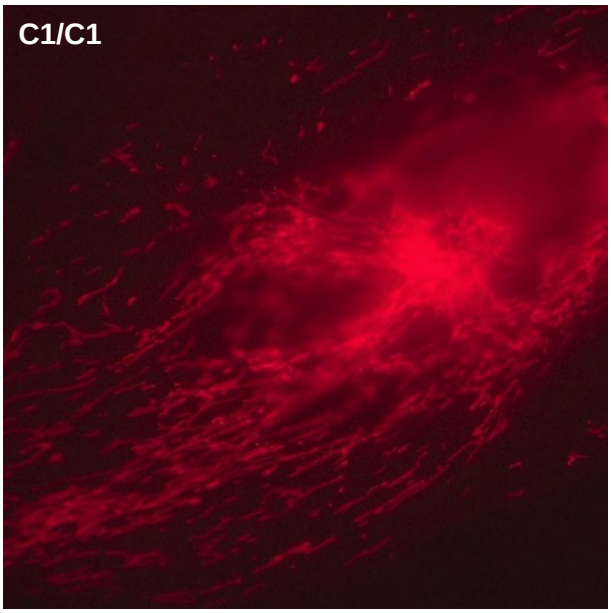
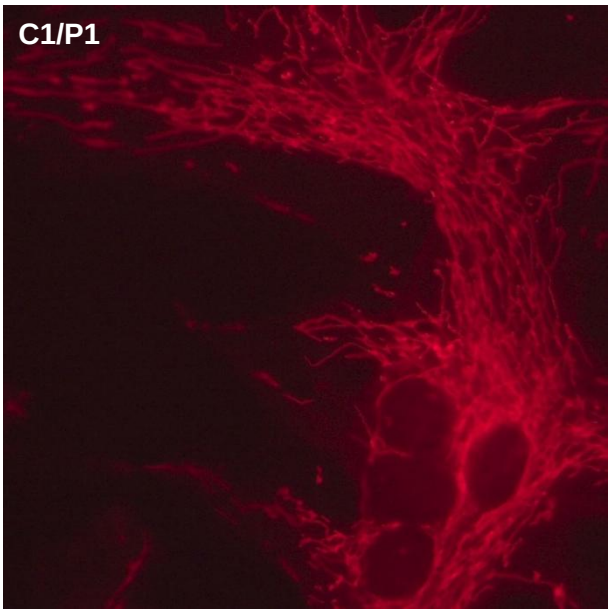
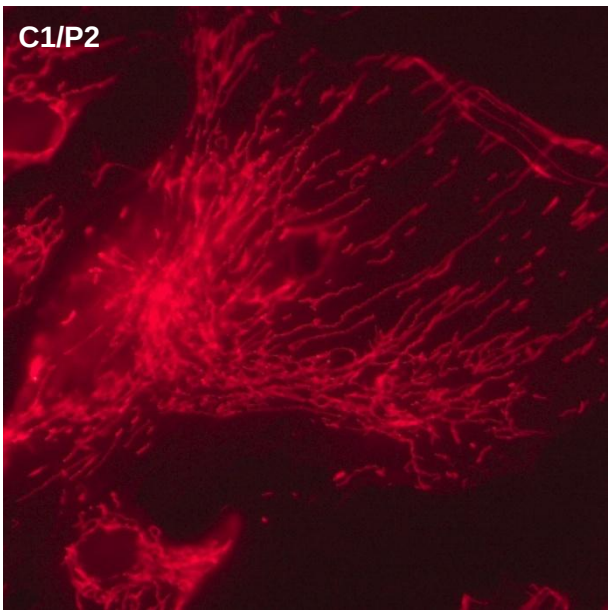
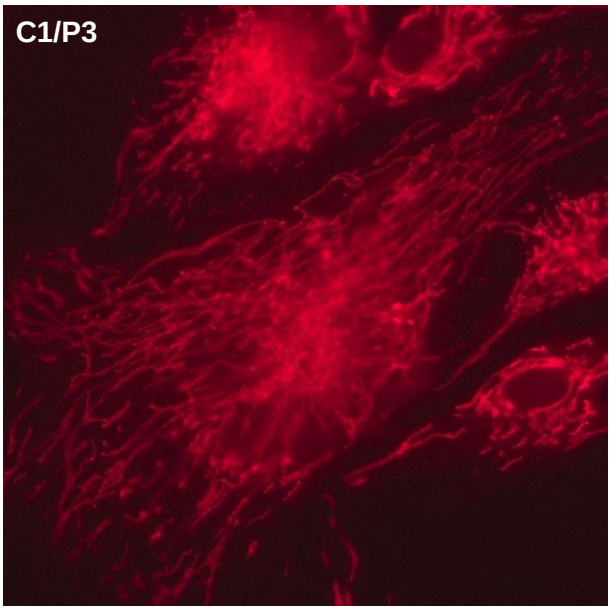


Figure 3.5 Staining of the mitochondrial matrix with JC-1 in fibroblasts from C1 and from patients under investigation. In cells of all patients, the mitochondrial reticulum was stained green with short tubular sections stained red, particularly in the extremities of cells. There was no difference in the ratio of red to green fluorescence between control cells and those from patients under investigation, although the morphology of the mitochondria highlighted by JC-1 staining was similar to that observed by MitoTracker® Red CMXRos staining in each case.


C1/C1


C1/P1


C1/P2



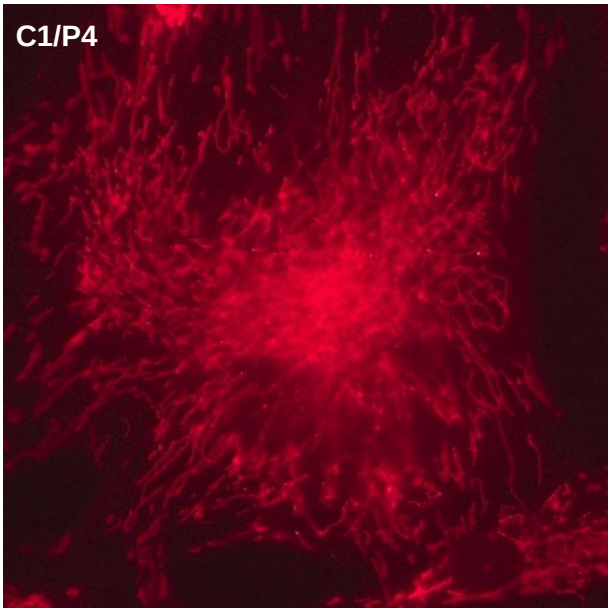
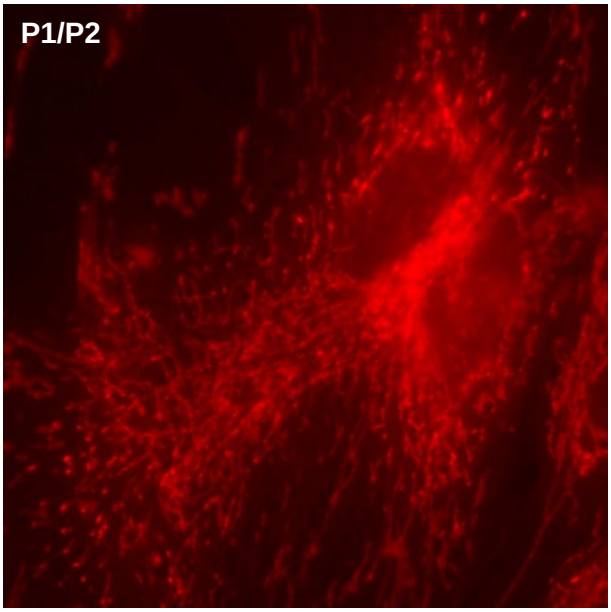
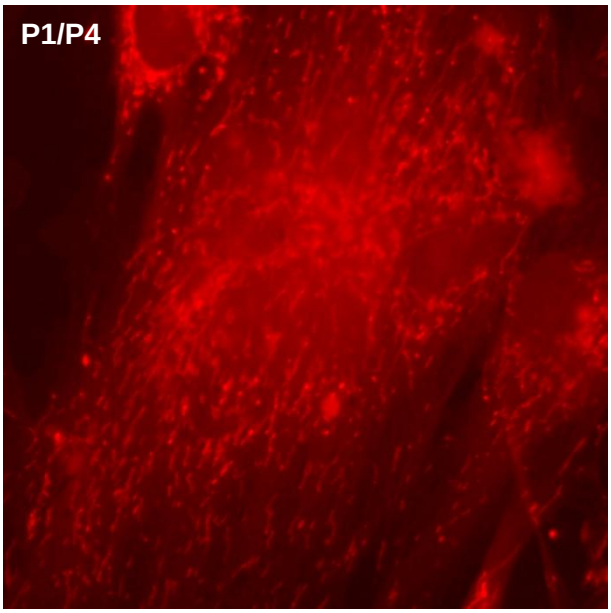
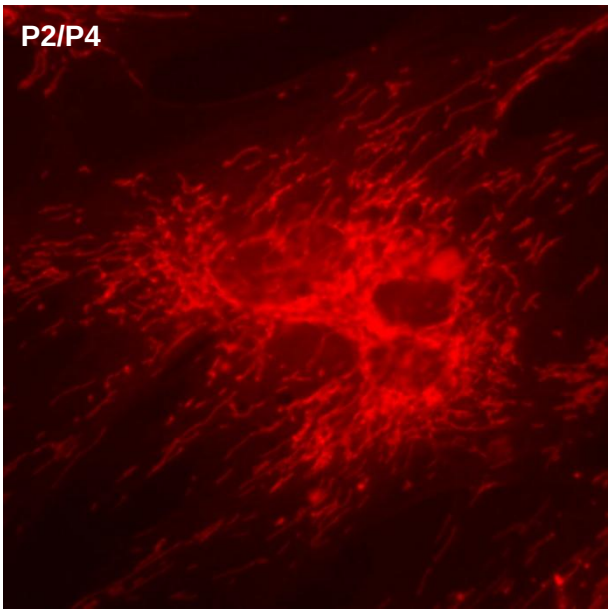
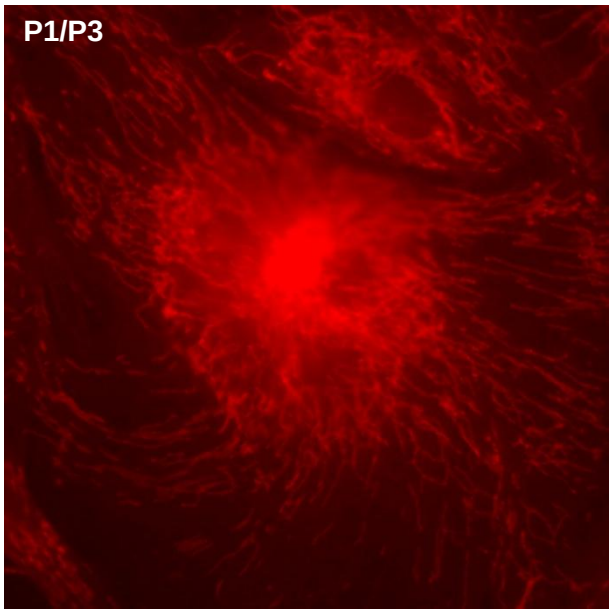


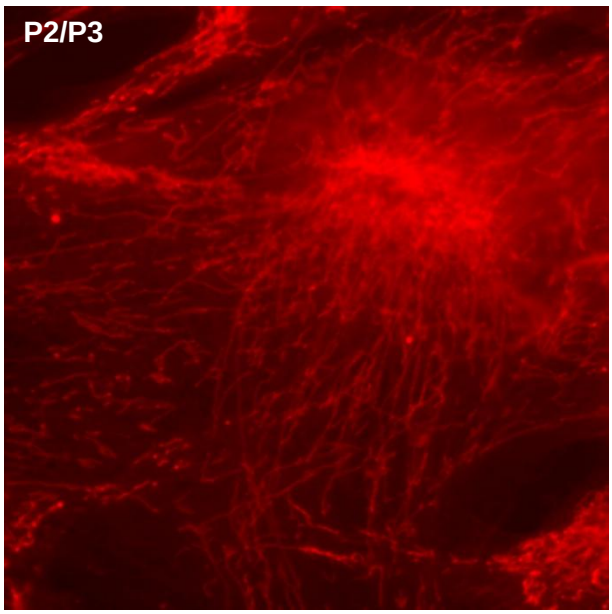
Figure 3.6 Heterokaryons produced by PEG-mediated fusion of fibroblasts from C1 with each other and with fibroblasts from each of the patients under investigation. The mitochondrial matrix was stained with MitoTracker® Red CMXRos in each case. Heterokaryons resulting from fusion of C1 cells to each other had a mitochondrial reticulum with morphology very similar to that of unfused cells. Fusion of C1 cells with cells from each of the patients under study resulted in complementation of mitochondrial morphology defects in 60-80 % of heterokaryons produced in each case.


P1/P2


P1/P4


P2/P4


P1/P3


P2/P3

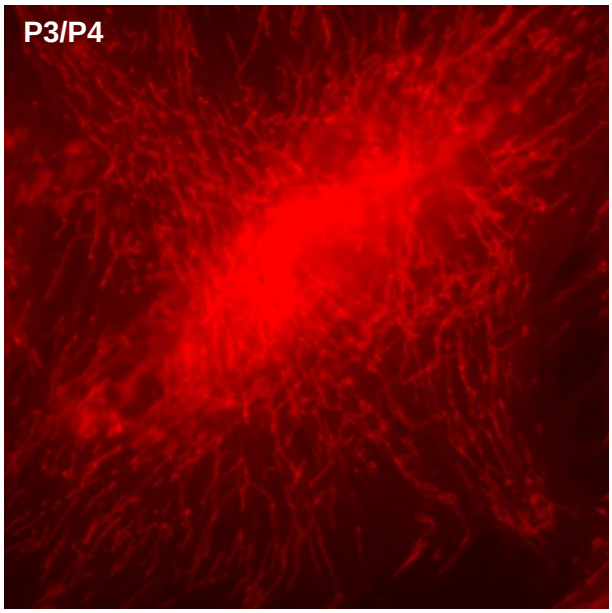

P3/P4

Figure 3.7 Heterokaryons produced by PEG-mediated fusion of fibroblasts from patients under investigation in pairwise combinations. The mitochondrial matrix was stained with MitoTracker® Red CMXRos in each case. No complementation of mitochondrial morphology defects was seen in heterokaryons resulting from pairwise fusions between cells from P1, P2 and P4. Some complementation was seen in heterokaryons resulting from fusion of cells from P3 with those of the other patients, particularly with those from P1. Most notably, no large mitochondrial aggregates were observed in these heterokaryons.

3.8 SEQUENCE ANALYSIS OF CANDIDATE GENES

Sequence variants in candidate genes were identified based on alignment of patient sequences with reference sequences defined in Section 2.12.2 (listed in Appendix 3). Sequence variants were described using standard rules of nomenclature (den Dunnen and Antonarakis, 2001), available at www.hgvs.org/mutnomen. Sequence variants were analysed at the level of DNA only therefore corresponding changes in protein sequence have been predicted not tested. Identification numbers are shown for sequence variants recorded as single nucleotide polymorphisms (SNPs) in the Ensembl database. BLAST searches of the human EST database were carried out for sequence variants not recorded as SNPs in the Ensembl database. Transcripts with deletions and/or insertions relative to the reference sequence are shown as a percentage of total transcripts, estimated from relative peak heights in sequencing chromatograms. Sequence variants found in candidate genes in patients under investigation are shown in Table 3.2. Sequence variants and splice variants in candidate genes in controls were not investigated, apart from those in the *TRAK1* gene. Each gene is discussed in turn below.

3.8.1 *AKAP1*

No sequence variants were found in the *AKAP1* coding sequence in P1 and P4. However, two silent SNPs, c.378T>C (ID rs2230772) and c.891T>C (ID rs1050515), were found in P2 and P3. P2 was homozygous for both SNPs. P3 was heterozygous for both SNPs.

Gene	Sequence variant			Patient			
	DNA	Protein (predicted)	Ensembl SNP ID	P1	P2	P3	P4
AKAP1	c.378T>C	-	rs2230772	-	Hom	Het	-
	c.891T>C	-	rs1050515	-	Hom	Het	-
DNM1L	c.120A>C	-	rs10844308	Het	Het	Het	-
	c.252G>A	-	rs2272238	Het	Het	Het	-
	c.918A>G	-	rs10844318	Het	Het	Het	-
	c.1597_1674del (c.EX15del)	p.S533_K558del	n/a	20 %	10 %	20 %	25 %
	c.1597_1707del (c.EX15_16del)	p.S533_N569del	n/a	60 %	55 %	45 %	50 %
	c.1968C>T	-		-	Het	-	-
FIS1	-	-	n/a	-	-	-	-
MFN1	c.1568C>G	p.P523R	rs7637065	Hom	Hom	Hom	Hom
MFN2	-	-	n/a	-	-	-	-
RHOT1	c.1458A>G	-	rs16967164	Het	-	Hom	Het
	c.1740_1835del (c.EX19del)	p.P580_F612delinsP	n/a	20 %	25 %	45 %	25 %
	c.1740_1958del (c.EX19_20del)	p.P580_R653delinsP	n/a	60 %	50 %	50 %	50 %
RHOT2	c.123C>G	-	rs7204542	Hom	Het	Het	Het
	c.223_276del (c.EX5del)	p.A75_K92del	n/a	10 %	10 %	10 %	10 %
	c.262G>A	p.A88T	rs11557858	-	Het	-	-
	c.306T>C	-	rs3752487	-	Het	-	-
	c.708C>T	-	rs3743912	-	Het	-	-
	c.734G>A	p.R245Q	rs1139897	-	Het	Het	Het
	c.748_749ins82bp (IN10)	p.G250delinsG250fsX341	n/a	20 %	35 %	50 %	35 %
	c.1273C>T	p.R425C	rs3177338	-	Hom	Het	Het
	c.1386A>G	-	rs1128550	-	Hom	Het	Het
TRAK2	c.424G>A	p.V142I	rs13022344	Het	Hom	Hom	Het
	c.888C>T	-	rs2256584	Hom	Hom	Hom	Hom
	c.1583C>T	p.T528I	rs2244438	Het	-	-	Het

Table 3.2 Sequence variants found in candidate genes in patients under investigation, based on alignment of patient sequences with reference sequences defined in Section 2.12.2 (listed in Appendix 3). Sequence variants were described using standard rules of nomenclature (den Dunnen and Antonarakis, 2001), available at www.hgvs.org/mutnomen. Sequence variants were analysed at the level of DNA only therefore corresponding changes in protein sequence shown in the table have been predicted not tested. Identification numbers are shown for sequence variants recorded as SNPs in the Ensembl database. -, no change from reference sequence. n/a, non-applicable. Hom, homozygous. Het, heterozygous. Transcripts with deletions and/or insertions relative to the reference sequence are shown as a percentage of total transcripts, estimated from relative peak heights in sequencing chromatograms. Amplification and sequencing of *TRAK1* is discussed in Section 3.8.8.

3.8.2 *DNM1L*

P1, P2 and P3 were heterozygous for three silent SNPs in the *DNM1L* coding sequence: c.120A>C (ID rs10844308), c.252G>A (ID rs2272238) and c.918A>G (ID rs10844318). P2 was also heterozygous for c.1968C>T, a sequence variant not listed in the Ensembl database or found in a BLAST search of the human EST database. None of the sequence variants were found in P4.

Skipping of exon 15, c.1597_1674del, and skipping of exons 15 and 16 together, c.1597_1707del, were observed in all four patients. However, the reading frame downstream remained the same in each case and the c.1597_1674del and c.1597_1707del transcripts correspond to the other two Ensembl transcripts validated by the CCDS project (IDs CCDS8730 and CCDS8728 respectively), suggesting that they occur as a result of normal *DNM1L* expression. The full-length, c.1597_1674del and c.1597_1707del transcripts were present in varying proportions in the patients, although the c.1597_1707del transcript was by far the most abundant in each case.

Gene	Sequence variant		Patient			
	DNA	Ensembl SNP ID	P1	P2	P3	P4
DNM1L	g.1596+66C>T (IN14)	rs7302970	Het	Het	Het	-
	g.1596+227_230del (IN14)		Het	Het	Het	-
	g.1596+248G>A (IN14)		Het	Het	Het	-
	g.1597_114C>T (IN14)		Het	Het	Hom	Hom
	g.1674+36T>A (IN15)	rs4506737	Het	Het	Het	-
	g.1707+637C>T (IN16)		-	-	-	Het
	g.1707+861_862del (IN16)		Het	Het	Het	-
	g.1708_778_779insAA (IN16)		Het	Het	Het	-
	g.1708_320C>T (IN16)		Het	Het	Het	-

Table 3.3 Sequence variants in introns 14, 15 and 16 of the *DNM1L* gene in patients under investigation. -, no change from reference sequence. Hom, homozygous. Het, heterozygous.

Exons 15 and 16 and adjacent introns were amplified from gDNA in all patients. In each case, the exonic coding sequences and intron/exon boundaries were normal. Various intronic

sequence variants were identified, as shown in Table 3.3, although there appeared to be no correlation between the pattern of intronic sequence variants and the relative levels of the full-length, c.1597_1674del and c.1597_1707del transcripts.

3.8.3 *FIS1*

No sequence variants were found in the *FIS1* coding sequence in any of the patients. However, P3 was homozygous for duplication of an 11 bp sequence, TCCTTTCCCTG, beginning 56 bp downstream of the STOP codon, in the 3'UTR. This sequence variant was not recorded in the Ensembl database but was present at a frequency of 9 % in a BLAST search of the human EST database, suggesting that it is not pathogenic.

3.8.4 *MFN1*

All four patients were homozygous for a SNP in *MFN1*, c.1568C>G (ID rs7637065), which results in the substitution of arginine for proline at position 523 in the protein.

3.8.5 *MFN2*

No sequence variants were found in the *MFN2* coding sequence in any of the patients.

3.8.6 *RHOT1*

The only SNP found in the *RHOT1* coding sequence, c.1458A>G (ID rs16967164), was silent. P1 and P4 were heterozygous for this SNP whereas P3 was homozygous. The SNP was not found in P2.

Skipping of exon 19, c.1740_1835del, and skipping of exons 19 and 20 together, c.1740_1958del, was observed in all four patients. However, the reading frame downstream remained the same in each case and the c.1740_1835del and c.1740_1958del transcripts correspond to the other two Ensembl transcripts validated by the CCDS project (IDs CCDS32611 and CCDS32612 respectively), suggesting that they occur as a result of normal RHOT1 expression. The full-length, c.1740_1835del and c.1740_1958del transcripts were present in varying proportions in the patients, although the c.1740_1958del transcript was by far the most abundant in each case.

Gene	Sequence variant		Patient			
	DNA	Ensembl SNP ID	P1	P2	P3	P4
RHOT1	g.1836_345G>T (IN19) g.1836_215T>A (IN19)		Het Het	- -	Hom -	Het -

Table 3.4 Sequence variants in intron 19 of the RHOT1 gene in patients under investigation. -, no change from reference sequence. Hom, homozygous. Het, heterozygous.

Exons 19 and 20 and adjacent intronic regions were amplified from gDNA in all patients. Introns 18 and 19 were sequenced in full but time constraints prevented complete sequencing of intron 20 (~13.4 kb). The exonic coding sequences and intron/exon boundaries were normal in each patient. Two sequence variants were found in intron 19, as shown in Table 3.4, although there appeared to be no correlation between the pattern of intronic sequence variants and the relative levels of the full-length, c.1740_1835del and c.1740_1958del transcripts.

3.8.7 *RHOT2*

Seven SNPs were found amongst the patients in the *RHOT2* coding sequence: c.123C>G (ID rs7204542), c.262G>A (ID rs11557858), c.306T>C (ID rs3752487), c.708C>T (ID rs3743912), c.734G>A (ID rs1139897), c.1273C>T (ID rs3177338) and c.1386A>G (ID rs1128550). Four of these SNPs are silent: c.123C>G, c.306T>C, c.708C>T and c.1386A>G. The three remaining

SNPs result in amino acid substitutions in the protein: c.262G>A results in substitution of threonine for alanine at position 88, c.734G>A results in substitution of glutamine for arginine at position 245, and c.1273C>T results in substitution of cysteine for arginine at position 425. P1 was homozygous for c.123C>G. P2 was heterozygous for c.123C>G, c.262G>A, c.306T>C, c.708C>T and c.734G>A, and homozygous for c.1273C>T and c.1386A>G. P3 and P4 were both heterozygous for c.123C>G, c.734G>A, c.1273C>T and c.1386A>G.

Low-level skipping of exon 5, c.223_276del, was found in all four patients to the same degree and did not alter the reading frame downstream.

Exonisation of intron 10 between exons 10 and 11, c.748_749insIN10, was observed to varying degrees in all four patients. This was confirmed by sequencing the cDNA PCR product with the reverse primer 5'-CTGGTCGTGCTTCTCAAACA-3', which binds in exon 12. Exonisation of intron 10 alters the reading frame downstream, introducing premature STOP codons into the sequence and resulting in a truncated protein of only 340 amino acid residues. In P3, as much as 50 % of all *RHOT2* transcripts showed exonisation of intron 10.

Gene	Sequence variant		Patient			
	DNA	Ensembl SNP ID	P1	P2	P3	P4
RHOT2	g.222+163G>A (IN4)		-	Het	-	-
	g.223-295T>C (IN4)		-	Hom	Het	Het
	g.223-224Gdel (IN4)		-	Het	Het	Het
	g.277-206G>C (IN5)		-	Hom	Het	Het
	g.277-190T>C (IN5)		-	Hom	Het	Het
	g.277-109A>C (IN5)		-	-	-	Het
	g.277-82C>T (IN5)	rs3752489	-	Het	Het	Het
	g.277-52G>A (IN5)	rs62032482	-	Het	-	-

Table 3.5 Sequence variants in introns 4 and 5 of the *RHOT2* gene in patients under investigation. -, no change from reference sequence. Hom, homozygous. Het, heterozygous.

Exons 5-10 and adjacent introns were amplified from gDNA in all patients. Sequence variants identified in these exons are shown in Table 3.2. All intron/exon boundaries were normal in

each patient. Various sequence variants were identified in introns 4 and 5, as shown in Table 3.5, but all other introns were normal and there appeared to be no correlation between the pattern of sequence variants and the skipping of exon 5 or the exonisation of intron 10.

3.8.8 *TRAK1*

TRAK1 amplified well from cDNA from the two controls but not from cDNA from patients under investigation, as shown in Figure 3.8 A. In each case, it was thought that this could be due to the introduction of a premature termination codon in the *TRAK1* coding sequence, as a result of either a point mutation or aberrant splicing that altered the reading frame downstream, which resulted in degradation of the *TRAK1* transcript by NMD. Cells from the two controls and from the patients under investigation were therefore cultured in emetine, as described in Section 2.2.4, to inhibit NMD. However, it was also not possible to amplify *TRAK1* from cDNA derived from emetine-treated cells from patients under investigation, whereas *TRAK1* amplified well from cDNA derived from emetine-treated control cells, as shown in Figure 3.8 B. The failure to amplify *TRAK1* was not due to the quality of the cDNA template because part of *POLG* (c.1044_2506), the housekeeping gene that encodes the catalytic subunit of the mtDNA polymerase, was amplified from cDNA from all patients to a similar degree, as shown in Figure 3.8 C. Taken together, these results suggest that *TRAK1* transcription is down-regulated in all four patients under investigation.

The sequence of *TRAK1* was analysed in cells from the two controls and the patients under investigation after culture in the presence and absence of emetine in each case. *TRAK1* was amplified by nested PCR, as described in Section 2.12.9, using PCR products shown in Figure 3.8 A and B as template DNA. *TRAK1* nested PCR products were then purified and sequenced as normal. All *TRAK1* sequencing results are shown in Tables 3.6-3.8.

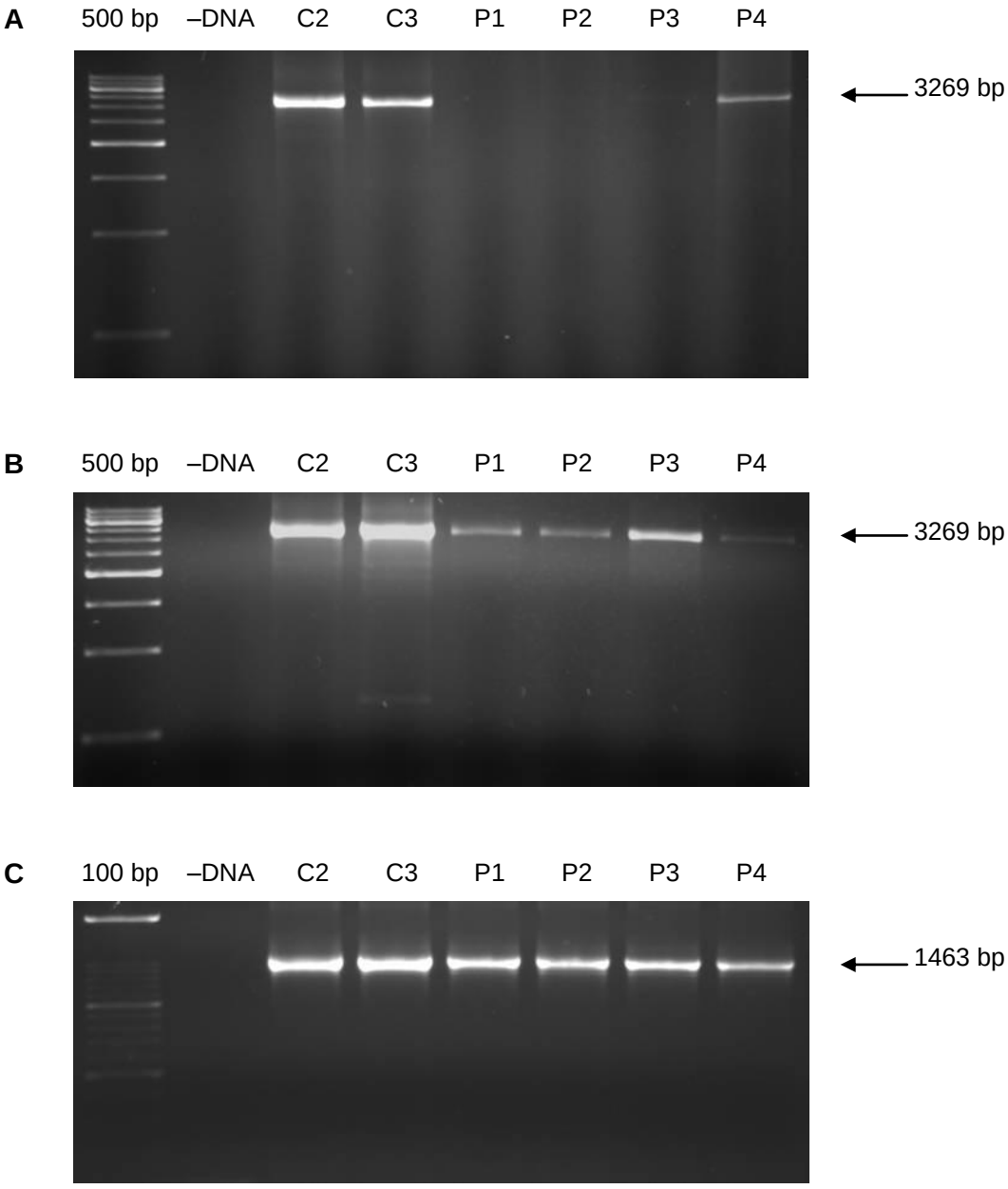


Figure 3.8 A, PCR amplification of *TRAK1* from cDNA. B, PCR amplification of *TRAK1* from cDNA derived from cells cultured in the presence of emetine, as described in Section 2.2.4. C, PCR amplification of *POLG* c.1044_2506 from cDNA. 500 bp, DNA Molecular Weight Marker XVII. 100 bp, DNA Molecular Weight Marker XIV.

In the controls, four silent SNPs were found in the *TRAK1* coding sequence: c.1095A>G (ID rs9851455), c.1749C>T (ID rs2290134), c.1815C>T (ID rs2290133) and c.2799T>C (ID rs12487911). C2 was homozygous for c.1095A>G, c.1749C>T and c.2799T>C. C3 was heterozygous for c.1095A>G, c.1749C>T and c.1815C>T. Deletion of the last 63 bp of exon

14, c.1901_1963del, was found in approximately 70 % transcripts in both controls. This deletion does not alter the reading frame downstream and is likely to be a result of normal *TRAK1* expression. Cell culture in emetine increased the ratio of full-length to c.1901_1963del transcripts to 50:50 but otherwise had no effect on the sequence of transcripts in either control. These results are shown in Table 3.6.

In the patients under investigation, *TRAK1* sequencing results were different for cells cultured in the presence and absence of emetine, as shown in Tables 3.7 and 3.8, and are therefore considered to be unreliable. However, it is likely that sequencing results from the emetine-treated samples are more reliable than those from the non-emetine-treated samples, at least in the case of P1, P2 and P3. Bands corresponding to PCR products can be clearly seen for all patients on the gel in Figure 3.8 B but not for P1, P2 and P3 on the gel in Figure 3.8 A, suggesting that levels of *TRAK1* transcripts are particularly low in cells of these patients cultured under normal conditions. Trace amounts of contaminating DNA in the PCR products may have been accidentally amplified by the nested PCR. Furthermore, *TRAK1* sequencing from emetine-treated samples did not identify any additional SNPs or deletions/insertions in transcripts from P1, P2 and P3 compared with those identified in transcripts in the controls. In any case, time constraints prevented full sequencing of the *TRAK1* gene from gDNA (>200 kb) so the true sequence of *TRAK1* transcripts in these patients remains unknown.

Skipping of exon 4 was observed in 50 % of transcripts sequenced from non-emetine-treated cells of P3, therefore exon 4 and adjacent intronic regions were amplified from gDNA in P3. The coding sequence and intron/exon boundaries were normal. Time constraints prevented full sequencing of introns 3 and 4 (~7.8 and 3.2 kb respectively).

All patients produced *TRAK1* transcripts with deletions and/or insertions at the end of exon 14, therefore exon 14 and adjacent intronic regions were amplified from gDNA in each patient. The coding sequence and intron/exon boundaries were normal in each case. Time constraints prevented full sequencing of introns 13 and 14 (~7.0 and 9.5 kb respectively), although the first section of intron 14 (covering the sequence included in transcripts from P2) was sequenced and found to contain a variation in the number of AGG repeats amongst the patients. P1 and P3 were homozygous for deletion of an AGG repeat, g.1963+130_132del (ID rs72193879). P2 was homozygous for insertion of an AGG repeat, g.1963+130_132dup (ID rs10530663). P4 and the controls were normal.

3.8.9 *TRAK2*

Three SNPs were found amongst the patients in the *TRAK2* coding sequence, c.424G>A (ID rs13022344), c.888C>T (ID rs2256584) and c.1583C>T (ID rs2244438). c.888C>T is silent whereas c.424G>A and c.1583C>T result in amino acid substitutions in the protein sequence, valine to isoleucine at position 142 and threonine to isoleucine at position 528 respectively. P1 and P4 were heterozygous for c.424G>A and c.1583C>T and homozygous for c.888C>T. P2 and P3 were homozygous for c.424G>A and c.888C>T and did not contain c.1583C>T.

Gene	Sequence variant			Patient (no emetine)		Patient (emetine)	
	DNA	Protein (predicted)	Ensembl SNP ID	C2	C3	C2	C3
TRAK1	c.1095A>G	-	rs9851455	Hom	Het	Hom	Het
	c.1749C>T	-	rs2290134	Hom	Het	Hom	Het
	c.1815C>T	-	rs2290133	-	Het	-	Het
	c.1901_1963del	p.G634_A655delinsA	n/a	70 %	70 %	50 %	50 %
	c.2799T>C	-	rs12487911	Hom	-	Hom	-

Table 3.6

Gene	Sequence variant			Patient (no emetine; nested PCR)			
	DNA	Protein (predicted)	Ensembl SNP ID	P1	P2	P3	P4
TRAK1	c.364_480del(c.EX4del)	p.K122_E160del	n/a	-	-	50 %	-
	c.1095A>G	-	rs9851455	Hom	Hom	Hom	Hom
	c.1749C>T	-	rs2290134	Hom	-	Hom	Hom
	c.1815C>T	-	rs2290133	-	-	Het	Hom
	c.1901_1963del	p.G634_A655delinsA	n/a	-	-	100 %	70 %
	c.1901_1963delins14bp*	p.G634_A655delinsD634fsX688	n/a	100 %	-	-	-
	c.1963_1964ins141bp**	p.A655delinsG655_A702	n/a	-	100 %	-	-
	c.1971T>C***	-		Het	-	-	-
	c.2799T>C	-	rs12487911	-	-	Het	-
	c.*45_*47del	n/a	rs3836498	Hom	Hom	-	-

Table 3.7

Gene	Sequence variant			Patient (emetine; nested PCR)			
	DNA	Protein (predicted)	Ensembl SNP ID	P1	P2	P3	P4
TRAK1	c.1095A>G	-	rs9851455	Hom	Hom	Hom	Het
	c.1749C>T	-	rs2290134	Hom	-	Hom	Het
	c.1815C>T	-	rs2290133	-	-	-	Het
	c.1901_1963del	p.G634_A655delinsA	n/a	50 %	50 %	50 %	35 %
	c.1901_1963delins****	p.G634_A655delins?	n/a	-	-	-	30 %
	c.2799T>C	-	rs12487911	Het	-	Hom	-
	c.*45_*47del	n/a	rs3836498	Het	Hom	-	-

Table 3.8

Table 3.6 Sequence variants found in the *TRAK1* gene in C2 and C3 after PCR amplification of *TRAK1* from cDNA derived from cells cultured in the presence and absence of emetine. -, no change from reference sequence. n/a, non-applicable. Hom, homozygous. Het, heterozygous. Transcripts with deletions and/or insertions relative to the reference sequence are shown as a percentage of total transcripts, estimated from relative peak heights in sequencing chromatograms.

Table 3.7 Sequence variants found in the *TRAK1* gene in patients under investigation after nested PCR amplification of *TRAK1* from cDNA derived from cells cultured under normal conditions. -, no change from reference sequence. n/a, non-applicable. Hom, homozygous. Het, heterozygous. Transcripts with deletions and/or insertions relative to the reference sequence are shown as a percentage of total transcripts, estimated from relative peak heights in sequencing chromatograms. *Deletion of the last 63 bp of exon 14 and insertion of 14 bp of gDNA sequence (ATCCAGTTAACAAG), 104-117 bp upstream of c.1964 (beginning of exon 15) in intron 14. The reading frame was altered downstream, introducing STOP codons and resulting in a truncated protein of 687 aa. **Insertion of 141 bp of gDNA sequence, immediately downstream of exon 14 in intron 14. The reading frame was maintained, resulting in an extended protein of 1000 aa. ***Not found in a BLAST search of the human EST database.

Table 3.8 Sequence variants found in the *TRAK1* gene in patients under investigation after nested PCR amplification of *TRAK1* from cDNA derived from cells cultured in the presence of emetine. -, no change from reference sequence. n/a, non-applicable. Hom, homozygous. Het, heterozygous. Transcripts with deletions and/or insertions relative to the reference sequence are shown as a percentage of total transcripts, estimated from relative peak heights in sequencing chromatograms. ****Deletion of the last 63 bp of exon 14 and insertion of some gDNA sequence, beginning 2251 bp upstream of c.1964 (beginning of exon 15) in intron 14. It was not possible to identify the end of the insertion sequence so it is not known if the reading frame was altered downstream.

CHAPTER 4: DISCUSSION AND FUTURE WORK

4.1 DISCUSSION

The patients studied in this project presented with early-onset metabolic disease, the key symptom of which was lactic acidosis, and acute encephalopathy. Skin fibroblasts from P1, P3 and P4 showed abnormalities in the activities of multiple mitochondrial enzymes, indicating generalised mitochondrial dysfunction. Skin fibroblasts from P2 showed highly variable PDH activity. Key features of the cellular phenotype in each patient are summarised in Table 4.1. Severe abnormalities in mitochondrial morphology were observed in each case, with concomitant abnormalities in the distributions of mitochondrial enzymes and in the amount and distribution of mtDNA.

Patient	Mitochondrial morphology	Distribution of PDH complex	Distribution/activity of COX	Distribution of mtDNA
C1	Tubular network	Puncta evenly distributed thoughout the entire network	Even distribution thoughout the entire network	Nucleoids evenly distributed thoughout the entire network
P1	Very short tubules	Fewer, larger puncta	Sparse, uneven distribution	Fewer, larger nucleoids
P2	Short tubules	Fewer, larger puncta	Sparse, uneven distribution	Fewer, larger nucleoids
P3	Collapsed around the nucleus; large aggregates in 50 % of cells	Puncta clustered around the nucleus; concentrated in large aggregates	Mosaic: 95 % negative cells; positive cells show faint, diffuse staining	Fewer, smaller nucleoids; mtDNA concentrated in large aggregates
P4	Tortuous, short tubules	Fewer, larger puncta	Mosaic: 20-40 % negative cells; positive cells show faint, diffuse staining	Fewer, smaller nucleoids; large nucleoids in some cells

Table 4.1 Key features of the cellular phenotype in patients under study relative to a control.

Several observations support the hypothesis of a primary genetic defect in mitochondrial dynamics, with secondary effects on mitochondrial metabolism, rather than *vice versa*. First, all four patients showed abnormalities in PDH activity and, since the PDH complex is entirely encoded by nuclear DNA, this argues against a primary defect in mtDNA or in a nuclear gene

encoding a protein involved in mtDNA maintenance. Second, in P1, P3 and P4, multiple enzymes are affected, arguing against a mutation in a single nuclear gene encoding an enzyme subunit or assembly factor. Third, fibroblasts from all four patients have severe abnormalities in mitochondrial morphology despite normal $\Delta\psi_m$ under basal culture conditions. In fibroblasts of patients with severe OXPHOS defects but no or only mild alterations in $\Delta\psi_m$, mitochondrial morphology is normal under basal culture conditions and dramatic alterations in mitochondrial fission and fusion rates are not observed (Guillery *et al.*, 2008a; Morán *et al.*, 2010). Fourth, mitochondrial enzymes and mtDNA are abnormally distributed throughout the matrix in a manner that reflects the abnormal mitochondrial morphology and is consistent with defects in mitochondrial connectivity.

With the exception of the single reported case of DRP1 deficiency (Waterham *et al.*, 2007), patients diagnosed with disorders of mitochondrial dynamics present first and foremost with neurological symptoms rather than metabolic disease, with onset occurring in the first two decades of life in many cases, as described in Section 1.4. It therefore seems that this project has characterised a novel group of patients with early-onset metabolic disease and encephalopathy due to a primary genetic defect in mitochondrial dynamics.

The cellular abnormalities in P1 and P2 most likely represent an imbalance in mitochondrial fission/fusion in favour of fission. In each case, the mitochondrial network is fragmented into short tubules rather than completely fragmented into small, spherical organelles, suggesting a reduction in fusion but not a complete lack of fusion (Chen *et al.*, 2003, 2005). The mitochondrial morphology in cells of P1 resembled that of *Mfn1*$^{-/-}$ MEFs, which exhibit very short mitochondrial tubules and small, spherical organelles of uniform size. The mitochondrial morphology in cells of P2 resembled that of *Mfn2*$^{-/-}$ MEFs, which show a mixture of medium-length and short tubules and spherical mitochondria of varying size. However, it is possible that the cellular abnormalities in P1 and P2 represent different severities of the same phenotype. In any case, *Mfn1*$^{-/-}$ and *Mfn2*$^{-/-}$ cells show only mild heterogeneity of

mitochondrial function, which is consistent with the partially reduced mitochondrial enzyme activities and the intact $\Delta\psi_m$ observed in the patients' cells (Chen *et al.*, 2003, 2005).

The mitochondrial morphology phenotype of P4 was also suggestive of an imbalance in mitochondrial fission/fusion in favour of fission, although several key differences were observed between the cellular phenotype of P4 and that of P1 and P2. Mitochondrial tubules were of intermediate length relative to those of P1 and P2 and were noticeably tortuous rather than straight, a morphological phenotype not reported in the literature. COX staining was mosaic in P4, with positive cells showing very faint, diffuse staining, whereas most cells stained for COX in P1 and P2. The reason for these differences is unknown.

P3 had a very different cellular phenotype from the other patients. The mitochondrial network was collapsed around the nucleus and consisted of highly elongated and interconnected mitochondrial tubules. In addition, large perinuclear "aggregates" of mitochondria were observed in 50 % of cells. mtDNA and proteins of the PDH complex were largely absent from the mitochondrial network and were concentrated in these mitochondrial "aggregates". Consistent with these observations, P3 showed the most severe biochemical phenotype of all four patients, with large reductions in the activities of the PDH complex and COX and a 2-fold increase in the activity of citrate synthase, possibly reflecting an increased mitochondrial mass. Using fluorescence microscopy, it was impossible to tell if the mitochondrial "aggregates" were clusters of mitochondria or individual swollen organelles. Some of these mitochondria were ring-shaped rather than solid spherical structures, although it was not clear if this represented circularisation of cristae or circularisation of the entire mitochondrion, including the OM.

Clusters of "giant mitochondria" have been observed in mammalian cells with defective or insufficient mitophagy (Navratil *et al.*, 2008) but a primary defect in mitophagy is unlikely in P3. PEG-mediated fusion of cells from P3 with control cells resulted in heterokaryons with a

normal mitochondrial morphology phenotype, indicating fusion of mitochondrial aggregates with the rest of the mitochondrial population. However, “giant mitochondria” resulting from defective or insufficient mitophagy do not fuse with each other or with other mitochondria in the cell (Navratil *et al.*, 2008). Furthermore, JC-1 staining of cells with “giant mitochondria” revealed that large areas of the cytoplasm have mitochondria with low $\Delta\psi_m$ (Navratil *et al.*, 2008), which was also not observed in cells of P3.

Swollen mitochondria have been observed in mammalian cells with defects in peroxisome biogenesis (Baumgart *et al.*, 2001) but a primary defect in peroxisome biogenesis is also unlikely in P3. Peroxisomal defects tend to affect mitochondrial ultrastructure rather than global dynamics. Dramatic mitochondrial tubulation and branching like that seen in cells of P3 has not been reported in cells of patients with peroxisome biogenesis disorders or in mouse models of these diseases (Baumgart *et al.*, 2001; Dirkx *et al.*, 2005; Goldfischer *et al.*, 1973). Interestingly however, a 2-fold increase in citrate synthase activity, like that seen in fibroblasts from P3, was observed in hepatocytes from mice with hepatocyte-selective elimination of peroxisomes (Dirkx *et al.*, 2005).

Based on the literature reviewed in Chapter 1, the morphological abnormalities of mitochondria observed in cells of P3 are most consistent with an imbalance in mitochondrial fission/fusion in favour of fusion (Rojo *et al.*, 2002; Santel and Fuller, 2001; Smirnova *et al.*, 1998; Yoon *et al.*, 2003), a defect in microtubule-based mitochondrial transport (Fransson *et al.*, 2006; Saotome *et al.*, 2008; Tanaka *et al.*, 1998; Varadi *et al.*, 2004), or a defect in AKAP149 (Rogne *et al.*, 2009).

Complementation analysis was carried out in order to place the patients into categories according to genotype. Patient fibroblasts were fused together in pairwise combinations and the resulting heterokaryons were stained with MitoTracker® Red CMXRos to check for complementation of the mitochondrial morphology defects. No complementation was

observed between cells of P1, P2 and P4, suggesting the possibility of a common primary genetic defect in these patients. Partial complementation was observed between cells of P3 and those of the other patients; heterokaryons showed variation in the length and branching of mitochondrial tubules but lacked the large mitochondrial aggregates seen in unfused cells of P3; this suggests the possibility of a different genetic defect in P3. These results are consistent with the mitochondrial morphology phenotypes observed in the patients. However, to assess complementation fully in this context, analysis of the distributions and activities of mitochondrial enzymes and mtDNA would be required in addition to MitoTracker® staining.

Gene	Protein	Primary function	Additional functions
AKAP1	AKAP149	OM scaffolding molecule for c-AMP-dependent phosphorylation events	Putative role in localisation of nuclear mRNAs to the OM
DNM1L	DRP1	OM fission	Peroxisomal fission
FIS1	FIS1	OM fission	Peroxisomal fission
MFN1	MFN1	OM fusion	-
MFN2	MFN2	OM fusion	Regulation of anterograde transport; ER-mitochondria tethering
RHOT1	MIRO1	Mitochondrial receptor for the anterograde transport machinery	Ca^{2+}-dependent regulation of mitochondrial fission
RHOT2	MIRO2	Mitochondrial receptor for the anterograde transport machinery	Ca^{2+}-dependent regulation of mitochondrial fission
TRAK1	TRAK1	Mitochondrial adaptor for the anterograde transport machinery	-
TRAK2	TRAK2	Mitochondrial adaptor for the anterograde transport machinery	-

Table 4.2 Candidate genes, their encoded proteins and the function(s) of those proteins in the regulation of mitochondrial dynamics in mammalian cells.

In an effort to identify the primary genetic defect in each patient, sequence analysis was carried out on candidate genes involved in mitochondrial fission, fusion and transport, as well as *AKAP1*. Candidate genes, their encoded proteins and the function(s) of those proteins in the regulation of mitochondrial dynamics are listed in Table 4.2. No pathogenic mutations were found amongst the patients, although two genetic anomalies were identified. First, *RHOT2* transcripts showed exonisation of intron 10 to varying degrees in all four patients. Exonisation of intron 10 between exons 10 and 11, c.748_749ins82bp, alters the reading frame downstream, introducing premature STOP codons into the sequence and resulting in a truncated protein of 340 amino acid residues. In P3, as much as 50 % of all *RHOT2*

transcripts showed exonisation of intron 10. Second, *TRAK1* transcription was severely downregulated in all four patients.

RHOT2 and *TRAK1* encode homologues of proteins involved in microtubule-based anterograde transport of mitochondria in *Drosophila*. *RHOT2* encodes MIRO2, one of the two human homologues of *Drosophila* dMiro, an OM protein that functions as the mitochondrial receptor for the anterograde transport machinery (Fransson *et al.*, 2003; Glater *et al.*, 2006; Guo *et al.*, 2005). *TRAK1* encodes one of the two human homologues of *Drosophila* Milton, thought to be the mitochondria-specific adaptor for the anterograde transport machinery, linking dMiro with Khc on microtubules (Brickley *et al.*, 2005; Glater *et al.*, 2006; Smith *et al.*, 2006; Stowers *et al.*, 2002). Loss of dMiro or Milton in *Drosophila* neurons results in detachment of mitochondria from kinesin, reduced anterograde transport, and perinuclear aggregation of mitochondria (Guo *et al.*, 2005; Stowers *et al.*, 2002). Conversely, overexpression of dMiro results in abnormal accumulation of mitochondria at distal synapses due to excessive anterograde transport along neuronal axons (Guo *et al.*, 2005).

The roles of dMiro and Milton in anterograde mitochondrial transport in *Drosophila* are well-defined. However, the situation in mammals is more complex and poorly understood. Both MIRO1 and MIRO2 interact with TRAK1 and TRAK2 (Fransson *et al.*, 2006) but the MIRO1-TRAK2 interaction seems to be the most important for mitochondrial transport *in vivo* (MacAskill *et al.*, 2009a,b). MIRO1 recruits TRAK2 to mitochondria, consistent with a role for TRAK2 as a mitochondria-specific adaptor (MacAskill *et al.*, 2009a). However, MIRO1 also directly interacts with KIF5 in a Ca^{2+}-dependent manner, resulting in dissociation of mitochondria from KIF5 and arrest of mitochondrial mobility at high cytosolic [Ca^{2+}] (MacAskill *et al.*, 2009b; Saotome *et al.*, 2008). The degree of functional redundancy between MIRO1 and MIRO2, and between TRAK1 and TRAK2, and the precise functions of these proteins in mitochondrial transport remain unclear.

MIRO1 and MIRO2 also influence mitochondrial fission/fusion in a Ca^{2+}-dependent manner, independently of their effects on mitochondrial transport, in both neuronal and non-neuronal cells. The MIRO proteins promote mitochondrial tubulation at resting cytosolic [Ca^{2+}] and mitochondrial fragmentation at high cytosolic [Ca^{2+}], by inhibition and activation of DRP1 respectively (Fransson *et al.*, 2006; Saotome *et al.*, 2008). It is therefore almost impossible to comment on whether the anomalies in *RHOT2* and *TRAK1* expression detected in the patients could account for the abnormal mitochondrial morphology phenotype in each case.

Based on the fact that abnormalities in mitochondrial morphology differed vastly amongst the patients' cells, and that P1, P2 and P4 were placed in a separate genetic complementation group from P3, a common primary defect in *RHOT2* or *TRAK1* is unlikely. Furthermore, *RHOT2* transcripts with exonisation of intron 10 would result in a truncated protein, $MIRO2_{1\text{-}340}$, which lacks the C-terminal GTPase domain and the TM domain that anchors the protein in the OM (Fransson *et al.*, 2006). $MIRO2_{1\text{-}340}$ would therefore have an aberrant cytosolic location; its expression would inhibit anterograde mitochondrial transport and promote mitochondrial fragmentation (Saotome *et al.*, 2008). Although P1, P2 and P4 exhibit mitochondrial morphologies consistent with an imbalance in fission/fusion in favour of fission, the opposite is true for P3, and this patient has the highest proportion of *RHOT2* transcripts with exonisation of intron 10. This is further evidence against the anomaly in *RHOT2* expression being the primary genetic defect in each case.

Interestingly, suppression of *TRAK1* transcription has been observed in conjunction with an increase in *RHOT1* expression in cultured COS7 cells, although the significance of this observation is unknown. Fransson *et al.* (2006) reported that ectopic expression of *TRAK1* or *TRAK2* with *RHOT1* in COS7 cells resulted in very low amounts of TRAK1 or TRAK2 proteins in cell lysates, compared with when these genes were expressed alone or with *RHOT2*. Levels of TRAK proteins did not increase after treatment of cells with protease inhibitors, indicating that the phenomenon was not dependent on proteasomal degradation of these

proteins but was most likely due to suppression of transcription (Fransson *et al.*, 2006). It is therefore possible that lack of *TRAK1* transcription is a secondary effect of increased *RHOT1* expression in the patients, but this hypothesis has not been explored.

Differences in the biochemical and clinical phenotypes amongst the patients also argue against the existence of a common primary genetic defect. P1, P3 and P4 showed abnormalities in the activities of multiple mitochondrial enzymes, indicating generalised mitochondrial dysfunction, whereas only PDH activity was altered in P2. All four patients presented with early-onset lactic acidosis and encephalopathy; however, P1 and P3 presented with hypotonia, whereas P2 and P4 did not, and P1 showed systemic disease. Importantly, despite the fact that P1 and P2 had very similar cellular phenotypes and were placed into the same genetic complementation group, these two patients showed the greatest contrast in their biochemical and clinical phenotypes.

Despite the differences in cellular, biochemical and clinical phenotypes amongst the patients, the possibility of a common primary defect in *RHOT2* or *TRAK1*, or even *RHOT1*, cannot be excluded. Pathogenic mutations in the same gene can have opposite effects on mitochondrial morphology and/or result in incredibly diverse sets of clinical symptoms in different patients. Examples of genes for which this is the case include the nuclear gene *NDUFS4*, encoding an accessory subunit of complex I, and the mitochondria tRNA genes. Some *NDUFS4* mutations decrease mitochondrial length and branching, some increase mitochondrial length and branching, and some are reported to have no effect on mitochondrial morphology whatsoever (Koopman *et al.*, 2007; Willems *et al.*, 2009). Pathogenic point mutations in mitochondrial tRNA genes, which each result in aberrant translation of multiple mitochondrial proteins, are associated with an incredible diversity of biochemical and clinical phenotypes, despite apparently generalised mitochondrial dysfunction in each case (Scaglia and Wong, 2008).

Even the same mutation can result in different clinical symptoms in different patients. In such cases it is thought that environmental factors, as well as the genetic background in each patient, modify the phenotype. Two unrelated patients homozygous for the same nonsense mutation in *NDUFS4*, c.316C>T p.R106X, do not have all symptoms in common; one patient shows atrophy of the brain but does not have cardiomyopathy, whereas the reverse is true for the other patient (Budde *et al.*, 2003). The most common pathogenic point mutation in mtDNA is m.3243A>G in the mitochondrial $tRNA^{Leu(UUR)}$ gene (Finsterer, 2007). Onset of symptoms can occur from early infancy to late adulthood. Patients can present with well-defined multisystemic disorders, such as mitochondrial encephalomyopathy with lactic acidosis and stroke-like episodes (MELAS syndrome), myoclonic epilepsy with ragged red fibres (MERRF syndrome), chronic progressive external ophthalmoplegia (CPEO), Kearns-Sayre syndrome, maternally-inherited diabetes and deafness (MIDD) and Leigh syndrome. Patients can also present with non-syndromic disorders, including hypertrophic cardiomyopathy, hypotonia and renal failure (Finsterer, 2007). In addition to environmental influences and the modifying effect of nuclear genes, the percentage of heteroplasmy in different tissues may account for this variability in clinical phenotype.

4.2 FUTURE WORK

4.2.1 Characterisation of the cellular phenotype

Further characterisation of the cellular phenotype in each patient may give more information about the nature of the defect in mitochondrial dynamics and thus the genetic defect in each case. First, levels of mitochondrial fusion could be assessed in patient fibroblasts by PEG-mediated cell fusion assays, as described by Chen *et al.* (2003, 2005). Second, ultrastructural analysis of mitochondrial aggregates will reveal whether they are clusters of smaller organelles, indicative of tethered intermediates that are unable to complete fusion, or individual swollen organelles. Third, Western blots will confirm reduced levels of TRAK1

protein and identify any changes in the expression levels of proteins encoded by other genes studied in the project. Fourth, immunofluorescent staining of these proteins may identify abnormalities in their subcellular distribution indicative of an alteration in their function. Fifth, confocal fluorescence microscopy analysis of the ER and peroxisomes will give information about their spatial relationship with mitochondria and may rule out abnormalities in mitochondrial morphology resulting from defects in ER-mitochondria tethering or peroxisomal biogenesis. Finally, candidate genes subjected to RNAi knockdown in fibroblasts from a control will create mutant phenotypes for comparison with the phenotypes of patients under study.

4.2.2 Genetic studies

The primary defect may lie outside of the coding region, for example, in the promoter or in an as yet unidentified regulatory element, in a gene already analysed in this project. As described above, Western blot analysis of proteins encoded by these genes may highlight abnormalities in their expression that will direct investigations of this kind. Alternatively, the defect may lie in a gene encoding a regulator of the mitochondrial fission, fusion or transport machineries. Of note, DRP1 is extensively post-translationally regulated by phosphorylation, ubiquitination and sumoylation (Santel and Frank, 2008), and the possibility of a defect in an enzyme involved in one of these processes has not been explored.

However, the primary defect may also lie in any number of other genes with putative roles in the regulation of mitochondrial and/or peroxisomal dynamics, as described in Chapter 1. These genes, their encoded proteins and the proposed function(s) of those proteins are listed in Table 4.3. These genes are all worthy of investigation based on their reported effects on mitochondrial morphology when under- or overexpressed. It would also be interesting to see if any of these genes lack mitochondrial targeting sequences and, if so, whether their 3'UTRs

contain elements of secondary structure, since these may represent binding sites for AKAP149.

Gene	Protein	Proposed function(s)
GDAP1	GDAP1	OM fission and/or IM fission
HSPD1	HSP60	Mitochondrial protein folding/import
MFF	MFF	OM fission; peroxisomal fission
MTFP1	MTP18	IM fission
OPA1	OPA1	IM fusion; cristae remodelling
PARK2	Parkin	Targeting mitochondria for mitophagy
PEX genes	Peroxins	Peroxisomal biogenesis

Table 4.3 Candidate genes, their encoded proteins and the function(s) of those proteins in the regulation of mitochondrial and/or peroxisomal dynamics in human cells.

4.3 CONCLUDING REMARKS

In conclusion, this project has characterised a novel group of patients with early-onset metabolic disease and abnormalities in mitochondrial dynamics. In each case, the primary genetic defect was not identified, but progress was made towards understanding the nature of the defect in the context of the cellular phenotype and suggestions have been made for future work. Based on the literature reviewed in Chapter 1, it is clear that the processes that regulate mitochondrial dynamics in mammalian cells are complex and interdependent, with several proteins playing multiple functionally-distinct roles in these processes. Genetic defects in different processes result in abnormal cellular phenotypes that are the same or show considerable overlap. Furthermore, it is likely that the full set of genes responsible for regulating these processes has not yet been identified. High-throughput screening of all genes reported to effect mitochondrial morphology and the characterisation of mutant phenotypes, both in cultured cells and in model organisms, may be crucial in the search for a molecular diagnosis.

APPENDIX 1: ZEISS FILTER SET SPECIFICATIONS

Zeiss filter set 02 (DAPI)

Excitation G365 nm
Emission LP420 nm

Zeiss filter set 10 (FITC)

Excitation BP450-490 nm
Emission BP515-565 nm

Zeiss filter set 13 (rhodamine)

Excitation BP470-490 nm
Emission BP505-530 nm

APPENDIX 2: APPROVED GENE SYMBOLS AND THEIR ALIASES

Approved gene symbol	Approved gene name	Aliases
AKAP1	A kinase (PRKA) anchor protein 1	AKAP121, AKAP149, SAKAP84, S-AKAP84, AKAP84
DNM1L	Dynamin 1-like	DRP1, DVLP, HDYNIV, DYMPLE, VPS1
FIS1	Fission 1 (mitochondrial outer membrane homolog) (*S. cerevisiae*)	CGI-135, H_NH0132A01.6, Fis1
MFN1	Mitofusin 1	FLJ20693
MFN2	Mitofusin 2	CPRP1, KIAA0214, MARF
RHOT1	Ras homolog gene family, member T1	MIRO-1, FLJ11040
RHOT2	Ras homolog gene family, member T2	MIRO-2
TRAK1	Trafficking protein, kinesin-binding 1	OIP106, KIAA1042
TRAK2	Trafficking protein, kinesin-binding 2	CALS-C, KIAA0549, GRIF-1, OIP98

Table A2: Symbols and names of candidate genes approved by the Human Genome Organisation (HUGO) were obtained from the HUGO Gene Nomenclature Committee (HGNC) Database, EMBL Outstation - Hinxton, European Bioinformatics Institute, Wellcome Trust Genome Campus, Hinxton, Cambridge, UK, available at www.genenames.org, in May 2010. Gene aliases, many of which are used in Chapter 1, are also shown.

APPENDIX 3: REFERENCE SEQUENCES

Gene	Chromosomal location	Transcript	Transcript ID	Length (bp)	No. of exons	Protein ID	Length (aa)	CCDS ID
AKAP1	Ch17:55,162,551-55,198,710 (forward)	AKAP1-001	ENST00000337714	3970	11	ENSP00000337736	903	CCDS11594
DNM1L	Ch12:32,832,137-32,898,584 (forward)	DNM1L-202	ENST00000266481	4612	20	ENSP00000266481	736	CCDS8729
FIS1	Ch7:100,882,893-100,888,366 (reverse)	FIS1-001	ENST00000223136	734	5	ENSP00000223136	152	CCDS43626
MFN1	Ch3:179,065,480-179,112,719 (forward)	MFN1-001	ENST00000471841	5224	18	ENSP00000420617	741	CCDS3228
MFN2	Ch1:12,040,238-12,073,571 (forward)	MFN2-001	ENST00000235329	4539	19	ENSP00000235329	757	CCDS30587
RHOT1	Ch17:30,469,473-30,552,746 (forward)	RHOT1-203	ENST00000358365	3309	21	ENSP00000351132	691	CCDS32610
RHOT2	Ch16:718,086-724,174 (forward)	RHOT2-001	ENST00000315082	2539	19	ENSP00000321971	618	CCDS10417
TRAK1	Ch3:42,055,294-42,267,381 (forward)	TRAK1-004	ENST00000327628	5293	16	ENSP00000328998	953	CCDS43072
TRAK2	Ch2:202,241,930-202,316,302 (reverse)	TRAK2-001	ENST00000332624	6510	16	ENSP00000328875	914	CCDS2347

Table A3: Reference sequences for candidate genes taken from the Ensembl database, available at www.ensembl.org/Homo_sapiens. For the majority of genes under study, the gDNA sequence was poorly defined and its annotation changed considerably throughout the course of the project, therefore a cDNA sequence was chosen as the reference sequence for each gene. Only those cDNA sequences validated by the collaborative consensus coding sequence (CCDS) project were considered. The CCDS project is a collaboration between the NCBI, Ensembl and UCSC Genome Browsers that tracks identical protein annotations with a stable identifier (CCDS ID) and reviews inconsistent protein annotations between sites, as well as annotations for which new evidence suggests a revision is needed, with the ultimate goal of identifying and accurately annotating all protein-coding genes on the reference mouse and human genomes (Pruit *et al.*, 2009). Of those cDNA sequences with CCDS IDs, the reference sequence was chosen as the cDNA sequence with the greatest number of exons.

APPENDIX 4: PREPARATION OF TEMPLATE NUCLEIC ACID FOR PCR

2.5 mg/ml RNase A

Stock RNase A solution was made by dissolving bovine pancreatic RNase A (Roche) in 10 mM Tris-HCl buffer pH 7.5 and 15 mM NaCl to a concentration of 2.5 mg/ml RNase A. The solution was heated to 100°C for 15 min, to inactivate any contaminating DNase, then allowed to cool slowly to room temperature before being stored at -20°C.

Extraction of gDNA from cultured cells

Cultured cells were harvested as described in Section 2.2.2.4 and gDNA was extracted using the Nucleon® BACC2 Genomic DNA Extraction Kit (Tepnel Life Sciences) according to the manufacturer's instructions. Pelleted cells were resuspended in 2 ml Reagent B. 15 µl 2.5 mg/ml RNase A was added and the tube was incubated in a shaking water bath at 37°C for 30 min. The contents of the tube were transferred to a 5 ml screw-capped polypropylene tube. 500 µl Sodium Perchlorate was added and contents of the tube were mixed gently, by tipping to and fro, for 5 min at room temperature. The tube was then incubated at 65°C for 5-10 min, with gently mixing as before, before being cooled on ice for 15 min. 2 ml chloroform, cooled to -20°C, was added and the tube was gently mixed as before. The tube was centrifuged at 800 g for 1 min before 300 µl Nucleon Resin was added and the tube was spun again at 1300 g for 3 min. The resin formed a layer halfway down the tube. The upper phase (approximately 2.5 ml) was transferred to a fresh centrifuge tube. This tube was centrifuged at 1300 g for 2 min, to spin down any resin accidentally transferred, and the supernatant was transferred to another fresh centrifuge tube. 2 volumes (approximately 5 ml) of absolute ethanol, cooled to -20°C, were added to this tube, which was gently mixed as before. The DNA appeared as white strands. The tube was centrifuged at 1000 g for 10 min to pellet the DNA. The supernatant was discarded and the pellet was resuspended in 1 ml 70 % v/v ethanol, cooled to -20°C, transferred to a 1.5 ml nuclease-free microcentrifuge tube and centrifuged at 13000 rpm for 1 min. The supernatant was discarded and the pellet was allowed to dry in air (approximately 10 min) before being resuspended in 50 µl TE buffer pH 8.0. The contents of the tube were mixed by flicking then the tube was incubated at 4°C for at least 24 hr or until the pellet had completely dissolved. The concentration of gDNA was measured using UV spectroscopy by absorption at 260 nm. Generally, concentrations of 0.5-2.0 µg/µl gDNA were obtained.

Extraction of mRNA from cultured cells

Cultured cells were harvested as described in Section 2.2.2.4 and mRNA was extracted using the High Pure RNA Isolation Kit (Roche) according to the manufacturer's instructions. Pelleted cells were resuspended in 200 µl PBS. 400 µl Lysis/-Binding Buffer was added and the mixture was vortexed for 15 s. The entire sample was then transferred into the upper reservoir of a High Pure Filter Tube, sitting in a High Pure Collection Tube. This assembly was centrifuged at 8000 g for 15 s and the flow-through was discarded. 90 µl DNase Incubation Buffer and 10 µl reconstituted DNase I solution were mixed in a nuclease-free microcentrifuge tube and pipetted into the centre of the glass filter fleece in the upper reservoir of the Filter Tube. This was incubated at room temperature for 15 min. 500 µl Wash Buffer I was added to the Filter Tube, the assembly was centrifuged at 8000 g for 15 s and the flow-through was discarded. 500 µl Wash Buffer II was added to the Filter Tube, the assembly was centrifuged again as before and the flow-through was discarded. Finally, 200 µl Wash Buffer II was added to the Filter Tube and the assembly was centrifuged at 13000 g for 2 min to remove any residual Wash Buffer. The Collection Tube was discarded and the Filter Tube was placed into a 1.5 ml nuclease-free microcentrifuge tube. 50 µl Elution Buffer was pipetted into the centre of the glass filter fleece in the upper reservoir of the Filter Tube and the assembly was centrifuged at 8000 g for 1 min to elute the mRNA. The Filter Tube

was discarded and the eluted RNA was stored at -20°C. The concentration of mRNA was measured using UV spectroscopy by absorption at 260 nm. Generally, concentrations of 0.5-1.0 µg/µl RNA were obtained.

Synthesis of cDNA from mRNA

cDNA was synthesised from mRNA using the AffinityScript^{TM} Multiple Temperature Reverse Transcriptase (Stratagene) according to the manufacturer's instructions. The following three components were added to a 0.5 ml nuclease-free microcentrifuge tube in the order shown: 3 µg total RNA, *x* µl of RNase-free water and 500 ng Primer $p(dT)_{15}$ (supplied as powder; Roche), where *x* was such that the total volume of the mixture was 14.2 µl. The mixture was thoroughly mixed by pipetting then incubated at 65°C for 5 min before being allowed to cool to room temperature (approximately 10 min). The following four components were then added to the mixture to give a final reaction volume of 20 µl: 2 µl 10x AffinityScript^{TM} RT buffer, 2 µl 100 mM DTT, 0.8 µl 100mM dNTP mix (25 mM each of dATP, dCTP, dGTP and dTTP) and 1 µl of AffinityScript^{TM} Multiple Temperature Reverse Transcriptase. The mixture was thoroughly mixed by pipetting then incubated at 42°C for 5 min, 53°C for 1 hr and 70°C for 15 min. cDNA was stored at -20°C.

APPENDIX 5: PRIMERS AND PROTOCOLS FOR PCR

Gene	Template	Target sequence	Primer sequence 5'→3'	Product Size (bp)	DNA polymerase -/+ Q-Solution™	PCR		
						Stage 1	Stage 2	Stage 3
AKAP1	cDNA	Coding sequence (first half)	(F) CCGCGCGTCTTCAGTATTTA (R) GTCTGACAACTCCCCCTTCA	1851	Taq + Q	94°C 2 min 1 cycle	94°C 1 min 61°C 1 min 72°C 2 min 40 cycles	72°C 4 min 1 cycle
	cDNA	Coding sequence (second half)	(F) CTCACCACCACCAAAGACCT (R) AAACCCTCTCAAGCAAGCAA	1831	Taq + Q	94°C 2 min 1 cycle	94°C 1 min 61°C 1 min 72°C 2 min 35 cycles	72°C 4 min 1 cycle
DNM1L	cDNA	Coding sequence	(F) GCCCCGTGTTTTCAGAGTC (R) ATCCACAGGCAAACTGCTTT	2544	Taq + Q	94°C 2 min 1 cycle	94°C 1 min 61°C 1 min 72°C 3 min 35 cycles	72°C 4 min 1 cycle
	gDNA	Intron 14-exon 16 inclusive (including part of intron 16)	(F) TTATGGCATGAGTCCCAACA (R) TCTCACAGTCCCCATTTGTTT	1781	Taq + Q	94°C 2 min 1 cycle	94°C 30 s 60°C 1 min 72°C 3 min 40 cycles	72°C 4 min 1 cycle
	gDNA	Intron 16 (remainder)	(F) TTTTTGGACATTTCCTTTCCTC (R) GTTGCCTGTGGTTGGTTCTT	1539	Taq + Q	94°C 2 min 1 cycle	94°C 30 s 60°C 1 min 72°C 2 min 40 cycles	72°C 4 min 1 cycle
FIS1	cDNA	Coding sequence + 3'UTR	(F) AGCTGGTGTCTGTGGAGGAC (R) CATCCATTCACCAGGGAACT	1946	Taq	94°C 2 min 1 cycle	94°C 1 min 61°C 1 min 72°C 2 min 30 s 35 cycles	72°C 4 min 1 cycle
	gDNA	Exon 1	(F) TACCCACCCTCTTTTTGCTG (R) GGGCCTGGACCTTTTATTGT	831	Taq + Q	94°C 2 min 1 cycle	94°C 1 min 61°C 1 min 72°C 1 min 35 cycles	72°C 4 min 1 cycle
MFN1	cDNA	Coding sequence	(F) ATGAGGCAGTTTGGGCATCT (R) CACAGGGCTTTGCTATTTAGG	2424	Taq + Q	94°C 2 min 1 cycle	94°C 1 min 61°C 1 min 72°C 3 min 35 cycles	72°C 4 min 1 cycle

Table A5: Primers and protocols for PCR amplification of candidate genes. F, forward primer. R, reverse primer. Q, Q-Solution™. Continued on next page.

Gene	Template	Target sequence	Primer sequence 5'→3'	Product Size (bp)	DNA polymerase -/+ Q-Solution™	PCR		
						Stage 1	Stage 2	Stage 3
MFN2	cDNA	Coding sequence	(F) CAGGACTGGTGGAGTCAACA (R) ACGAGACTGGGTGCTTCATT	2554	Taq + Q	94°C 2 min 1 cycle	94°C 1 min 61°C 1 min 72°C 3 min 35 cycles	72°C 4 min 1 cycle
RHOT1	cDNA	Coding sequence	(F) CTCTTGCGGGGAAGCAACT (R) TGGCCTACCACAACTGACTG	2548	Taq + Q	94°C 2 min 1 cycle	94°C 1 min 58°C 1 min 72°C 3 min 40 cycles	72°C 4 min 1 cycle
	gDNA	Intron 18-exon 20 inclusive	(F) CTCCACCACAAGCCTTCACT (R) AGTTGGGCATCAGTCAGCTT	3130	Taq + Q	94°C 2 min 1 cycle	94°C 30 s 61°C 1 min 72°C 3 min 30 s 38 cycles	72°C 4 min 1 cycle
RHOT2	cDNA	Coding sequence	(F) GAGCGAAAGGCTTGAGGAC (R) CTCCGGTCCTCTGCTACAAC	2407	Taq + Q	94°C 2 min 1 cycle	94°C 1 min 58°C 1 min 72°C 3 min 40 cycles	72°C 4 min 1 cycle
	gDNA	Intron 4-intron 10 inclusive	(F) CCGCAGTGGAGTCTCTTTGT (R) AGCGTGTTCAGGAAGAGGAA	2477	Taq + Q	94°C 2 min 1 cycle	94°C 1 min 61°C 1 min 72°C 3 min 40 cycles	72°C 4 min 1 cycle
TRAK1	cDNA	Coding sequence	(F) GGATTTGCCCTAACAAGCAA (R) CGTCCTCGTGAGAGTGATGA	3269	TopTaq™	94°C 3 min 1 cycle	94°C 30 s 63°C 30 s 72°C 4 min 40 cycles	72°C 10 min 1 cycle
	gDNA	Exon 5	(F) AGGCTTCCCTTTCCTTGTGT (R) TGATCAGCCTGCATCGTTAG	689	Taq + Q	94°C 2 min 1 cycle	94°C 1 min 61°C 1 min 72°C 1 min 40 cycles	72°C 4 min 1 cycle
	gDNA	Exon 15	(F) ATTTTCCCCCTTCCATTTTG (R) ATCATCACCCACACAGACGA	864	Taq	94°C 2 min 1 cycle	94°C 1 min 58°C 1 min 72°C 1 min 40 cycles	72°C 4 min 1 cycle
TRAK2	cDNA	Coding sequence	(F) GAGTGCTCGTTGCTACGGAT (R) TCACAACCCTTGTGCAACAT	3025	TopTaq™	94°C 3 min 1 cycle	94°C 30 s 61°C 30 s 72°C 3 min 30 s 40 cycles	72°C 10 min 1 cycle

Table A5 continued.

APPENDIX 6: PRIMERS AND PROTOCOLS FOR SEQUENCING

Gene	PCR product	Primer sequence 5'→3'
AKAP1	Coding sequence (first half)	(F) CCGCGCGTCTTCAGTATTTA (F) ACAGGTGGTGAAGCCAAATC (R) GTCTGACAACTCCCCCTTCA
	Coding sequence (second half)	(F) CTCACCACCACCAAAGACCT (F) TTTCAACCCTGCCTTACACC
DNM1L	Coding sequence	(F) TATCCTCGCTGTCACTGCTG (R) TGGAATAACCCTTCCCATCA (F) AGCGGCAAATCAAACGTCTA (F) AATTATGCCAGCCAGTCCAC (R) TGATGTGTTCTGCAATTTGG
	Intron 14-exon 16 inclusive (including part of intron 16)	(F) CCTTGAATTCTTTGCCAGAAA (R) TCTGCCTTATTTCCTTCACCA (F) GTTGACATGCTTTTGCTTGC
	Intron 16 (remainder)	(F) TTTTTGGACATTTCCTTTCCTC (F) TGTTTGTCACATTCCGCATT (R) TTCTCCCACCCTTCAAACAC
FIS1	Coding sequence + 3'UTR	(R) CTTCAGGAAAGGGAGGAAGG (R) TCCTCCCTACTCCTGTGCTG (R) CATCCATTCACCAGGGAACT
	Exon 1	(F) TACCCACCCTCTTTTTGCTG
MFN1	Coding sequence	(R) TCTTTCCATGTGCTGTCTGC (F) TTGGTCGCAAACTCTGAATC (F) TTACTTCCAGCTGGTATACAGGA
MFN2	Coding sequence	(R) TGTCCATCAAAACGAGGTCA (F) AGGGCTCAGAGGAAAAGAGG (R) CACCACTCCTCCAACAACAA (F) CTACAATGACCAGGCAAGCA
RHOT1	Coding sequence	(F) TACTGCCCAGAGGAGAAGGA (R) CCAGAGCTTGAGGAGCTAATG (F) CAGTGGACGCTCACGACTTA (R) TGGCCTACCACAACTGACTG
	Intron 18-exon 20	(F) CTCCACCACAAGCCTTCACT (F) ATGGCATTCGCCTCAAGTAG (F) TGTAGAAACGCACTGCTTGG (F) TGGTTTTCAGGCATGTGTGT (R) AGATGGCACCCTCGTCTAAA
RHOT2	Coding sequence	(F) GAGCGAAAGGCTTGAGGAC (F) TTCCAGAAATCCTGCTTTGG (F) GCCTTCCTGCAGGCCTTTC
	Intron 4-intron 10 inclusive	(F) GCGGTCCTGTCACTCTGTCT (R) CCCTCAGAGAAGCCTCTTCC (F) TCTTTCTTCCCCAGTTTCCA (F) GCCAAGAACCTGAGGAACAT
TRAK1	Coding sequence	(F) AACACATCAGGGAGGAGGTG (R) GCCTCGGATCGAAGTACAAC (F) CACCAGAAGCGTGTCTTTGA (F) ATGTCCCCACCTTGACTGAG (R) GTGACAGTGGGGCATCTGAG
	Exon 5	(F) AGGCTTCCCTTTCCTTGTGT
	Exon 15	(F) TCCTTCTGAGCATGGTAGGG (R) GGCTCCTGCATCTCCTCTG
TRAK2	Coding sequence	(F) GCAGCATGAGCTATGCAAGA (R) GCTTTTCTTGCAGCATTTCC (F) CAGGATTGCCAATGACACAC (F) TTCCTGCCACCCATTACTTC

Table A6: Primers for sequencing products of PCR reactions detailed in Table A5. F, forward primer. R, reverse primer.

AKAP1 (first half)

Some patients were heterozygous for deletion of a T nucleotide 13 bp upstream of the START codon, resulting in double sequence downstream though the START codon when sequencing with forward primer 5'-CCGCGCGTCTTCAGTATTTA-3'. In these patients, the reverse primer 5'-CCTGTCTCTCTTGCCCTCTC-3' was used to sequence the first part of the coding sequence, sequencing upstream though the START codon.

DNM1L

Skipping of exons 15-16 and exon 15 alone resulted in double sequence downstream from the start of exon 15, sequencing with forward primer 5'-AGCGGCAAATCAAACGTCTA-3', and upstream from the end of exon 16, sequencing with reverse primer 5'-TGATGTGTTCTGCAATTTGG-3'. Exons 15 and 16 and their adjacent introns were therefore amplified and sequenced from gDNA. Some patients were heterozygous for deletion of ATTT in intron 14, beginning 223 bp downstream from the end of exon 14, which resulted in double sequence upstream when sequencing with reverse primer 5'-TCTGCCTTATTTCCTTCACCA-3'. In these patients, the forward primer 5'-AGGAACAAAGGAGAAACAGGCTA-3' was used to sequence downstream through the first part of intron 14.

FIS1

The *FIS1* 5'UTR is very short and GC-rich and it was not possible to design a suitable PCR primer to bind in this region. The forward PCR primer 5'-AGCTGGTGTCTGTGGAGGAC-3' was designed to bind downstream of the START codon in exon 1. In order to sequence the beginning of the gene, exon 1 was amplified and sequenced from gDNA.

RHOT1

Skipping of exons 19-20 and exon 19 alone resulted in double sequence downstream from the start of exon 19, sequencing with forward primer 5'-CAGTGGACGCTCACGACTTA-3', and upstream from the end of exon 20, sequencing with reverse primer 5'-TGGCCTACCACAACTGACTG-3'. Exons 19 and 20 and their adjacent introns were therefore amplified and sequenced individually from gDNA.

RHOT2

Low-level skipping of exon 5 resulted in messy sequence downstream from the start of exon 5. Heterozygous exonisation of intron 10 (82 bp) resulted in double sequence downstream from the start of exon 11, although this tailed off quite rapidly. Exonisation of intron 10 altered the reading frame downstream and introduced STOP codons into the sequence. In order to sequence exons 5-10 accurately, a reverse primer would have to be designed such that it bound downstream of the forward primer 5'-TTCCAGAAATCCTGCTTTGG-3' and upstream of the boundary of exons 10 and 11, but this was not possible due to the presence of several common SNPs in this region. Instead, two reverse primers were designed: one primer that bound across the exon 10/exon 11 boundary and one primer that bound across the exon 10/intron 10 boundary. However, these primers gave poor sequence for every patient analysed. Exons 5-10 and their adjacent introns were therefore amplified in one piece from gDNA, since both exons and introns are short. Some patients were heterozygous for deletion of a G nucleotide in intron 4, 224 bp upstream of the start of exon 5, which resulted in double sequence downstream through exon 5 when sequencing with forward primer 5'-GCGGTCCTGTCACTCTGTCT-3'. In these patients, the reverse primer 5'-GAACAAAGCTGGTGGGAGAA-3', which binds just downstream of forward primer 5'-TCTTTCTTCCCCAGTTTCCA-3' in intron 5, was used to sequence upstream through exon 5.

APPENDIX 7: GEL ELECTROPHORESIS

5x TBE buffer pH 8.0

TBE buffer pH 8.0 was made up as a 5x concentrated stock solution, containing 90 mM Tris-borate and 2 mM EDTA, stored at room temperature. The buffer was diluted 1:4 in dH_2O for use in gel electrophoresis.

1 % w/v agarose gels with 0.5 µg/ml EtBr

Agarose gels contained 1 % w/v SeaKem® LE-agarose with 0.5 µg/ml EtBr (Gene Choice) in 1x TBE buffer pH 8.0.

DNA Molecular Weight Markers XIV and XVII (Roche)

DNA Molecular Weight Markers XIV and XVII (Roche) were diluted 1:4 in 1x TBE buffer to make stocks, which were stored at -20°C. Stocks were diluted 1:5 in 1x TBE buffer for gel loading.

Bromophenol blue and xylene cyanol FF loading dyes

Stock loading dyes contained 0.25 % w/v loading dye and 30 % w/v glycerol in dH_20 and were stored at 4°C. Stocks were diluted 1:5 in 1x TBE buffer for gel loading. PCR products of size 1 kb or greater were run with bromophenol blue. PCR products of size less than 1 kb were run with xylene cyanol FF.

APPENDIX 8: PURIFICATION OF PCR PRODUCTS

PCR products were purified using the QIAquick® PCR Purification Kit (Qiagen) and a microcentrifuge according to the manufacturer's instructions. All steps in the purification protocol were carried out at room temperature. 5 volumes of Buffer PB were mixed with 1 volume of PCR products, which were then added to a QIAquick® column sitting in a QIAquick® collection tube and centrifuged at 13000 rpm for 1 min. The flow-through was discarded, 0.75 ml Buffer PE was added to the column and the assembly was again centrifuged at 13000 rpm for 1 min. The flow-through was discarded and the assembly was spun again as before to remove residual wash buffer. The column was placed in a 1.5 ml nuclease-free microcentrifuge tube, 30-50 µl Buffer EB was added to the centre of the QIAquick® membrane, and the assembly was centrifuged at 13000 rpm for 1 min to elute the DNA, which was stored at 4˚C.

REFERENCES

Agsteribbe E., Huckriede A., Veenhuis M., Ruiters M. H., Niezenkoning K. E., Skjeldal O. H., Skullerud K., Gupta R. S., Hallberg R., Vandiggelen O. P. and Scholte H. R. (1993). A fatal, systemic mitochondrial disease with decreased mitochondrial enzyme activities, abnormal ultrastructure of the mitochondria and deficiency of heat shock protein 60. *Biochemical and Biophysical Research Communications*, 193(1):146-154.

Alexander C., Votruba M., Pesch U. E., Thiselton D. L., Mayer S., Moore A., Rodriguez M., Kellner U., Leo-Kottler B., Auburger G., Bhattacharya S. S. and Wissinger B. (2000). *OPA1*, encoding a dynamin-related GTPase, is mutated in autosomal dominant optic atrophy linked to chromosome 3q28. Nature Genetics, 26(2):211-215.

Amati-Bonneau P., Milea D., Bonneau D., Chevrollier A., Ferré M., Guillet V., Gueguen N., Loiseau D., de Crescenzo M A., Verny C., Procaccio V., Lenaers G. and Reynier P. (2009). OPA1-associated disorders: phenotypes and pathophysiology. *The International Journal of Biochemistry and Cell Biology*, 41(10):1855-1865.

Amiott E. A., Lott P., Soto J., Kang P. B., McCaffery J. M., DiMauro S., Abel E. D., Flanigan K. M., Lawson V. H. and Shaw J. M. (2008). Mitochondrial fusion and function in Charcot-Marie-Tooth type 2A patient fibroblasts with mitofusin 2 mutations. *Experimental Neurology*, 211(1):115-127.

Ashley N., Harris D. and Poulton J. (2005). Detection of mitochondrial DNA depletion in living human cells using PicoGreen staining. *Experimental Cell Research*, 303(2):432-446.

Aubourg P. (2007). X-linked adrenoleukodystrophy. *Annales d'Endocrinologie*, 68(6):403-411.

Aubourg P., Robain O., Rocchiccioli F., Dancea S. and Scotto J. (1985). The cerebro-hepato-renal (Zellweger) syndrome: lamellar lipid profiles in adrenocortical, hepatic mesenchymal, astrocyte cells and increased levels of very long chain fatty acids and phytanic acid in the plasma. *Journal of the Neurological Sciences*, 69(1):9-25.

Bach D., Pich S., Soriano F. X., Vega N., Baumgartner B., Oriola J., Daugaard J. R., Lloberas J., Camps M., Zierath J. R., Rabasa-Lhoret R., Wallberg-Henriksson H., Laville M., Palacín M., Vidal H., Rivera F., Brand M. and Zorzano A (2003). Mitofusin-2 determines mitochondrial network architecture and mitochondrial metabolism. A novel regulatory mechanism altered in obesity. *The Journal of Biological Chemistry*, 278(19):17190-17197.

Bakeeva L. E., Chentsov Y. S. and Skulachev V. P. (1981). Ontogenesis of mitochondrial reticulum in rat diaphragm muscle. *European Journal of Cell Biology*, 25(1):175-181.

Baloh R. H., Schmidt R. E., Pestronk A. and Milbrandt J. (2007). Altered axonal mitochondrial transport in the pathogenesis of Charcot-Marie-Tooth disease from mitofusin 2 mutations. *The Journal of Neuroscience*, 27(2):422-430.

Baumgart E., Vanhorebeek I., Grabenbauer M., Borgers M., Declercq P. E., Fahimi H. D. and Baes M. (2001). Mitochondrial alterations caused by defective peroxisomal biogenesis in a mouse model for Zellweger syndrome (*PEX5* knockout mouse). *The American Journal of Pathology*, 159(4):1477-1494.

Baxter R. V., Ben Othmane K., Rochelle J. M., Stajich J. E., Hulette C., Dew-Knight S., Hentati F., Ben Hamida M., Bel S., Stenger J. E., Gilbert J. R., Pericak-Vance M. A. and Vance J. M. (2002). Ganglioside-induced differentiation-associated protein-1 is mutant in Charcot-Marie-Tooth disease type 4A/8q21. *Nature Genetics*, 30(1):21-22.

Beene D. L. and Scott J. D. (2007). A-kinase anchoring proteins take shape. *Current Opinion in Cell Biology*, 19(2):192-198.

Benard G., Bellance N., James D., Parrone P., Fernandez H., Letellier T. and Rossignol R. (2007). Mitochondrial bioenergetics and structural network organization. *Journal of Cell Science*, 120(5):838-848.

Benshalom G. and Reese T. S. (1985). Ultrastructural observations on the cytoarchitecture of axons processed by rapid-freezing and freeze-substitution. *Journal of Neurocytology*, 14(6):943-960.

Beregi E., Regius O., Hüttl T. and Göbl Z. (1988). Age-related changes in skeletal muscle cells. *Zeitschrift für Gerontologie*, 21(2):83-86.

Bereiter-Hahn J. (1990). Behavior of mitochondria in the living cell. *International Review of Cytology*, 122:1-63.

Bereiter-Hahn J. and Vöth M. (1994). Dynamics of mitochondria in living cells: shape changes, dislocations, fusion, and fission of mitochondria. *Microscopy Research and Technique*, 27(3):198-219.

Bereiter-Hahn J., Vöth M., Mai S. and Jendrach M. (2008). Structural implications of mitochondrial dynamics. *Biotechnology Journal*, 3(6):765-780.

Bleazard W., McCaffery J. M., King E. J., Bale S., Mozdy A., Tieu Q., Nunnari J and Shaw J. M. (1999). The dynamin-related GTPase Dnm1 regulates mitochondrial fission in yeast. *Nature Cell Biology*, 1(5):298-304.

Bloethner S., Mould A., Stark M. and Hayward N. K. (2008). Identification of ARHGEF17, DENND2D, FGFR3, and RB1 mutations in melanoma by inhibition of nonsense-mediated mRNA decay. *Genes, Chromosomes and Cancer*, 47(12):1076-1085.

Boichard A., Venet L., Naas T., Boutron A., Chevret L., Ogier de Baulny H., De Lonlay P., Legrand A., Nordman P. and Brivet M. (2008). Two silent substitutions in the *PDHA1* gene cause exon 5 skipping by disruption of a putative exonic splicing enhancer. *Molecular Genetics and Metabolism*, 93(3):323-330.

Breckenridge D. G., Stojanovic M., Marcellus R. C. and Shore G. C. (2003). Caspase cleavage product of BAP31 induces mitochondrial fission through endoplasmic reticulum calcium signals, enhancing cytochrome c release to the cytosol. *The Journal of Cell Biology*, 160(7):1115-1127.

Brickley K., Smith M. J., Beck M. and Stephenson F. A. (2005). GRIF-1 and OIP106, members of a novel gene family of coiled-coil domain proteins: association *in vivo* and *in vitro* with kinesin. *The Journal of Biological Chemistry*, 280(15):14723-14732.

Bridgman P.D. (2004). Myosin-dependent transport in neurons. *Journal of Neurobiology*, 58(2):164-174.

Briones P., Vilaseca M. A., Ribes A., Vernet A., Lluch M., Cusi V., Huckriede A. And Agsteribbe E. (1997). A new case of multiple mitochondrial enzyme deficiencies with decreased amount of heat shock protein 60. *Journal of Inherited Metabolic Disease*, 20(4):569-577.

Bross P., Li Z., Hansen J., Hansen J. J., Nielsen M. N., Corydon T. J., Georgopoulos C., Ang D., Lundemose J. B., Niezen-Koning K., Eiberg H., Yang H., Kølvraa S., Bolund L. and Gregersen N. (2007). Single-nucleotide variations in the genes encoding the mitochondrial Hsp60/Hsp10 chaperone system and their disease-causing potential. *Journal of Human Genetics*, 52(1):56-65.

Brunk U. T. and Terman A. (2002). The mitochondrial-lysosomal axis theory of aging: accumulation of damaged mitochondria as a result of imperfect autophagocytosis. *European Journal of Biochemistry*, 269(8):1996-2002.

Budde S. M., van den Heuvel L. P., Smeets R. J., Skladal D., Mayr J. A., Boelen C., Petruzzella V., Papa S. and Smeitink J. A. (2003). Clinical heterogeneity in patients with mutations in the *NDUFS4* gene of mitochondrial complex I. *Journal of Inherited Metabolic Disease*, 26(8):813-815.

Camões F., Bonekamp N., Delille H. and Schrader M. (2009). Organelle dynamics and dysfunction: a closer link between peroxisomes and mitochondria. *Journal of Inherited Metabolic Disease*, 32(2):163-180.

Carafoli E. (2003). Historical review. Mitochondria and calcium: ups and downs of an unusual relationship. *Trends in Biochemical Sciences*, 28(4):175-181.

Cartoni R. and Martinou J.-C. (2009). Role of mitofusin 2 mutations in the physiopathology of Charcot-Marie-Tooth disease type 2A. *Experimental Neurology*, 218(2):268-273.

Chada S. R. and Hollenbeck P. J. (2003). Mitochondrial movement and positioning in axons: the role of growth factor signaling. *The Journal of Experimental Biology*, 206(12):1985-1992.

Chada S. R. and Hollenbeck P. J. (2004). Nerve growth factor signaling regulates motility and docking of axonal mitochondria. *Current Biology*, 14(14):1272-1276.

Chen H., Chomyn A. and Chan D. C. (2005). Disruption of fusion results in mitochondrial heterogeneity and dysfunction. *The Journal of Biological Chemistry*, 280(28):26185-26192.

Chen H., Detmer S. A., Ewald A. J., Griffin E. E., Fraser S. E. and Chan D. C. (2003). Mitofusins Mfn1 and Mfn2 co-ordinately regulate mitochondrial fusion and are essential for embryonic development. *The Journal of Cell Biology*, 160(2):189-200.

Chen H., McCaffery J. M. and Chan D. C. (2007). Mitochondrial fusion protects against neurodegeneration in the cerebellum. *Cell*, 130(3):548-562.

Chen K. H., Guo X., Ma D., Guo Y., Li Q., Yang D., Li P., Qiu X., Wen S., Xiao R. P. and Tang J. (2004). Dysregulation of HSG triggers vascular proliferative disorders. *Nature Cell Biology*, 6(9):872-883.

Chen Q., Lin R.-Y. and Rubin C. S. (1997). Organelle-specific targeting of protein kinase All (PKAII). Molecular and *in situ* characterization of murine A kinase anchor proteins that recruit regulatory subunits of PKAII to the cytoplasmic surface of mitochondria. *The Journal of Biological Chemistry*, 272(24):15247-15257.

Chen T. R. (1977). *In situ* detection of mycoplasma contamination in cell cultures by fluorescent Hoechst 33258 stain. *Experimental Cell Research*, 104(2):255-262.

Chomyn A., Martinuzzi A., Yoneda M., Daga A., Hurko O., Johns D., Lai S. T., Nonaka I., Angelini C. and Attardi G. (1992). MELAS mutation in mtDNA binding site for transcription termination factor causes defects in protein synthesis and in respiration but no change in levels of upstream and downstream mature transcripts. *Proceedings of the National Academy of Sciences of the United States of America*, 89(10):4221-4225.

Chung K. W., Kim S. B., Park K. D., Choi K. G., Lee J. H., Eun H. W., Suh J. S., Hwang J. H., Kim W. K., Seo B. C., Kim S. H., Son I. H., Kim S. M., Sunwoo I. N. and Choi B. O. (2006). Early onset severe and late-onset mild Charcot-Marie-Tooth disease with *mitofusin 2* (*MFN2*) mutations. *Brain*, 129(8):2103-2118.

Cipolat S., Martins de Brito O., Dal Zilio B. and Scorrano L. (2004). OPA1 requires mitofusin 1 to promote mitochondrial fusion. *Proceedings of the National Academy of Sciences of the United States of America*, 101(45):15927-15932.

Cipolat S., Rudka T., Hartmann D., Costa V., Serneels L., Craessaerts K., Metzger K., Frezza C., Annaert W., D'Adamio L., Derks C., Dejaegere T., Pellegrini L., D'Hooge R., Scorrano L. and De Strooper B. (2006). Mitochondrial rhomboid PARL regulates cytochrome c release during apoptosis *via* OPA1-dependent cristae remodeling. *Cell*, 126(1):163-175.

Claramunt R., Pedrola L., Sevilla T., López de Munain A., Berciano J., Cuesta A., Sánchez-Navarro B., Millán J. M., Saifi G. M., Lupski J. R., Vílchez J. J., Espinós C. and Palau F. (2005). Genetics of Charcot-Marie-Tooth disease type 4A: mutations, inheritance, phenotypic variability, and founder effect. *Journal of Medical Genetics*, 42(4):358-365.

Coleman R., Silbermann M., Gershon D. and Reznick A. Z. (1987). Giant mitochondria in the myocardium of aging and endurance-trained mice. *Gerontology*, 33(1):34-39.

Collinson I. R., Runswick M. J., Buchanan S. K., Fearnley I. M., Skehel J. M., van Raaij M. J., Griffiths D. E. and Walker J. E. (1994). Fo membrane domain of ATP synthase from bovine heart mitochondria: purification, subunit composition, and reconstitution with F1-ATPase. *Biochemistry*, 33(25):7971-7978.

Corral-Debrinski M. (2007). mRNA specific subcellular localization represents a crucial step for fine-tuning of gene expression in mammalian cells. *Biochimica et Biophysica Acta – Molecular Cell Research*, 1773(4):473-475.

Csordás G., Renken C., Várnai P., Walter L., Weaver D., Buttle K. F., Balla T., Mannella C. A. and Hajnóczky G. (2006). Structural and functional features and significance of the physical linkage between ER and mitochondria. *The Journal of Cell Biology*, 174(7):915-921.

Cuesta A., Pedrola L., Sevilla T., García-Planells J., Chumillas M. J., Mayordomo F., LeGuern E., Marín I., Vílchez J. J. and Palau F. (2002). The gene encoding ganglioside-induced differentiation-associated protein 1 is mutated in axonal Charcot-Marie-Tooth type 4A disease. *Nature Genetics*, 30(1):22-25.

Davidson R. L. and Gerald P. S. (1976a). Improved techniques for the induction of mammalian cell hybridization by polyethylene glycol. *Somatic Cell Genetics*, 2(2):165-176.

Davidson R. L. and Gerald P. S. (1977). Induction of mammalian somatic cell hybridization by polyethylene glycol. *Methods in Cell Biology*, 15:325-338.

Davidson R. L., O'Malley K. A. and Wheeler T. B. (1976b). Polyethylene glycol-induced mammalian cell hybridization: effect of polyethylene glycol molecular weight and concentration. *Somatic Cell Genetics*, 2(3):271-280.

De Brito O. M. and Scorrano L. (2008). Mitofusin-2 tethers endoplasmic reticulum to mitochondria. *Nature*, 456(7222):605-610.

De Vos K. J., Sable J., Miller K. E. and Sheetz M. P. (2003). Expression of phosphatidylinositol (4,5) bisphosphate-specific pleckstrin homology domains alters direction but not the level of axonal transport of mitochondria. *Molecular Biology of the Cell*, 14(9):3636-3649.

Deacon S. W., Serpinskaya A. S., Vaughan P. S., Lopez Fanarraga M., Vernos I., Vaughan K. T. and Gelfand V. I. (2003). Dynactin is required for bidirectional organelle transport. The *Journal of Cell Biology*, 160(3):297-301.

Delettre C., Griffoin J.-M., Kaplan J., Dollfus H., Lorenz B., Faivre L., Lenaers G., Belenguer P. and Hamel C. P. (2001). Mutation spectrum and splicing variants in the *OPA1* gene. *Human Genetics*, 109(6):584-591.

Delettre C., Lenaers G., Griffoin J.-M., Gigarel N., Lorenzo C., Belenguer P., Pelloquin L., Grosgeorge J., Turc-Carel C., Perret E., Astarie-Dequeker C., Lasquellec L., Arnaud B., Ducommun B., Kaplan J. and Hamel C. P. (2000). Nuclear gene *OPA1*, encoding a mitochondrial dynamin-related protein, is mutated in dominant optic atrophy. *Nature Genetics*, 26(2):207-210.

Den Dunnen J. T. and Antonarakis S. E. (2001). Nomenclature for the description of human sequence variations. *Human Genetics*, 109(1):121-124.

Detmer S. A. and Chan D. C. (2007). Complementation between mouse Mfn1 and Mfn2 protects mitochondrial fusion defects caused by CMT2A disease mutations. *The Journal of Cell Biology*, 176(4):405-414.

Detmer S. A., Velde C. V., Cleveland D. W. and Chan D. C. (2008). Hindlimb gait defects due to motor axon loss and reduced distal muscles in a transgenic mouse model of Charcot-Marie-Tooth type 2A. *Human Molecular Genetics*, 17(3):367-375.

Dirkx R., Vanhorebeek I., Martens K., Schad A., Grabenbauer M., Fahimi D., Declercq P., Van Veldhoven P. P. and Baes M. (2005). Absence of peroxisomes in mouse hepatocytes causes mitochondrial and ER abnormalities. *Hepatology*, 41(4):868-878.

Dohm J. A., Lee S. J., Hardwick J. M., Hill R. B. and Gittis A. G. (2004). Cytosolic domain of the human mitochondrial fission protein fis1 adopts a TPR fold. *Proteins*, 54(1):153-156.

Duvezin-Caubet S., Jagasia R., Wagener J., Hofmann S., Trifunovic A., Hansson A., Chomyn A., Bauer M. F., Attardi G., Larsson N.-G., Neupert W. and Reichert A. S. (2006). Proteolytic processing of OPA1 links mitochondrial dysfunction to alterations in mitochondrial morphology. *The Journal of Biological Chemistry*, 281(49):37972-37979.

Elmore S. P., Qian T., Grissom S. F. and Lemasters J. J. (2001). The mitochondrial permeability transition initiates autophagy in rat hepatocytes. *The FASEB Journal*, 15(12):2286-2287.

Finsterer J. (2007). Genetic, pathogenetic, and phenotypic implications of the mitochondrial A3243G tRNALeu(UUR) mutation. *Acta Neurologica Scandinavica*, 116(1):1-14.

Forss-Petter S., Werner H., Berger J., Lassmann H., Molzer B., Schwab M. H., Bernheimer H., Zimmermann F. and Nave K. A. (1997). Targeted inactivation of the X-linked adrenoleukodystrophy gene in mice. *Journal of Neuroscience Research*, 50(5):829-843.

Fransson A., Ruusala A. and Aspenström P. (2003). Atypical Rho GTPases have roles in mitochondrial homeostasis and apoptosis. *The Journal of Biological Chemistry*, 278(8):6495-6502.

Fransson S., Ruusala A. and Aspenström P. (2006). The atypical Rho GTPases Miro-1 and Miro-2 have essential roles in mitochondrial trafficking. *Biochemical and Biophysical Research Communications*, 344(2):500-510.

Frederick R. L., McCaffery J. M., Cunningham K. W., Okamoto K. and Shaw J. M. (2004). Yeast Miro GTPase, Gem1p, regulates mitochondrial morphology *via* a novel pathway. *The Journal of Cell Biology*, 167(1):87-98.

Frey T. G. and Mannella C. A. (2000). The internal structure of mitochondria. *Trends in Biochemical Sciences*, 25(7):319-324.

Frezza C., Cipolat S., Martins de Brito O., Micaroni M., Beznoussenko G. V., Rudka T., Bartoli D., Polishuck R. S., Danial N. N., De Strooper B. and Scorrano L. (2006). OPA1 controls apoptotic cristae remodeling independently from mitochondrial fusion. *Cell*, 126(1):177-189.

Gandre-Babbe S. and van der Bliek A. M. (2008). The novel tail-anchored membrane protein Mff controls mitochondrial and peroxisomal fission in mammalian cells. *Molecular Biology of the Cell*, 19(6):2402-2412.

Ginsberg M. D., Feliciello A., Jones J. K., Avvedimento E. V. and Gottesman M. E. (2003). PKA-dependent binding of mRNA to the mitochondrial AKAP121 protein. *Journal of Molecular Biology*, 327(4):885-897.

Glater E. E., Megeath L. J., Stowers R. S. and Schwarz T. L. (2006). Axonal transport of mitochondria requires milton to recruit kinesin heavy chain and is light chain independent. *The Journal of Cell Biology*, 173(4):545-557.

Goldfischer S., Moore C. L., Johnson A. B., Spiro A. J., Valsamis M. P., Wisniewski H. K., Ritch R. H., Norton W. T., Rapin I. and Gartner L. M. (1973). Peroxisomal and mitochondrial defects in the cerebro-hepato-renal syndrome. *Science*, 182(107):62-64.

Gomes L. C. and Scorrano L. (2008). High levels of Fis1, a pro-fission mitochondrial protein, trigger autophagy. *Biochimica et Biophysica Acta – Bioenergetics*, 1777(7):860-866.

Greene J. C., Whitworth A. J., Kuo I., Andrews L. A., Feany M. B. and Pallanck L. J. (2003). Mitochondrial pathology and apoptotic muscle degeneration in *Drosophila* parkin mutants. *Proceedings of the National Academy of Sciences of the United States of America*, 100(7):4078-4083.

Griparic L., van der Wel N. N., Orozco I. J., Peters P. J. and van der Bliek A. M. (2004). Loss of the intermembrane space protein Mgm1/Opa1 induces swelling and localized constrictions along the lengths of mitochondria. *The Journal of Biological Chemistry*, 279(18):18792-18798.

Guillery O., Malka F., Frachon P., Milea D., Rojo M. and Lombès A. (2008a). Modulation of mitochondrial morphology by bioenergetics defects in primary human fibroblasts. *Neuromuscular Disorders*, 18(4):319-330.

Guillery O., Malka F., Landes T., Guillou E., Blackstone C., Lombès A., Belenguer P., Arnoult D. and Rojo M. (2008b). Metalloprotease-mediated OPA1 processing is modulated by the mitochondrial membrane potential. *Biology of the Cell*, 100(5):315-325.

Guo X., Chen K. H., Guo Y., Liao H., Tang J. and Xiao R. P. (2007). Mitofusin 2 triggers vascular smooth muscle cell apoptosis *via* mitochondrial death pathway. *Circulation Research*, 101(11):1113-1122.

Guo X., Macleod G. T., Wellington A., Hu F., Panchumarthi S., Schoenfield M., Marin L., Charlton M. P., Atwood H. L. and Zinsmaier K. E. (2005). The GTPase dMiro is required for axonal transport of mitochondria to *Drosophila* synapses. *Neuron*, 47(3):379-393.

Habermann A., Schroer T. A., Griffiths G. and Burkhardt J. K. (2001). Immunolocalization of cytoplasmic dynein and dynactin subunits in cultured macrophages: enrichment on early endocytic organelles. *Journal of Cell Science*, 114(1):229-240.

Hales K. G. and Fuller M. T. (1997). Developmentally regulated mitochondrial fusion mediated by a conserved, novel, predicted GTPase. *Cell*, 90(1):121-129.

Hayashi J., Ohta S., Kagawa Y., Takai D., Miyabayashi S., Tada K., Fukushima H., Inui K., Okada S., Goto Y. and Nonaka I. (1994). Functional and morphological abnormalities of mitochondria in human cells containing mitochondrial DNA with pathogenic point mutations in tRNA genes. *The Journal of Biological Chemistry*, 269(29):19060-19066.

Herlan M., Vogel F., Bornhovd C., Neupert W. and Reichert A. S. (2003). Processing of Mgm1 by the rhomboid-type protease Pcp1 is required for maintenance of mitochondrial morphology and of mitochondrial DNA. *The Journal of Biological Chemistry*, 278(30):27781-27788.

Hermann G. J., Thatcher J. W., Mills J. P., Hales K. G., Fuller M. T., Nunnari J. and Shaw J. M. (1998). Mitochondrial fusion in yeast requires the transmembrane GTPase Fzo1p. *The Journal of Cell Biology*, 143(2):359-373.

Hirokawa N. (1982). Cross-linker system between neurofilaments, microtubules, and membranous organelles in frog axons revealed by the quick-freeze, deep-etching method. *The Journal of Cell Biology*, 94(1):129-142.

Hollenbeck P. J. (1996). The pattern and mechanism of mitochondrial transport in axons. *Frontiers in Bioscience*, 1:d91-d102.

Hollenbeck P. J. and Saxton W. M. (2005). The axonal transport of mitochondria. *Journal of Cell Science*, 118(23):5411-5419.

Huckriede A. and Agsteribbe E. (1994). Decreased synthesis and inefficient mitochondrial import of hsp60 in a patient with a mitochondrial encephalomyopathy. *Biochimica et Biophysica Acta*, 1227(3):200-206.

Huckriede A., Heikema A., Sjollema K., Briones P. and Agsteribbe E. (1995). Morphology of the mitochondria in heat shock protein 60 deficient fibroblasts from mitochondrial myopathy patients. Effects of stress conditions. *Virchows Archiv*, 427(2):159-165.

Iancu T. C., Mason W. H. and Neustein H. B. (1977). Ultrastructural abnormalities of liver cells in Reye's syndrome. *Human Pathology*, 8(4):421-431.

Ichimura Y., Kirisako T., Takao T., Satomi Y., Shimonishi Y., Ishihara N., Mizushima N., Tanida I., Kominami E., Ohsumi M., Noda T. and Ohsumi Y. (2000). A ubiquitin-like system mediates protein lipidation. *Nature*, 408(6811):488-492.

Ingerman E., Perkins E. M., Marino M., Mears J. A., McCaffery J. M., Hinshaw J. E. and Nunnari J. (2005). Dnm1 forms spirals that are structurally tailored to fit mitochondria. *The Journal of Cell Biology*, 170(7):1021-1027.

Ishihara N., Eura Y. and Mihara K. (2004). Mitofusin 1 and 2 play distinct roles in mitochondrial fusion reactions *via* GTPase activity. *Journal of Cell Science*, 117(26):6535-6546.

Ishihara N., Fujita Y., Oka T. and Mihara K. (2006). Regulation of mitochondrial morphology through proteolytic cleavage of OPA1. *The EMBO Journal*, 25(13):2966-2977.

James D. I., Parone P. A., Mattenberger Y. and Martinou J.-C. (2003). hFis1, a novel component of the mammalian mitochondrial fission machinery. *The Journal of Biological Chemistry*, 278(38):36373-36379.

Jiménez A., Carrasco L. and Vázquez D. (1977). Enzymic and nonenzymic translocation by yeast polysomes. Site of action of a number of inhibitors. *Biochemistry*, 16(21):4727-4730.

Jones B. A. and Fangman W. L. (1992). Mitochondrial DNA maintenance in yeast requires a protein containing a region related to the GTP-binding domain of dynamin. *Genes and Development*, 6(3):380-389.

Kabeya Y., Mizushima N., Ueno T., Yamamoto A., Kirisako T., Noda T., Kominami E., Ohsumi Y. and Yoshimori T. (2000). LC3, a mammalian homologue of yeast Apg8p, is localized in autophagosome membranes after processing. *The EMBO Journal*, 19(21):5720-5728.

Kabeya Y., Mizushima N., Yamamoto A., Oshitani-Okamoto S., Ohsumi Y. and Yoshimori T. (2004). LC3, GABARAP and GATE16 localize to autophagosomal membrane depending on form-II formation. *Journal of Cell Science*, 117(13):2805-2812.

Kang J.-S., Tian J.-H., Pan P.-Y., Zald P., Li C., Deng C. and Sheng Z.-H. (2008). Docking of axonal mitochondria by syntaphilin controls their mobility and affects short-term facilitation. *Cell*, 132(1):137-148.

Kemp S., Wei H. M., Lu J. F., Braiterman L. T., McGuinness M. C., Moser A. B., Watkins P. A. and Smith K. D. (1998). Gene redundancy and pharmacological gene therapy: implications for X-linked adrenoleukodystrophy. *Nature Medicine*, 4(11):1261-1268.

Kim I., Mizushima N. and Lemasters J. J. (2006). Selective removal of damaged mitochondria by autophagy (mitophagy). *Hepatology*, 44(Suppl1):241A Abstract.

Kim I., Rodriguez-Enriquez S., Mizushima N., Ohsumi Y. and Lemasters J. J. (2004). Autophagic degradation of mitochondria in GFP-LC3 transgenic mouse hepatocytes after nutrient deprivation. *Hepatology*, 40(Suppl1):291A Abstract.

Kirisako T., Ichimura Y., Okada H., Kabeya Y., Mizushima N., Yoshimori T., Ohsumi M., Takao T., Noda T. and Ohsumi Y. (2000). The reversible modification regulates the membrane-binding state of Apg8/Aut7 essential for autophagy and the cytoplasm to vacuole targeting pathway. *The Journal of Cell Biology*, 151(2):263-276.

Kitada T., Asakawa S., Hattori N., Matsumine H., Yamamura Y., Minoshima S., Yokochi M., Mizuno Y. and Shimizu N. (1998). Mutations in the parkin gene cause autosomal recessive juvenile parkinsonism. *Nature*, 392(6676):605-608.

Kobayashi S., Tanaka A. and Fujiki Y. (2007). Fis1, DLP1, and Pex11p co-ordinately regulate peroxisome morphogenesis. *Experimental Cell Research*, 313(8):1675-1686.

Kobayashi T., Shinnoh N., Kondo A. and Yamada T. (1997). Adrenoleukodystrophy protein-deficient mice represent abnormality of very long chain fatty acid metabolism. *Biochemical and Biophysical Research Communications*, 232(3):631-636.

Koch A., Schneider G., Lüers G. H. and Schrader M. (2004). Peroxisome elongation and constriction but not fission can occur independently of dynamin-like protein 1. *Journal of Cell Science*, 117(17):3995-4006.

Koch A., Thiemann M., Grabenbauer M., Yoon Y., McNiven M. A. and Schrader M. (2003). Dynamin-like protein 1 is involved in peroxisomal fission. *The Journal of Biological Chemistry*, 278(10):8597-8605.

Koch A., Yoon Y., Bonekamp N. A., McNiven M. A. and Schrader M. (2005). A role for Fis1 in both mitochondrial and peroxisomal fission in mammalian cells. *Molecular Biology of the Cell*, 16(11):5077-5086.

Koepke J. I., Nakrieko K.-A., Wood C. S., Boucher K. K., Terlecky L. J., Walton P. A. and Terlecky S. R. (2007). Restoration of peroxisomal catalase import in a model of human cellular aging. *Traffic*, 8(11):1590-600.

Koepke J. I., Wood C. S., Terlecky L. J., Walton P. A. and Terlecky S. R. (2008). Progeric effects of catalase inactivation in human cells. *Toxicology and Applied Pharmacology*, 232(1):99-108.

Koopman W. J., Verkaart S., Visch H. J., van Emst-de Vries S., Nijtmans L. G., Smeitink J. A. and Willems P. H. (2007). Human NADH:ubiquinone oxidoreductase deficiency: radical changes in mitochondrial morphology? *American Journal of Physiology – Cell Physiology*, 293(1):C22-C29.

Koshiba T., Detmer S. A., Kaiser J. T., Chen H., McCaffery J. M. and Chan D. C. (2004). Structural basis of mitochondrial tethering by mitofusin complexes. *Science*, 305(5685):858-862.

Köttgen M., Benzing T., Simmen T., Tauber R., Buchholz B., Feliciangeli S., Huber T. B., Schermer B., Kramer-Zucker A., Höpker K., Simmen K. C., Tschucke C. C., Sandford R., Kim E., Thomas G. and Walz G. (2005). Trafficking of TRPP2 by PACS proteins represents a novel mechanism of ion channel regulation. *The EMBO Journal*, 24(4):705-716.

Labrousse A. M., Zappaterra M. D., Rube D. A. and van der Bliek A. M. (1999). *C. elegans* dynamin-related protein DRP-1 controls severing of the mitochondrial outer membrane. *Molecular Cell*, 4(5):815-826.

Lao G., Scheuss V., Gerwin C. M., Su Q., Mochida S., Rettig J. and Sheng Z. H. (2000). Syntaphilin: a syntaxin-1 clamp that controls SNARE assembly. *Neuron*, 25(1):191-201.

Lazarow P. B., Black V., Shio H., Fujiki Y., Hajra A. K., Datta N. S., Bangaru B. S., Dancis J. (1985). Zellweger syndrome: biochemical and morphological studies on two patients treated with clofibrate. *Pediatric Research*, 19(12):1356-1364.

Legesse-Miller A., Massol R. H. and Kirchhausen T. (2003). Constriction and Dnm1p recruitment are distinct processes in mitochondrial fission. *Molecular Biology of the Cell*, 14(5):1953-1963.

Legros F., Lombès A., Frachon P. and Rojo M. (2002). Mitochondrial fusion in human cells is efficient, requires the inner membrane potential, and is mediated by mitofusins. *Molecular Biology of the Cell*, 13(12):4343-4354.

Li X. and Gould S. J. (2003). The dynamin-like GTPase DLP1 is essential for peroxisome division and is recruited to peroxisomes in part by PEX11. *The Journal of Biological Chemistry*, 278(19):17012-17020.

Ligon L. A. and Steward O. (2000). Role of microtubules and actin filaments in the movement of mitochondria in the axons and dendrites of cultured hippocampal neurons. *The Journal of Comparative Neurology*, 427(3):351-361.

Lin R.-Y., Moss S. B. and Rubin C. S. (1995). Characterization of S-AKAP84, a novel developmentally regulated A kinase anchor protein of male germ cells. *The Journal of Biological Chemistry,* 270(46):27804–27811.

Loiseau D., Chevrollier A., Verny C., Guillet V., Gueguen N., Pou de Crescenzo M.-A., Ferré M., Malinge M.-C., Guichet A., Nicolas G., Amati-Bonneau P., Malthièry Y., Bonneau D. and Reynier P. (2007). Mitochondrial coupling defect in Charcot-Marie-Tooth type 2A disease. *Annals of Neurology*, 61(4):315-323.

Lowry O. H., Rosebrough N. J., Farr A. L. and Randall R. J. (1951). Protein measurement with the Folin phenol reagent. *The Journal of Biological Chemistry*, 193(1):265-275.

Lu J. F., Lawler A. M., Watkins P. A., Powers J. M., Moser A. B., Moser H. W. and Smith K. D. (1997). A mouse model for X-linked adrenoleukodystrophy. *Proceedings of the National Academy of Sciences of the United States of America*, 94(17):9366-9371.

MacAskill A. F., Brickley K., Stephenson F. A. and Kittler J. T. (2009a). GTPase dependent recruitment of Grif-1 by Miro1 regulates mitochondrial trafficking in hippocampal neurons. *Molecular and Cellular Neurosciences*, 40(3):301-312.

MacAskill A. F., Rinholm J. E., Twelvetrees A. E., Arancibia-Carcamo I. L., Muir J., Fransson A., Aspenstrom P., Attwell D. and J. T. Kittler J. T. (2009b). Miro1 is a calcium sensor for glutamate receptor-dependent localization of mitochondria at synapses. *Neuron*, 61(4):541-555.

Malka F., Guillery O., Cifuentes-Diaz C., Guillou E., Belenguer P., Lombès A. and Rojo M. (2005). Separate fusion of outer and inner mitochondrial membranes. *EMBO Reports*, 6(9):853-859.

Mannella C. A. (2006). Structure and dynamics of the mitochondrial inner membrane cristae. *Biochimica et Biophysica Acta – Molecular Cell Research*, 1763(5):542-548.

Mannella C. A. (2008). Structural diversity of mitochondria: functional implications. *Annals of the New York Academy of Sciences*, 1147:171-179.

Mannella C. A., Buttle K., Rath B. K. and Marko M. (1998). Electron microscopic tomography of rat-liver mitochondria and their interaction with the endoplasmic reticulum. *Biofactors*, 8(3):225-228.

Margineantu D. H., Brown R. M., Brown G. K., Marcus A. H. and Capaldi R. A. (2002). Heterogeneous distribution of pyruvate dehydrogenase in the matrix of mitochondria. *Mitochondrion*, 1(4):327-338.

Marsh B. J., Mastronarde D. N., Buttle K. F., Howell K. E. and McIntosh J. R. (2001). Organellar relationships in the Golgi region of the pancreatic beta cell line, HIT-T15, visualized by high resolution electron tomography. *Proceedings of the National Academy of Sciences of the United States of America*, 98(5):2399-2406.

Mayorov V. I., Lowrey A. J., Biousse V., Newman N. J., Cline S. D. and Brown M. D. (2008). Mitochondrial oxidative phosphorylation in autosomal dominant optic atrophy. *BMC Biochemistry*, 9:22-28.

McCormack J. G., Halestrap A. P. and Denton R. M. (1990). Role of calcium ions in regulation of mammalian intramitochondrial metabolism. *Physiological Reviews*, 70(2):391-425.

McGuinness M. C., Lu J. F., Zhang H. P., Dong G. X., Heinzer A. K., Watkins P. A., Powers J. and Smith K. D. (2003). Role of ALDP (ABCD1) and mitochondria in X-linked adrenoleukodystrophy. *Molecular and Cellular Biology*, 23(2):744-753.

McGuinness M. C., Zhang H. P. and Smith K. D. (2001). Evaluation of pharmacological induction of fatty acid beta-oxidation in X-linked adrenoleukodystrophy. *Molecular Genetics and Metabolism*, 74(1):256-263.

McQuibban G. A., Saurya S. and Freeman M. (2003). Mitochondrial membrane remodelling regulated by a conserved rhomboid protease. *Nature*, 423(6939):537-541.

Meeusen S., DeVay R., Block J., Cassidy-Stone A., Wayson S., McCaffery J. M. and Nunnari J. (2006). Mitochondrial inner-membrane fusion and crista maintenance requires the dynamin-related GTPase Mgm1. *Cell*, 127(2):383-395.

Meeusen S., McCaffery J. M. and Nunnari J. (2004). Mitochondrial fusion intermediates revealed *in vitro*. *Science*, 305(5691):1747-1752.

Meier P. J., Spycher M. A. and Meyer U. A. (1981). Isolation and characterization of rough endoplasmic reticulum associated with mitochondria from normal rat liver. *Biochimica et Biophysica Acta – Biomembranes*, 646(2):283-297.

Messerschmitt M., Jakobs S., Vogel F., Fritz S., Dimmer K. S., Neupert W. and Westermann B. (2003). The inner membrane protein Mdm33 controls mitochondrial morphology in yeast. *The Journal of Cell Biology*, 160(4):553-564.

Mironov S. L. and Symonchuk N. (2006). ER vesicles and mitochondria move and communicate at synapses. *Journal of Cell Science*, 119(23):4926-4934.

Misko A., Jiang S., Wegorzewska I., Milbrandt J. and Baloh R. H. (2010). Mitofusin 2 is necessary for transport of axonal mitochondria and interacts with the Miro/Milton complex. *The Journal of Neuroscience*, 30(12):4232-4240.

Mizushima N., Ohsumi Y. and Yoshimori T. (2002). Autophagosome formation in mammalian cells. *Cell Structure and Function*, 27(6):421-429.

Mizushima N., Yamamoto A., Matsui M., Yoshimori T. and Ohsumi Y. (2004). *In vivo* analysis of autophagy in response to nutrient starvation using transgenic mice expressing a fluorescent autophagosome marker. *Molecular Biology of the Cell*, 15(3):1101-1111.

Morán M., Rivera H., Sánchez-Aragó M., Blázquez A., Merinero B., Ugalde C., Arenas J., Cuezva J. M. and Martín M. A. (2010). Mitochondrial bioenergetics and dynamics interplay in complex I-deficient fibroblasts. *Biochimica et Biophysica Acta – Molecular Basis of Disease*, 1802(5):443-453.

Morris R. L. and Hollenbeck P. J. (1993). The regulation of bidirectional mitochondrial transport is coordinated with axonal outgrowth. *Journal of Cell Science*, 104(3):917-927.

Morris R. L. and Hollenbeck P. J. (1995). Axonal transport of mitochondria along microtubules and F-actin in living vertebrate neurons. *The Journal of Cell Biology*, 131(5):1315-1326.

Mosser J., Douar A. M., Sarde C. O., Kioschis P., Feil R., Moser H., Poustka A. M., Mandel J. L. and Aubourg P. (1993). Putative X-linked adrenoleukodystrophy gene shares unexpected homology with ABC transporters. *Nature*, 361(6414):726-730.

Mosser J., Lutz Y., Stoeckel M. E., Sarde C. O., Kretz C., Douar A. M., Lopez J., Aubourg P. and Mandel J. L. (1994). The gene responsible for adrenoleukodystrophy encodes a peroxisomal membrane protein. *Human Molecular Genetics*, 3(2):265-271.

Mozdy A. D., McCaffery J. M. and Shaw J. M. (2000). Dnm1p GTPase-mediated mitochondrial fission is a multi-step process requiring the novel integral membrane component Fis1p. *The Journal of Cell Biology*, 151(2):367-380.

Narendra D., Tanaka A., Suen D.-F. and Youle R. J. (2008). Parkin is recruited selectively to impaired mitochondria and promotes their autophagy. *The Journal of Cell Biology*, 183(5):795-803.

Navratil M., Terman A. and Arriaga E. A. (2008). Giant mitochondria do not fuse and exchange their contents with normal mitochondria. *Experimental Cell Research*, 314(1):164-172.

Neuspiel M., Schauss A. C., Braschi E., Zunino R., Rippstein P., Rachubinski R. A., Andrade-Navarro M. A. and McBride H. M. (2008). Cargo-selected transport from the mitochondria to peroxisomes is mediated by vesicular carriers. *Current Biology*, 18(2):102-108.

Nicholls D. G. and Crompton M. (1980). Mitochondrial calcium transport. *FEBS Letters*, 111(2):261-268.

Niemann A., Ruegg M., La Padula V., Schenone A. and Suter U. (2005). Ganglioside-induced differentiation associated protein 1 is a regulator of the mitochondrial network: new implications for Charcot-Marie-Tooth disease. *The Journal of Cell Biology*, 170(7):1067-1078.

Olichon A., Baricault L., Gas N., Guillou E., Valette A., Belenguer P. and Lenaers G. (2003). Loss of OPA1 perturbates the mitochondrial inner membrane structure and integrity, leading to cytochrome c release and apoptosis. *The Journal of Biological Chemistry*, 278(10):7743-7746.

Otsuga D., Keegan B. R., Brisch E., Thatcher J. W., Hermann G. J., Bleazard W. and Shaw J. M. (1998). The dynamin-related GTPase, Dnm1p, controls mitochondrial morphology in yeast. *The Journal of Cell Biology*, 143(2):333-349.

Overly C. C., Rieff H. I. and Hollenbeck P. J. (1996). Organelle motility and metabolism in axons vs dendrites of cultured hippocampal neurons. *Journal of Cell Science*, 109(5):971-980.

Pannese E., Procacci P., Ledda M., Arcidiacono G., Frattola D. and Rigamonti L. (1986). Association between microtubules and mitochondria in myelinated axons of *Lacerta muralis*. A quantitative analysis. *Cell and Tissue Research*, 245(1):1-8.

Pedrola L., Espert A., Valdés-Sánchez T., Sánchez-Piris M., Sirkowski E. E., Scherer S. S., Fariñas I. and Palau F. (2008). Cell expression of GDAP1 in the nervous system and pathogenesis of Charcot-Marie-Tooth type 4A disease. *Journal of Cellular and Molecular Medicine*, 12(2):679-689.

Pellegrini L. and Scorrano L. (2007). A short cut to death: Parl and Opa1 in the regulation of mitochondrial morphology and apoptosis. *Cell Death and Differentiation*, 14(7):1275-1284.

Petiot A., Ogier-Denis E., Blommaart E. F., Meijer A. J. and Codogno P. (2000). Distinct classes of phosphatidylinositol 3'-kinases are involved in signalling pathways that control macroautophagy in HT-29 cells. *The Journal of Biological Chemistry*, 275(2):992-998.

Pham N.-A., Richardson T., Cameron J., Chue B. and Robinson B. H. (2004). Altered mitochondrial structure and motion dynamics in living cells with energy metabolism defects revealed by real time microscope imaging. *Microscopy and Microanalysis*, 10(2):247-260.

Pich S., Bach D., Briones P., Liesa M., Camps M., Testar X., Palacín M. and Zorzano A. (2005). The Charcot-Marie-Tooth type 2A gene product, Mfn2, up-regulates fuel oxidation through expression of OXPHOS system. *Human Molecular Genetics*, 14(11):1405-1415.

Pilling A. D., Horiuchi D., Lively C. M. and Saxton W. M. (2006). Kinesin-1 and Dynein are the primary motors for fast transport of mitochondria in *Drosophila* motor axons. *Molecular Biology of the Cell*, 17(4):2057-2068.

Pitts K. R., Yoon Y., Krueger E. W. and McNiven M. A. (1999). The dynamin-like protein DLP1 is essential for normal distribution and morphology of the endoplasmic reticulum and mitochondria in mammalian cells. *Molecular Biology of the Cell*, 10(12):4403-4417.

Poot M., Zhang Y. Z., Krämer J. A., Wells K. S., Jones L. J., Hanzel D. K., Lugade A. G., Singer V. L. and Haugland R. P. (1996). Analysis of mitochondrial morphology and function with novel fixable fluorescent stains. *The Journal of Histochemistry and Cytochemistry*, 44(12):1363-1372.

Powers J. M., DeCiero D. P., Cox C., Richfield E. K., Ito M., Moser A. B. and Moser H. W. (2001). The dorsal root ganglia in adrenomyeloneuropathy: neuronal atrophy and abnormal mitochondria. *Journal of Neuropathology and Experimental Neurology*, 60(5):493-501.

Price R. L., Lasek R. J. and Katz M. J. (1991). Microtubules have special physical associations with smooth endoplasmic reticula and mitochondria in axons. *Brain Research*, 540(1):209-216.

Pruitt K. D., Harrow J., Harte R. A., Wallin C., Diekhans M., Maglott D. R., Searle S., Farrell C. M., Loveland J. E., Ruef B. J., Hart E., Suner M.-M., Landrum M. J., Aken B., Ayling S., Baertsch R., Fernandez-Banet J., Cherry J. L., Curwen V., Dicuccio M., Kellis M., Lee J., Lin M. F., Schuster M., Shkeda A., Amid C., Brown G., Dukhanina O., Frankish A., Hart J., Maidak B. L., Mudge J., Murphy M. R., Murphy T., Rajan J., Rajput B., Riddick L. D., Snow C., Steward C., Webb D., Weber J. A., Wilming L., Wu W., Birney E., Haussler D., Hubbard T., Ostell J., Durbin R. and Lipman D. (2009). The consensus coding sequence (CCDS) project: Identifying a common protein-coding gene set for the human and mouse genomes. *Genome Research*, 19(7):1316-1323.

Quintero O. A., DiVito M. M., Adikes R. C., Kortan M. B., Case L. B., Lier A. J., Panaretos N. S., Slater S. Q., Rengarajan M., Feliu M. and Cheney R. E. (2009). Human Myo19 is a novel myosin that associates with mitochondria. *Current Biology*, 19(23):2008-2013.

Rapaport D., Brunner M., Neupert W. and Westermann B. (1998). Fzo1p is a mitochondrial outer membrane protein essential for the biogenesis of functional mitochondria in *Saccharomyces cerevisiae*. *The Journal of Biological Chemistry*, 273(32):20150-20155.

Reers M., Smith T. W. and Chen L. B. (1991). J-aggregate formation of a carbocyanide as a quantitative fluorescent indicator of membrane potential. *Biochemistry*, 30(18):4480-4486.

Rizzuto R., Brini M., Murgia M. and Pozzan T. (1993). Microdomains with high Ca^{2+} close to IP_3-sensitive channels that are sensed by neighbouring mitochondria. *Science*, 262(5134):744-747.

Rizzuto R., Duchen M. R. and Pozzan T. (2004). Flirting in little space: the ER/mitochondria Ca^{2+} liaison. *Science STKE*, 2004(215):re1.

Rizzuto R., Marchi S., Bonora M., Aguiari P., Bononi A., De Stefani D., Giorgi C., Leo S., Rimessi A., Siviero R., Zecchini E. and Pinton P. (2009). Ca(2+) transfer from the ER to mitochondria: when, how and why. *Biochimica et Biophysica Acta*, 1787(11):1342-1351.

Rizzuto R., Pinton P., Carrington W., Fay F. S., Fogarty K. E., Lifshitz L. M., Tuft R. A. and Pozzan T. (1998). Close contacts with the endoplasmic reticulum as determinants of mitochondrial Ca^{2+} responses. *Science*, 280(5370):1763-1766.

Rizzuto R., Simpson A. W., Brini M. and Pozzan T. (1992). Rapid changes of mitochondrial Ca^{2+} revealed by specifically targeted recombinant aequorin. *Nature*, 358(6384):325-327.

Rodionov V. I., Gyoeva F. K., Tanaka E., Bershadsky A. D., Vasiliev J. M. and Gelfand V. I. (1993). Microtubule-dependent control of cell shape and pseudopodial activity is inhibited by the antibody to kinesin motor domain. *The Journal of Cell Biology*, 123(6Pt2):1811-1820.

Rodriguez-Enriquez S., Kim I., Currin R. T. and Lemasters J. J. (2006). Tracker dyes to probe mitochondrial autophagy (mitophagy) in rat hepatocytes. *Autophagy*, 2(1):39-46.

Rogne M., Landsverk H. B., Van Eynde A., Beullens M., Bollen M., Collas P. and Küntziger T. (2006). The KH-Tudor domain of A-kinase anchoring protein 149 mediates RNA-dependent self-association. *Biochemistry*, 45(50):14980-14989.

Rogne M., Stokka A. J., Taskén K., Collas P. and Küntziger T. (2009). Mutually exclusive binding of PP1 and RNA to AKAP149 affects the mitochondrial network. *Human Molecular Genetics*, 18(5):978-987.

Rojo M., Legros F., Chateau D. and Lombès A. (2002). Membrane topology and mitochondrial targeting of mitofusins, ubiquitous mammalian homologs of the transmembrane GTPase Fzo. *Journal of Cell Science*, 115(8):1663-1674.

Rozen S. and Skaletsky H. (2000). Primer3 on the WWW for general users and for biologist programmers. *Methods in Molecular Biology*, 132:365-386.

Russo A., Russo G., Cuccurese M., Garbi C. and Pietropaolo C. (2006). The 3'-untranslated region directs ribosomal protein-encoding mRNAs to specific cytoplasmic regions. *Biochimica et Biophysica Acta – Molecular Cell Research*, 1763(8):833-843.

Santel A. and Frank S. (2008). Shaping mitochondria: The complex posttranslational regulation of the mitochondrial fission protein DRP1. *IUBMB Life*, 60(7):448-455.

Santel A.and Fuller M. T. (2001). Control of mitochondrial morphology by a human mitofusin. *Journal of Cell Science*, 114(5):867-874.

Saotome M., Safiulina D., Szabadkai G., Das S., Fransson A., Aspenstrom P., Rizzuto R. and Hajnóczky G. (2008). Bidirectional Ca^{2+}-dependent control of mitochondrial dynamics by the Miro GTPase. *Proceedings of the National Academy of Sciences of the United States of America*, 105(52):20728-20733.

Sarnat H. B., Machin G., Darwish H. Z. And Rubin S. Z. (1983). Mitochondrial myopathy of cerebro-hepato-renal (Zellweger) syndrome. *The Canadian Journal of Neurological Sciences*, 10(3):170-177.

Scaglia F. and Wong L.-J. (2008). Human mitochondrial transfer RNAs: role of pathogenic mutation in disease. *Muscle and Nerve*, 37(2):150-171.

Schnapp B. J. and Reese T. S. (1982). Cytoplasmic structure in rapid-frozen axons. *The Journal of Cell Biology*, 94(3):667-669.

Schrader M. (2006). Shared components of mitochondrial and peroxisomal division. *Biochimica et Biophysica Acta – Molecular Cell Research*, 1763(5):531-541.

Schrader M. and Fahimi H. D. (2008). The peroxisome: still a mysterious organelle. *Histochemistry and Cell Biology*, 129(4):421-440.

Schrader M., Reuber B. E., Morrell J. C., Jimenez-Sanchez G., Obie C., Stroh T. A., Valle D., Schroer T. A. and Gould S. J. (1998). Expression of PEX11beta mediates peroxisome proliferation in the absence of extracellular stimuli. *The Journal of Biological Chemistry*, 273(45):29607-29614.

Seligman A. M., Karnovsky M. J., Wasserkrug H. L. and Hanker J. S. (1968). Nondroplet ultrastructural demonstration of cytochrome oxidase activity with a polymerizing osmiophilic reagent, diaminobenzidine (DAB). *The Journal of Cell Biology*, 38(1):1-14.

Senderek J., Bergmann C., Ramaekers V. T., Nelis E., Bernert G., Makowski A., Züchner S., De Jonghe P., Rudnik-Schöneborn S., Zerres K. and Schröder J. M. (2003). Mutations in the ganglioside-induced differentiation-associated protein-1 (GDAP1) gene in intermediate type autosomal recessive Charcot-Marie-Tooth neuropathy. *Brain*, 126(3):642-649.

Sesaki H., Southard S. M., Hobbs A. E. and Jensen R. E. (2003). Cells lacking Pcp1p/Ugo2p, a rhomboid-like protease required for Mgm1p processing, lose mtDNA and mitochondrial structure in a Dnm1p-dependent manner, but remain competent for mitochondrial fusion. *Biochemical and Biophysical Research Communications*, 308(2):276-283.

Shore G. C. and Tata J. R. (1977). Two fractions of rough endoplasmic reticulum from rat liver. I. Recovery of rapidly sedimenting endoplasmic reticulum in association with mitochondria. *The Journal of Cell Biology*, 72(3):714-725.

Simmen T., Aslan J. E., Blagoveshchenskaya A. D., Thomas L., Wan L., Xiang Y., Feliciangeli S. F., Hung C. H., Crump C. M. and Thomas G. (2005). PACS-2 controls endoplasmic reticulum-mitochondria communication and Bid-mediated apoptosis. *The EMBO Journal*, 24(4):717-729.

Singer V. L., Jones L. J., Yue S. T. and Haugland R. P. (1997). Characterization of PicoGreen reagent and development of a fluorescence-based solution assay for double-stranded DNA quantitation. *Analytical Biochemistry*, 249(2):228-238.

Smiley S. T., Reers M., Mottola-Hartshorn C., Lin M., Chen A., Smith T. W., Steele G. D. Jr and Chen L. B. (1991). Intracellular heterogeneity in mitochondrial membrane potentials revealed by a J-aggregate-forming lipophilic cation JC-1. *Proceedings of the National Academy of Sciences of the United States of America*, 88(9):3671-3675.

Smirnova E., Griparic L., Shurland D. L. and van der Bliek A. M. (2001). Dynamin-related protein Drp1 is required for mitochondrial division in mammalian cells. *Molecular Biology of the Cell*, 12(8):2245-2256.

Smirnova E., Shurland D. L., Ryazantsev S. N. and van der Bliek A. M. (1998). A human dynamin-related protein controls the distribution of mitochondria. *The Journal of Cell Biology*, 143(2):351-358.

Smith M. J., Pozo K., Brickley K. and Stephenson F. A. (2006). Mapping the GRIF-1 binding domain of the kinesin, KIF5C, substantiates a role for GRIF-1 as an adaptor protein in the anterograde trafficking of cargoes. *The Journal of Biological Chemistry*, 281(37):27216-27228.

Spinazzi M., Cazzola S., Bortolozzi M., Baracca A., Loro E., Casarin A., Solaini G., Sgarbi G., Casalena G., Cenacchi G., Malena A., Frezza C., Carrara F., Angelini C., Scorrano L., Salviati L. and Vergani L. (2008). A novel deletion in the GTPase domain of OPA1 causes defects in mitochondrial morphology and distribution, but not in function. *Human Molecular Genetics*, 17(21):3291-3302.

Steen R. L., Martins S. B., Taskén K. and Collas P. (2000). Recruitment of protein phosphatase 1 to the nuclear envelope by A-kinase anchoring protein AKAP149 is a prerequisite for nuclear lamina assembly. *The Journal of Cell Biology*, 150(6):1251-1262.

Stowers R. S., Megeath L. J., Górska-Andrzejak J., Meinertzhagen I. A. and Schwarz T. L. (2002). Axonal transport of mitochondria to synapses depends on milton, a novel *Drosophila* protein. *Neuron*, 36(6):1063-1077.

Stroikin Y., Dalen H., Lööf S. and Terman A. (2004). Inhibition of autophagy with 3-methyladenine results in impaired turnover of lysosomes and accumulation of lipofuscin-like material. *European Journal of Cell Biology*, 83(10):583-590.

Suzuki M., Jeong S. Y., Karbowski M., Youle R. J. and Tjandra N. (2003). The solution structure of human mitochondrial fission protein Fis1 reveals a novel TPR-like helix bundle. *Journal of Molecular Biology*, 334(3):445-458.

Sylvestre J., Margeot A., Jacq C., Dujardin G. and Corral-Debrinski M. (2003a). The role of the 3' untranslated region in mRNA sorting to the vicinity of mitochondria is conserved from yeast to human cells. *Molecular Biology of the Cell*, 14(9):3848-3856.

Sylvestre J., Vialette S., Corral-Debrinski M. and Jacq C. (2003b). Long mRNAs coding for yeast mitochondrial proteins of prokaryotic origin preferentially localize to the vicinity of mitochondria. *Genome Biology*, 4(7):R44.

Szabadkai G., Bianchi K., Várnai P., De Stefani D., Wieckowski M. R., Cavagna D., Nagy A. I., Balla T. and Rizzuto R. (2006). Chaperone-mediated coupling of endoplasmic reticulum and mitochondrial Ca^{2+} channels. *The Journal of Cell Biology*, 175(6):901-911.

Szabadkai G., Simoni A. M., Chami M., Wieckowski M. R., Youle R. J. and Rizzuto R. (2004). Drp-1-dependent division of the mitochondrial network blocks intraorganellar Ca^{2+} waves and protects against Ca^{2+}-mediated apoptosis. *Molecular Cell*, 16(1):59-68.

Szalai G., Krishnamurthy R. and Hajnóczky G. (1999). Apoptosis driven by IP(3)-linked mitochondrial calcium signals. *The EMBO Journal*, 18(22):6349-6361.

Tanaka Y., Kanai Y., Okada Y., Nonaka S., Takeda S., Harada A. and Hirokawa N. (1998). Targeted disruption of mouse conventional kinesin heavy chain, kif5B, results in abnormal perinuclear clustering of mitochondria. *Cell*, 93(7):1147-1158.

Tanida I., Komatsu M., Ueno T. and Kominami E. (2003). GATE-16 and GABARAP are authentic modifiers mediated by Apg7 and Apg3. *Biochemical and Biophysica Research Communications*, 300(3):637-644.

Terman A., Dalen H., Eaton J. W., Neuzil J. and Brunk U. T. (2003). Mitochondrial recycling and aging of cardiac myocytes: the role of autophagocytosis. *Experimental Gerontology*, 38(8):863-876.

Terman A., Dalen H., Eaton J. W., Neuzil J. and Brunk U. T. (2004). Aging of cardiac myocytes in culture: oxidative stress, lipofuscin accumulation, and mitochondrial turnover. *Annals of the New York Academy of Sciences*, 1019:70-77.

Tinel H., Cancela J. M., Mogami H., Gerasimenko J. V., Gerasimenko O. V., Tepikin A. V. and Petersen O. H. (1999). Active mitochondria surrounding the pancreatic acinar granule region prevent spreading of inositol trisphosphate-evoked local cytosolic Ca(2+) signals. *The EMBO Journal*, 18(18):4999-5008.

Tondera D., Czauderna F., Paulick K., Schwarzer R., Kaufmann J. and Santel A. (2005). The mitochondrial protein MTP18 contributes to mitochondrial fission in mammalian cells. *Journal of Cell Science*, 118(14):3049-3059.

Tondera D., Santel A., Schwarzer R., Dames S., Giese K., Klippel A. and Kaufmann J. (2004). Knockdown of MTP18, a novel phosphatidylinositol 3-kinase-dependent protein, affects mitochondrial morphology and induces apoptosis. *The Journal of Biological Chemistry*, 279(30):31544-31555.

Trendelenburg G., Hummel M., Riecken E. O. and Hanski C. (1996). Molecular characterization of AKAP149, a novel A kinase anchor protein with a KH domain. *Biochemical and Biophysical Research Communications*, 225(1):313-319.

Tucker E. J., Compton A. G. and Thorburn D. R. (2010). Recent advances in the genetics of mitochondrial encephalopathies. *Current Neurology and Neuroscience Reports*, 10(4):277-285.

Twig G., Elorza A., Molina A. J., Mohamed H., Wikstrom J. D., Walzer G., Stiles L., Haigh S. E., Katz S., Las G., Alroy J., Wu M., Py B. F., Yuan J., Deeney J. T., Corkey B. E. and Shirihai O. S. (2008a). Fission and selective fusion govern mitochondrial segregation and elimination by autophagy. *The EMBO Journal*, 27(2):433-446.

Twig G., Graf S. A., Wikstrom J. D., Mohamed H., Haigh S. E., Elorza A., Deutsch M., Zurgil N., Reynolds N. and Shirihai O. S. (2006). Tagging and tracking individual networks within a complex mitochondrial web with photoactivatable GFP. *American Journal of Physiology – Cell Physiology*, 291(1):C176-C184.

Twig G., Hyde B. and Shirihai O. S. (2008b). Mitochondrial fusion, fission and autophagy as a quality control axis: the bioenergetic view. *Biochimica et Biophysica Acta – Bioenergetics*, 1777(9):1092-1097.

Vale R. D. (2003). The molecular motor toolbox for intracellular transport. *Cell*, 112(4):467-480.

Valverde R., Edwards L. and Regan L. (2008). Structure and function of KH domains. *The FEBS Journal*, 275(11):2712-2726.

Vanneste J. and van den Bosch de Aguilar P. (1981). Mitochondrial alterations in the spinal ganglion neurons in ageing rats. *Acta Neuropathologica*, 54(1): 83-87.

Varadi A., Ainscow E. K., Allan V. J. and Rutter G. A. (2002). Involvement of conventional kinesin in glucose-stimulated secretory granule movements and exocytosis in clonal pancreatic beta-cells. *Journal of Cell Science*, 115(21):4177-4189.

Varadi A., Johnson-Cadwell L. I., Cirulli V., Yoon Y., Allan V. J. and Rutter G. A. (2004). Cytoplasmic dynein regulates the subcellular distribution of mitochondria by controlling the recruitment of the fission factor dynamin-related protein-1. *Journal of Cell Science*, 117(19):4389-4400.

Verstreken P., Ly C. V., Venken K. J., Koh T. W., Zhou Y. and Bellen H. J. (2005). Synaptic mitochondria are critical for mobilization of reserve pool vesicles at *Drosophila* neuromuscular junctions. *Neuron*, 47(3):365-378.

Waterham H. R., Koster J., van Roermund C. W., Mooyer P. A., Wanders R. J. and Leonard J. V. (2007). A lethal defect of mitochondrial and peroxisomal fission. *The New England Journal of Medicine*, 356(17):1736-1741.

Welte M. A. (2004). Bidirectional transport along microtubules. *Current Biology*, 14(13):R525-R537.

Whitworth A. J., Theodore D. A., Greene J. C., Benes H., Wes P. D. and Pallanck L. J. (2005). Increased glutathione S-transferase activity rescues dopaminergic neuron loss in a *Drosophila* model of Parkinson's disease. *Proceedings of the National Academy of Sciences of the United States of America*, 102(22):8024-8029.

Willems P. H., Smeitink J. A. and Koopman W. J. (2009). Mitochondrial dynamics in human NADH:ubiquinone oxidoreductase deficiency. *The International Journal of Biochemistry and Cell Biology*, 41(10):1773-1782.

Wong E. D., Wagner J. A., Gorsich S. W., McCaffery J. M., Shaw J. M. and Nunnari J. (2000). The dynamin-related GTPase, Mgm1p, is an intermembrane space protein required for maintenance of fusion competent mitochondria. *The Journal of Cell Biology*, 151(2):341-352.

Wong E. D., Wagner J. A., Scott S. V., Okreglak V., Holewinske T. J., Cassidy-Stone A. and Nunnari J. (2003). The intramitochondrial dynamin-related GTPase, Mgm1p, is a component of a protein complex that mediates mitochondrial fusion. *The Journal of Cell Biology*, 160(3):303-311.

Xie Z. and Klionsky D. J. (2007). Autophagosome formation: core machinery and adaptations. *Nature Cell Biology*, 9(10):1102-1109.

Yi M., Weaver D. and Hajnóczky G. (2004). Control of mitochondrial motility and distribution by the calcium signal: a homeostatic circuit. *The Journal of Cell Biology*, 167(4):661-672.

Yoon Y., Krueger E. W., Oswald B. J. and McNiven M. A. (2003). The mitochondrial protein hFis1 regulates mitochondrial fission in mammalian cells through an interaction with the dynamin-like protein DLP1. *Molecular and Cellular Biology*, 23(15): 5409-5420.

Yoon Y., Pitts K. R. and McNiven M. A. (2001). Mammalian dynamin-like protein DLP1 tubulates membranes. *Molecular Biology of the Cell*, 12(9):2894-2905.

Yu T., Fox R. J., Burwell L. S. and Yoon Y. (2005). Regulation of mitochondrial fission and apoptosis by the mitochondrial outer membrane protein hFis1. *Journal of Cell Science*, 118(18):4141-4151.

Yu-Wai-Man P., Sitarz K. S., Samuels D. C., Griffiths P. G., Reeve A. K., Bindoff L. A., Horvath R. and Chinnery P. F. (2010). *OPA1* mutations cause cytochrome c oxidase deficiency due to loss of wild-type mtDNA molecules. *Human Molecular Genetics*, 19(15): 3043-3052.

Zanna C., Ghelli A., Porcelli A. M., Karbowski M., Youle R. J., Schimpf S., Wissinger B., Pinti M., Cossarizza A., Vidoni S., Valentino M. L., Rugolo M. and Carelli V. (2008). OPA1 mutations associated with dominant optic atrophy impair oxidative phosphorylation and mitochondrial fusion. *Brain*, 131(2):352-367.

Züchner S., De Jonghe P., Jordanova A., Claeys K. G., Guergueltcheva V., Cherninkova S., Hamilton S. R., Van Stavern G., Krajewski K. M., Stajich J., Tournev I., Verhoeven K., Langerhorst C. T., de Visser M., Baas F., Bird T., Timmerman V., Shy M. and Vance J. M. (2006). Axonal neuropathy with optic atrophy is caused by mutations in *mitofusin 2*. *Annals of Neurology*, 59(2):276-281.

Züchner S., Mersiyanova I. V., Muglia M., Bissar-Tadmouri N., Rochelle J., Dadali E. L., Zappia M., Nelis E., Patitucci A., Senderek J., Parman Y., Evgrafov O., Jonghe P. D., Takahashi Y.,Tsuji S., Pericak-Vance M. A., Quattrone A., Battaloglu E., Polyakov A. V., Timmerman V., Schröder J. M. and Vance J. M. (2004). Mutations in the mitochondrial GTPase mitofusin 2 cause Charcot-Marie-Tooth neuropathy type 2A. *Nature Genetics*, 36(5):449-451.